AD_____

Award Number: DAMD17-02-1-0238

TITLE: Endometase in Androgen-Repressed Human Prostate Cancer

PRINCIPAL INVESTIGATOR: Qing-Xiang Amy Sang, Ph.D.

CONTRACTING ORGANIZATION: Florida State University
Tallahassee, FL 32306-4166

REPORT DATE: March 2004

TYPE OF REPORT: Annual

PREPARED FOR: U.S. Army Medical Research and Materiel Command
Fort Detrick, Maryland 21702-5012

DISTRIBUTION STATEMENT: Approved for Public Release;
Distribution Unlimited

The views, opinions and/or findings contained in this report are those of the author(s) and should not be construed as an official Department of the Army position, policy or decision unless so designated by other documentation.

REPORT DOCUMENTATION PAGE

Form Approved
OMB No. 074-0188

1. AGENCY USE ONLY (Leave blank)	2. REPORT DATE	3. REPORT TYPE AND DATES COVERED
	March 2004	Annual (25 Feb 2003 - 25 Feb 2004)

4. TITLE AND SUBTITLE

Endometase in Androgen-Repressed Human Prostate Cancer

5. FUNDING NUMBERS

DAMD17-02-1-0238

6. AUTHOR(S)

Qing-Xiang Amy Sang, Ph.D.

7. PERFORMING ORGANIZATION NAME(S) AND ADDRESS(ES)

Florida State University
Tallahassee, FL 32306-4166

E-Mail: sang@chem.fsu.edu

8. PERFORMING ORGANIZATION REPORT NUMBER

9. SPONSORING / MONITORING AGENCY NAME(S) AND ADDRESS(ES)

U.S. Army Medical Research and Materiel Command
Fort Detrick, Maryland 21702-5012

10. SPONSORING / MONITORING AGENCY REPORT NUMBER

11. SUPPLEMENTARY NOTES

Original contains color plates: ALL DTIC reproductions will be in black and white

12a. DISTRIBUTION / AVAILABILITY STATEMENT

Approved for Public Release; Distribution Unlimited

12b. DISTRIBUTION CODE

13. ABSTRACT (Maximum 200 Words)

The spread of prostate cancer cells to other parts of the body is the leading cause of patient death. In 2000, we reported the discovery, cloning, and characterization of human matrix metalloproteinase-26 (MMP-26), **endometase**. We have been testing three specific hypotheses: 1) The expression levels of MMP-26 is correlated with the metastatic potentials and the degrees of malignancy of human prostate cells; 2) MMP-26 has unique structure and enzymatic function; 3) MMP-26 enhances prostate cancer invasion by digesting extracellular matrix proteins and inactivating serine proteinase inhibitors, and specific inhibitors of MMP-26 block prostate cancer invasion. We have showed that the levels of MMP-26 protein in human prostate carcinomas from multiple patients were significantly higher than those in prostatitis, benign prostate hyperplasia, and normal prostate glandular tissues. Human breast carcinoma *in situ* also expressed high levels of MMP-26 protein. Prostate cancer cells transfected with MMP-26 cDNA are more invasive than the parental cell lines. MMP-26 promoted prostate cancer invasion via activation of pro-gelatinase B/MMP-9. The endometase active site structure has been revealed to have an intermediate S1′ pocket using synthetic metalloproteinase inhibitors. Endometases may be a novel marker for prostate cancer detection and a new target for therapy. Reprints published by Sang lab are attached.

14. SUBJECT TERMS

Matrix metalloproteinase-26, endometase, advanced human prostate cancer, novel proteinases, cell biology and biochemistry

15. NUMBER OF PAGES

54

16. PRICE CODE

17. SECURITY CLASSIFICATION OF REPORT	18. SECURITY CLASSIFICATION OF THIS PAGE	19. SECURITY CLASSIFICATION OF ABSTRACT	20. LIMITATION OF ABSTRACT
Unclassified	Unclassified	Unclassified	Unlimited

Table of Contents

DAMD17-02-1-0238 Annual/Midterm Report

Endometase in Androgen-Repressed Human Prostate Cancer

Introduction

Our long term goal is to understand the biochemical and cellular functions of matrix metalloproteinases (MMPs, matrixins) so that we may reveal the molecular steps and pathways of cancer angiogenesis (new blood formation to provide nutrients, oxygen, and passages for cancer cell growth and spread) and metastasis (the spread of cancer). We discovered a novel matrix metalloproteinase (MMP-26, endometase) recently. Endometase is a special biological catalyst that specifically digests some of the connective tissue barrier proteins and may facilitate tumor growth, invasion, and new blood vessel formation. *Endometase* was found to be specifically associated with the androgen-repressed human prostate cancer *(ARCaP)* cells. It was *not* expressed by normal human prostate tissues and early stage prostate cancer cells. ARCaP cells were isolated from a human patient who died of metastasis of prostate cancer. Most importantly, endometase gene was turned on in human prostate cancer tissues from patients. This project has investigated a role of endometase in advanced human prostate cancer and provided knowledge for new strategies to detect and attack prostate cancer. To understand the functions of endometase, we have identified some of its physiological and pathological substrates and developed potent proteinase inhibitors targeting this protein. We have tested the *hypothesis* that this unique endometase is partially responsible for promoting cancer cell growth and invasion because of its activity as "a molecular power drill" that breaks down connective tissue barriers. Together with our collaborators Drs. Martin A. Schwartz and Leland W.K. Chung, we have been developing and testing new MMP inhibitors and identify potent and selective compounds to target endometase. The inhibitors are useful tools for the investigations of the endometase active site structure and functions, and more importantly, the prostate cancer invasion and angiogenesis. We have revealed that the active site of endometase has an intermediate S1' pocket by enzyme inhibition kinetic studies, protein sequence analyses, and homology modeling. We have also examined the endometase expression pattern in human prostate and breast cancer tissues and clinical specimens and studied its pathological role in human prostate and breast cancers. This project may identify a novel marker for prostate cancer detection and a new target for prostate cancer treatment.

Body

Statement of Work

Endometase in Androgen-Repressed Human Prostate Cancer

Task 1. **To examine the endometase (matrix metalloproteinase-26, MMP-26) expression pattern in normal and malignant prostate cell lines and to correlate the endometase protein expression levels with the known malignancy and metastatic potentials of the cells (Months 1-8):**

a. Culture normal and malignant prostate cells.
b. Measure the endometase expression levels by enzyme-linked immunosorbent assay (ELISA) and immunoblot using enhanced chemiluminescence (ECL). There are four specific endometase antibodies (Abs) available at the P.I.'s lab; three Abs are against the catalytic domain, one Ab is against the pro-domain.

This task has been accomplished. For more details please see Fig. 2 and Fig. 3 of the following published paper: Y.-G. Zhao, A. Xiao, R.G. Newcomer, H.I. Park, T. Kang, L.W.K. Chung, M.G. Swanson, H. E. Zhau, J. Kurhanewicz, and **Q.-X. Sang*** (2003) Activation of Pro-Gelatinase B by Endometase/Matrilysin-2 Promotes Invasion of Human Prostate Cancer Cells. *J. Biol. Chem.* **278**, 15056-15064. Please see attached reprint.

Task 2. **To over-express endometase in endometase-negative human prostate cells and characterize endometase positive cells (Months 5-25):**

a. Prepare endometase over-expression vectors.
b. Transfect pCIMMP-26 into normal human prostate cells, an androgen-dependent prostate cancer cell line LNCaP, and an androgen-independent prostate cancer cell line DU-145.
c. Identify endometase positive cells by immunological methods (ELISA and immunoblot).
d. Characterize endometase positive cells *in vitro* (colony formation on soft agar).

This task is in excellent progress. For more details please see Fig. 5 and Fig. 6 of the following paper published: Y.-G. Zhao, A. Xiao, R.G. Newcomer, H.I. Park, T. Kang, L.W.K. Chung, M.G. Swanson, H. E. Zhau, J. Kurhanewicz, and **Q.-X. Sang*** (2003) Activation of Pro-Gelatinase B by Endometase/Matrilysin-2 Promotes Invasion of Human Prostate Cancer Cells. *J. Biol. Chem.* **278**, 15056-15064. Please also see attached reprint and the following preliminary results (Fig. 1 and Fig. 2).

Task 3. **Analyze structure-function relationships of the endometase active site using synthetic matrix metalloproteinase (MMP) inhibitors and identify specific and potent endometase inhibitors for the cell invasion assays (Months 10-30):**

a. Optimize the synthetic fluorogenic peptide substrate cleavage assays using a Perkin-Elmer LS-50B luminescence spectrometer.
b. Measure the IC_{50} (inhibitor concentration at 50% enzyme activity) values and inhibition constants (k_I values) of new synthetic MMP inhibitors with endometase listed in *Table 1* and *Figure 2* of the proposal. Determine the inhibition kinetics and mechanisms.

This task has been accomplished. Please see attached reprints for more details:

H.I. Park, B.E. Turk, F.E. Gerkema, L.C. Cantley, and **Q.-X. Sang*** (2002) Peptide substrate specificities and protein cleavage sites of human endometase/matrilysin-2/matrix metalloproteinase-26. *J. Biol. Chem.* **277,** 35168-35175.

H.I. Park, Y. Jin, D.R. Hurst, C.A. Monroe, S. Lee, M.A. Schwartz, and **Q.-X. Sang*** (2003) The intermediate S1' pocket of the endometase/matrilysin-2 active site revealed by enzyme inhibition kinetic studies, protein sequence analyses, and homology modeling. *J. Biol. Chem.*, 278:51646-51653.

Task 4. **Identify new substrates of endometase, compare the degrees of invasiveness of the human prostate cells selected from *Task 1* and *Task 2*, and test the efficacies of MMP inhibitors selected from *Task 3* in the prostate cell invasion (Months 20-36):**

a. Test intracelluar proteins, extracellular matrix proteins, and cell surface proteins of ARCaP and other cells to identify new endometase substrates, hence, understand its putative functions.

This task is in progress. Please see the following published paper Figs. 6-8 and tables I and II for more details. H.I. Park, B.E. Turk, F.E. Gerkema, L.C. Cantley, and **Q.-X. Sang*** (2002) Peptide substrate specificities and protein cleavage sites of human endometase/matrilysin-2/matrix metalloproteinase-26. *J. Biol. Chem.* **277,** 35168-35175.

b. Test and compare the degrees of invasiveness of human normal, malignant, and endometase over-expression prostate cells, respectively, using modifed Boyden Chambers coated with extracellular matrix proteins or cell surface proteins.
c. Test and compare the efficacies of selective MMP inhibitors from *Task 3* in prostate cell invasion. Identify specific inhibitors that may lead to future cancer therapeutics.

This task is in excellent progress. For more details please see Figs. 4-8 of the following paper published. Y.-G. Zhao, A. Xiao, R.G. Newcomer, H.I. Park, T. Kang, L.W.K. Chung, M.G. Swanson, H. E. Zhau, J. Kurhanewicz, and **Q.-X. Sang*** (2003) Activation of Pro-Gelatinase B by Endometase/Matrilysin-2 Promotes Invasion of Human Prostate Cancer Cells. *J. Biol. Chem.* **278,** 15056-15064. Please see attached reprint and the following preliminary results (Fig. 1 and Fig. 2).

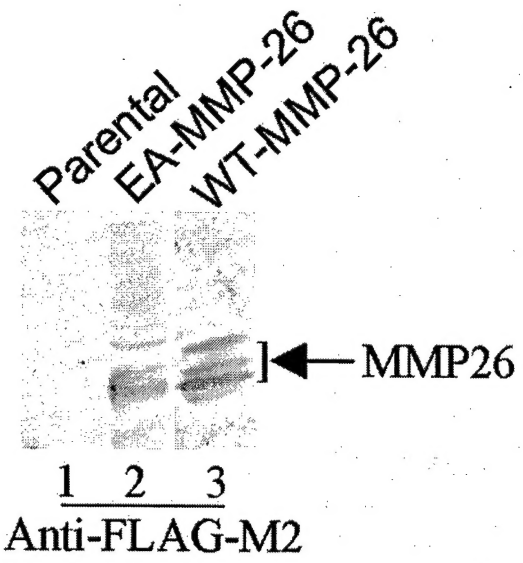

Fig. 1. Detection of MMP-26 in androgen-dependent LNCaP cells stably expressing MMP-26 wild type or an inactive form. LNCaP cells, a human prostate cancer cell line, were stably transfected with MMP-26 wild type (WT-MMP-26), or an inactive form (EA-MMP-26), both of which were tagged with FLAG tags at their C-termini. Cells were routinely cultured in DMEM supplemented with 10% fetal bovine serum and 400 μg/L of G418. For experiments, they were seeded into 24-well-plates until they reached 100% confluence. Cells were lysed with RIPA buffer, and cell lysates were analyzed by Western blotting using anti-FLAG-M2 antibody.

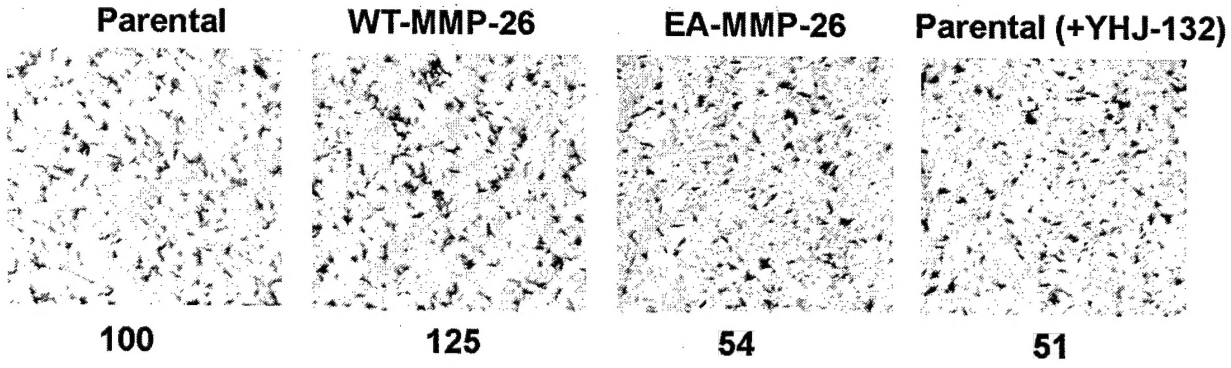

Fig. 2. MMP-26 plays a vital role in the invasion of androgen-dependent LNCaP cells. Parental LNCaP cells or its derivatives stably over-expressing MMP-26 wild type (WT-MMP-26) or inactive form (EA-MMP-26) were subjected to invasion assays utilizing a modified Boyden chamber coated with type IV collagen (25 μg/well). Following 48 hours incubation in serum-free medium alone or containing **10 μM YHJ-132, an MMP inhibitor synthesized by our group**, the inner chambers were fixed and the invading cells were photographed. Quantification of the invading cells was performed by integrated morphometry analysis (IMA); untreated parental LNCaP cells (Parental) were controls as 100% invasive. The WT-MMP-26 cells showed a 25% increase in invading cells, while the EA-MMP-26 or parental cells treated with YHJ-132 showed decreased invasion, at 54% and 51% of the parental cells, respectively.

Task 5. **Alternative approaches: Test and compare the rates of cell proliferation and apoptosis of the human prostate cells selected from *Task 1* and *Task 2* (Months 26-36):**

a. Test and compare the rates of cell proliferation of human normal, malignant, and endometase over-expression prostate cells, respectively, cultured on extracellular matrix proteins. Cell proliferation rates will be determined by assaying for 5-bromo-2'-deoxyuridine (BrdU) incorporation using the colorimetric ELISA assay kit from Boehringer Mannheim Co.

b. Test and compare the rates of cell apoptosis of human normal, malignant, and endometase over-expression prostate cells, respectively, cultured on extracellular matrix proteins. A quantitative Cell Death Detection ELISA^{PLUS} colorimetric assay kit (also from Boehringer Mannheim Co.) will be used. This assay is useful for the quantitation of apoptosis without cell labeling; it differentiates apoptosis from necrosis.

This task is in progress.

Blockage of ARCaP cell invasion by MMP-26 antibodies is not due to the effects of the antibodies on cell attachment to extracellular matrix, cell proliferation, cytotoxicity, and apoptosis. Further investigation shows that the functional blocking antibodies do not affect ARCaP cell attachment to the substrates, do not inhibit ARCaP cell proliferation (**Fig. 3**), have no cytotoxicity, and do not promote the cell apoptosis, demonstrating that the diminished invasiveness of ARCaP cells is due to the functional neutralizing activity of the antibodies against MMP-26 and is not due to reduced cell numbers and is not due to reduced cell attachment to the extracellular matrix substrates.

Cells attachment experiments. 2.25×10^5 ARCap/LNCap/DU145/ PC-3 cells in serum free DMEM media containing different concentrations of one of the pre-immune-IgGs or anti-MMP-26 IgGs were cultured in fibronectin, and matrigel coated 24-well plates. The growing cells were stopped at 3 hours, 6 hours, 12 hours, 24 hours, 48 hours, and 60 hours by rinsing with PBS and fixing in 4% PFA/PBS solution. Then the cells were stained with 0.1% Crystal Violet (Sigma, USA) solution. The attached cells number was counted under in 10 high power fields (400x) of each of the duplicate samples under a microscope.

Results: The ARCaP cells number attached on the FN and Matrigel coated 24-well plate had no significant difference among the untreated wells, pre-immune IgGs treated wells and the anti-MMP-26 antibodies treated the wells ($p>0.05$) at the time points of 3 hours, 6 hours, 12 hours, 24 hours, 48 hours, and 60 hours (data not shown). These results indicate that the inhibition of ARCaP cell invasion by anti-MMP-26 antibodies is not due to the effect on the cells attachment to extracellular matrix components.

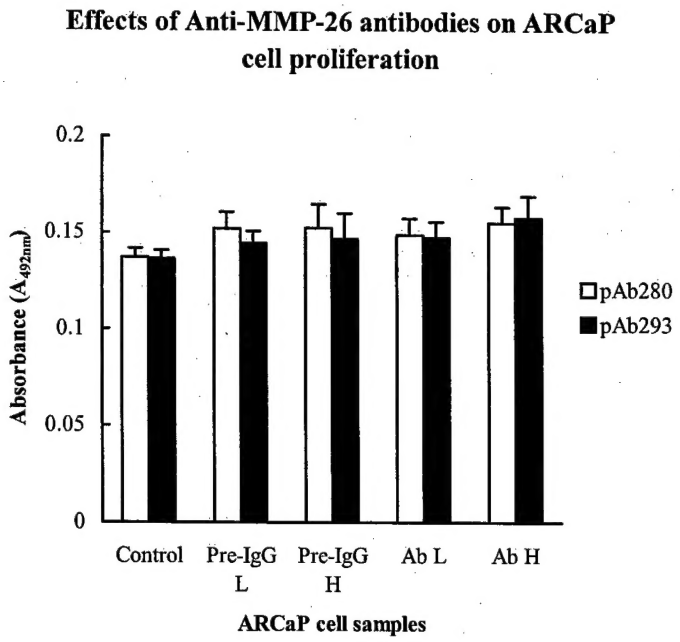

Fig. 3. The anti-MMP-26 polyclonal Abs have no effect on the proliferation of ARCaP cells. The ARCaP cells proliferation was determined using the BrdU Labeling Cell Proliferation ELISA (Roche Molecular Biochemicals, Indianapolis, IN) according to the manufacturer's instructions. **Pre-IgG L**, preimmune IgG low concentration (10μg/ml); **Pre-IgG H,** preimmune IgG high concentration (50μg/ml); **Ab L**, antibody low concentration (10μg/ml); and **Ab H**, antibody high concentration (50μg/ml).

Cells proliferation assays. ARCaP cell proliferation was determined using the Cell Proliferation ELISA from Roche Molecular Biochemicals (Indianapolis, IN) following the manufacturer's instructions. In brief, the ARCap cells were plated in a fibronectin, and matrigel pre-coated 96-well tissue culture plate (Falcon, Becton Dickinson Labware, Lincoln Park, New Jersey) at a density of 1 x 10^4 cells/well in DMEM medium containing 10% FBS for 24 hours. Then the cells were cultured in serum free DMEM medium in the presence of pre-immune IgG of 98R3, pre-immune IgG of 98R12, pAb280 and pAb293 (10μg/ml, 50μg/ml, respectively) in duplicate wells for another 24 hours. After adding BrdU (100μM) labeling solution for 12 hours in 37° C, 5%CO_2, the cells were fixed by adding FixDenat solution for 30mins at room temperature. Followed by adding anti-BrdU POD and incubated for 90 min at room temperature. Finally, added substrate and incubate for 30 mins and the values of absorbance were read at 492 nm using an Automatic Microplate Reader (Titertek Multiskan MC-340, Flow Laboratories, Virginia). Standard deviations were calculated and were presented as error bars in the Figures.

Key Research Accomplishments

1. This research project has addressed many of the tasks listed in the "Statement of Work", generated three papers published in "The Journal of Biological Chemistry", one "Cancer Research" paper, and one "Biochemical Journal paper". The grant also supported training of research students and postdoctoral associates.

2. This work has verified a putative biochemical mechanism by which endometase/matrilysin-2/matrix metalloproteinase-26 (MMP-26) may promote human prostate cancer cell invasion.

3. We showed that the levels of MMP-26 protein in human prostate carcinomas from multiple patients were significantly higher than those in prostatitis, benign prostate hyperplasia, and normal prostate glandular tissues. Statistical analyses have been performed.

4. MMP-26 was capable of activating pro-MMP-9 by cleavage at the Ala^{93}-Met^{94} site of the prepro-enzyme. This activation proceeded in a time- and dose-dependent manner, facilitating the efficient cleavage of fibronectin by MMP-9. The activated MMP-9 products generated by MMP-26 appeared more stable than those cleaved by MMP-7 under the conditions tested.

5. To investigate the contribution of MMP-26 to cancer cell invasion via the activation of MMP-9, highly invasive and metastatic human prostate carcinoma cells, androgen-repressed prostate cancer (ARCaP) cells, were selected as a working model. ARCaP cells express both MMP-26 and MMP-9. Specific anti-MMP-26 and anti-MMP-9 functional blocking antibodies both reduced the invasiveness of ARCaP cells across fibronectin or type IV collagen.

6. The introduction of MMP-26 antisense cDNA into ARCaP cells reduced the MMP-26 protein level in these cells and strongly suppressed the invasiveness of ARCaP cells.

7. Double immunofluorescence staining and confocal laser scanning microscopic images revealed that MMP-26 and MMP-9 were co-localized in parental and MMP-26 sense-transfected ARCaP cells. Moreover, MMP-26 and MMP-9 proteins were both expressed in the same human prostate carcinoma tissue samples examined.

8. These results indicate that MMP-26 may be a physiological and pathological activator of pro-MMP-9, and the activation of pro-MMP-9 by MMP-26 may be an important mechanism contributing to the invasive capabilities of prostate carcinomas.

9. Peptide libraries were used to profile the substrate specificity of MMP-26 from the P4 to P4′ sites. The optimal cleavage motifs for MMP-26 were Lys-Pro-Ile/Leu-Ser (P1)-Leu/Met (P1′)-Ile/Thr-Ser/Ala-Ser.

10. The strongest preference was observed at the P1′ and P2 sites where hydrophobic residues were favored. Proline was preferred at P3 and Serine at P1. The overall specificity was similar to that of other MMPs except that more flexibility was observed at P1, P2′, and P3′.

11. Synthetic inhibitors of gelatinases and collagenases inhibited MMP-26 with similar efficacy. A pair of stereoisomers had a only 40-fold difference in K_i^{app} values against MMP-26 compared to a 250-fold difference against neutrophil collagenase, indicating that MMP-26 is less stereo-selective for its inhibitors.

12. MMP-26 auto-digested itself during the folding process; two of the major autolytic sites were Leu^{49}-Thr^{50} and Ala^{75}–Leu^{76}, which still left the cysteine switch sequence (PH**C**^{82}GVPD) intact. This suggests that Cys^{82} may not play a role in the latency of the zymogen.

13. MMP-26 cleaved Phe^{352}–Leu^{353} and Pro^{357}–Met^{358} in the reactive loop of alpha 1 proteinase inhibitor and His^{140}–Val^{141} in insulin-like growth factor binding protein-1, likely rendering these substrates inactive.

14. Among the fluorescent peptide substrates analyzed, Mca-Pro-Leu-Ala-Nva-Dpa-Ala-Arg-NH_2 displayed the highest specificity constant (30000 / Molar second) with MMP-26.

15. The intermediate S1' pocket of the endometase active site has been revealed by enzyme inhibition kinetic studies using our novel MMP inhibitors, protein sequence analyses, and molecular modeling/computational biochemistry.

16. Potent and selective inhibitors of endometase have been identified and tested in biochemical experiments, and some preliminary data were also obtained for the inhibition of human prostate cancer cell invasion by one of the potent inhibitors.

17. Transgenic human prostate cancer cell lines (both androgen-repressed and androgen-dependent) have been made and MMP-26 over-expression cells, knock out cells, and dominant-negative catalytically inactive mutants have been generated and tested. The degree of invasiveness of these human prostate cancer cell lines were correlated with the expression levels of MMP-26 protein. These results verified our hypotheses.

18. Human breast cancer tissues were examined as controls for prostate cancer studies. Breast carcinoma *in situ* also expressed high levels of MMP-26 and MMP-26 may play a role in the initiation of invasion of human breast cancers.

19. Tissue inhibitors of metalloproteinases TIMP-2 and TIMP-4 are potent inhibitors of MMP-26 and they have inhibited the activation of pro-MMP-9 by MMP-26.

20. MMP-26 gene is expressed by human breast carcinoma/epithelial cancer cells as examined by *in situ* hybridization, confirming MMP-26 is expressed by epithelial cells

and its epithelial origin. These data have been reported in the "Cancer Research" paper. Please see attached reprints.

21. This report proposes a working model for the future studies of proMMP-26 activation, the design of inhibitors, and the identification of optimal physiological and pathological substrates of MMP-26 *in vivo*.

Reportable Outcomes

1. Published papers and manuscripts:

H.I. Park, B.E. Turk, F.E. Gerkema, L.C. Cantley, and **Q.-X. Sang*** (2002) Peptide substrate specificities and protein cleavage sites of human endometase/matrilysin-2/matrix metalloproteinase-26. *J. Biol. Chem.* **277,** 35168-35175.

Y.-G. Zhao, A. Xiao, R.G. Newcomer, H.I. Park, T. Kang, L.W.K. Chung, M.G. Swanson, H. E. Zhau, J. Kurhanewicz, and **Q.-X. Sang*** (2003) Activation of Pro-Gelatinase B by Endometase/Matrilysin-2 Promotes Invasion of Human Prostate Cancer Cells. *J. Biol. Chem.* **278,** 15056-15064.

H.I. Park, Y. Jin, D.R. Hurst, C.A. Monroe, S. Lee, M.A. Schwartz, and **Q.-X. Sang*** (2003) The intermediate S1' pocket of the endometase/matrilysin-2 active site revealed by enzyme inhibition kinetic studies, protein sequence analyses, and homology modeling. *J. Biol. Chem.*, 278:51646-51653.

D. R. Hurst, M.A. Schwartz, M.A. Ghaffari, Y. Jin, H. Tschesche, G.B. Fields, and **Q.-X. Sang*** (2004) Catalytic- and ecto-domains of membrane type 1-matrix metalloproteinase have similar inhibition profiles but distinct endopeptidase activities. *Biochem. J.* **377**, 775-779.

Y.-G. Zhao, A.-Z. Xiao, H.I. Park, R.G. Newcomer, M. Yan, Y.-G. Man, S.C. Heffelfinger, and **Q.-X. Sang*** (2004) Endometase/matrilysin-2 in human breast ductal carcinoma *in situ* and its inhibition by tissue inhibitors of metalloproteinases-2 and -4: a putative role in the initiation of breast cancer invasion. *Cancer Res.* **64,** 590-598.

2. In addition to the Principal Investigator, Dr. Sang, the following students and research associates at Professor Sang's laboratory have been partially funded by this grant.

Douglas R. Hurst, Graduate Student Research Assistant
Dr. Hyun I. Park, Postdoctoral Research Associate
Margaret Mary Coryn, Student Assistant
Sara C. Monroe, Research Assistant
Tiebang Kang, Postdoctoral Research Associate
Aizhen Xiao, Postdoctoral Research Associate

Conclusions

The spread of prostate cancer cells to other parts of the body is the leading cause of patient death. In 2000, we reported the discovery, cloning, and characterization of human matrix metalloproteinase-26 (MMP-26), **endometase**. We have been testing three specific hypotheses: 1) The expression levels of MMP-26 is correlated with the metastatic potentials and the degrees of malignancy of human prostate cells; 2) MMP-26 has unique structure and enzymatic function; 3) MMP-26 enhances prostate cancer invasion by digesting extracellular matrix proteins and inactivating serine proteinase inhibitors, and specific inhibitors of MMP-26 block prostate cancer invasion. We have showed that the levels of MMP-26 protein in human prostate carcinomas from multiple patients were significantly higher than those in prostatitis, benign prostate hyperplasia, and normal prostate glandular tissues. High levels of MMP-26 is also expressed by human breast ductal carcinoma *in situ*. Both MMP-26 gene and protein are expressed by the carcinoma cells confirming its epithelial origin. MMP-26 promoted prostate cancer invasion via activation of pro-gelatinase B/MMP-9. Functional blocking antibodies against either MMP-26 or MMP-9 blocked human prostate cancer cell invasion. Furthermore, antisense cDNA of MMP-26 and catalytically inactive mutant MMP-26 also inhibited prostate cancer cell invasion. The over-expression of MMP-26 cDNA in both androgen-dependent and independent cells lines enhanced the invasiveness of these cells. Tissue inhibitors of metalloproteinases TIMP-2 and TIMP-4 are also potent inhibitors of MMP-26. The endometase active site structure and function have been investigated and revealed to have an intermediate S1' pocket using synthetic metalloproteinase inhibitors, protein sequence analyses and homology modeling studies. These findings may aid in rational inhibitor/potential drug design for the development of more potent and selective inhibitors of MMP-26. Optimal peptide substrate specificity and protein cleavage sites have been identified in both peptide libraries and potentially physiologically relevant proteins. These results suggest that endometase/MMP-26 may promote human prostate and breast cancer cell invasion and it is specifically expressed in human prostate and breast cancer tissues. MMP-26 may be a novel marker for prostate cancer detection and a new target for prostate cancer treatment.

References

Please see references cited in the following five papers:

H.I. Park, B.E. Turk, F.E. Gerkema, L.C. Cantley, and **Q.-X. Sang*** (2002) Peptide substrate specificities and protein cleavage sites of human endometase/matrilysin-2/matrix metalloproteinase-26. *J. Biol. Chem.* **277,** 35168-35175.

Y.-G. Zhao, A. Xiao, R.G. Newcomer, H.I. Park, T. Kang, L.W.K. Chung, M.G. Swanson, H. E. Zhau, J. Kurhanewicz, and **Q.-X. Sang*** (2003) Activation of Pro-Gelatinase B by Endometase/Matrilysin-2 Promotes Invasion of Human Prostate Cancer Cells. *J. Biol. Chem.* **278,** 15056-15064.

H.I. Park, Y. Jin, D.R. Hurst, C.A. Monroe, S. Lee, M.A. Schwartz, and **Q.-X. Sang*** (2003) The intermediate S1' pocket of the endometase/matrilysin-2 active site revealed by enzyme inhibition kinetic studies, protein sequence analyses, and homology modeling. *J. Biol. Chem.*, 278:51646-

51653.

D. R. Hurst, M.A. Schwartz, M.A. Ghaffari, Y. Jin, H. Tschesche, G.B. Fields, and **Q.-X. Sang*** (2004) Catalytic- and ecto-domains of membrane type 1-matrix metalloproteinase have similar inhibition profiles but distinct endopeptidase activities. *Biochem. J.* **377**, 775-779.

Y.-G. Zhao, A.-Z. Xiao, H.I. Park, R.G. Newcomer, M. Yan, Y.-G. Man, S.C. Heffelfinger, and **Q.-X. Sang*** (2004) Endometase/matrilysin-2 in human breast ductal carcinoma *in situ* and its inhibition by tissue inhibitors of metalloproteinases-2 and -4: a putative role in the initiation of breast cancer invasion. *Cancer Res.* **64,** 590-598.

Appendices

The following five papers/reprints are attached.

H.I. Park, B.E. Turk, F.E. Gerkema, L.C. Cantley, and **Q.-X. Sang*** (2002) Peptide substrate specificities and protein cleavage sites of human endometase/matrilysin-2/matrix metalloproteinase-26. *J. Biol. Chem.* **277,** 35168-35175.

Y.-G. Zhao, A. Xiao, R.G. Newcomer, H.I. Park, T. Kang, L.W.K. Chung, M.G. Swanson, H. E. Zhau, J. Kurhanewicz, and **Q.-X. Sang*** (2003) Activation of Pro-Gelatinase B by Endometase/Matrilysin-2 Promotes Invasion of Human Prostate Cancer Cells. *J. Biol. Chem.* **278,** 15056-15064.

H.I. Park, Y. Jin, D.R. Hurst, C.A. Monroe, S. Lee, M.A. Schwartz, and **Q.-X. Sang*** (2003) The intermediate S1' pocket of the endometase/matrilysin-2 active site revealed by enzyme inhibition kinetic studies, protein sequence analyses, and homology modeling. *J. Biol. Chem.*, 278:51646-51653.

D. R. Hurst, M.A. Schwartz, M.A. Ghaffari, Y. Jin, H. Tschesche, G.B. Fields, and **Q.-X. Sang*** (2004) Catalytic- and ecto-domains of membrane type 1-matrix metalloproteinase have similar inhibition profiles but distinct endopeptidase activities. *Biochem. J.* **377**, 775-779.

Y.-G. Zhao, A.-Z. Xiao, H.I. Park, R.G. Newcomer, M. Yan, Y.-G. Man, S.C. Heffelfinger, and **Q.-X. Sang*** (2004) Endometase/matrilysin-2 in human breast ductal carcinoma *in situ* and its inhibition by tissue inhibitors of metalloproteinases-2 and -4: a putative role in the initiation of breast cancer invasion. *Cancer Res.* **64,** 590-598.

THE JOURNAL OF BIOLOGICAL CHEMISTRY
Vol. 278, No. 17, Issue of April 25, pp. 15056–15064, 2003
Printed in U.S.A.

Activation of Pro-gelatinase B by Endometase/Matrilysin-2 Promotes Invasion of Human Prostate Cancer Cells*

Received for publication, October 28, 2002, and in revised form, February 10, 2003
Published, JBC Papers in Press, February 13, 2003, DOI 10.1074/jbc.M210975200

Yun-Ge Zhao‡, Ai-Zhen Xiao‡, Robert G. Newcomer‡, Hyun I. Park‡, Tiebang Kang‡, Leland W. K. Chung§, Mark G. Swanson¶, Haiyen E. Zhau§, John Kurhanewicz¶, and Qing-Xiang Amy Sang‡‖

From the ‡Department of Chemistry and Biochemistry and Institute of Molecular Biophysics, Florida State University, Tallahassee, Florida 32306-4390, the §Molecular Urology and Therapeutics Program, Emory University Winship Cancer Institute, Atlanta, Georgia 30322, and the ¶Magnetic Resonance Science Center, University of California, San Francisco, California 94143-1290

This work has explored a putative biochemical mechanism by which endometase/matrilysin-2/matrix metalloproteinase-26 (MMP-26) may promote human prostate cancer cell invasion. Here, we showed that the levels of MMP-26 protein in human prostate carcinomas from multiple patients were significantly higher than those in prostatitis, benign prostate hyperplasia, and normal prostate glandular tissues. The role of MMP-26 in prostate cancer progression is unknown. MMP-26 was capable of activating pro-MMP-9 by cleavage at the Ala^{93}–Met^{94} site of the prepro-enzyme. This activation proceeded in a time- and dose-dependent manner, facilitating the efficient cleavage of fibronectin by MMP-9. The activated MMP-9 products generated by MMP-26 appeared more stable than those cleaved by MMP-7 under the conditions tested. To investigate the contribution of MMP-26 to cancer cell invasion via the activation of MMP-9, highly invasive and metastatic human prostate carcinoma cells, androgen-repressed prostate cancer (ARCaP) cells were selected as a working model. ARCaP cells express both MMP-26 and MMP-9. Specific anti-MMP-26 and anti-MMP-9 functional blocking antibodies both reduced the invasiveness of ARCaP cells across fibronectin or type IV collagen. Furthermore, the introduction of *MMP-26* antisense cDNA into ARCaP cells significantly reduced the MMP-26 protein level in these cells and strongly suppressed the invasiveness of ARCaP cells. Double immunofluorescence staining and confocal laser scanning microscopic images revealed that MMP-26 and MMP-9 were co-localized in parental and *MMP-26* sense-transfected ARCaP cells. Moreover, MMP-26 and MMP-9 proteins were both expressed in the same human prostate carcinoma tissue samples examined. These results indicate that MMP-26 may be a physiological and pathological activator of pro-MMP-9.

During the initial phases of carcinoma cell invasion, as tumor cells begin to spread and infiltrate into the surrounding normal tissues, these cells must first degrade the basement membrane and other elements of the extracellular matrix (ECM),[1] including type IV collagen, laminin, and fibronectin (FN) (1). Multiple protease families, including the matrix metalloproteinases (MMPs), serine proteases, and cysteine proteases, are suspected of contributing to the invasive and metastatic abilities of a variety of malignant tumors (2–5), but the specific biochemical mechanisms that facilitate these invasive behaviors remain elusive.

More than 23 human *MMPs*, and numerous homologues from other species, have been reported (5), and matrix metalloproteinase-26 (*MMP-26*)/endometase/matrilysin-2 is a novel member of this enzyme family that was recently cloned and characterized by our group (6) and others (7–9). *MMP-26* mRNA is primarily expressed in epithelial cancers, such as lung, breast, endometrial, and prostate carcinomas, in their corresponding cell lines (6–9), and in a very limited number of normal adult tissues, such as the uterus (6, 8), placenta (7, 8), and kidney (9). Recently, we have found that the levels of *MMP-26* gene and protein expression are higher in a malignant choriocarcinoma cell line (JEG-3) than in normal human cytotrophoblast cells (10). Our preliminary studies indicate that expression of *MMP-26* may be correlated with the malignant transformation of human prostate and breast epithelial cells. The specific expression of *MMP-26* in malignant tumors and the proteolytic activity of this enzyme against multiple components of the ECM, including fibronectin, type IV collagen, vitronectin, gelatins, and fibrinogen, as well as non-ECM proteins such as insulin-like growth factor-binding protein 1 and α1-protease inhibitor (6–9), indicate that MMP-26 may possess an important function in tumor progression.

Another member of the *MMP* family considered to be an important contributor to the processes of invasion, metastasis, and angiogenesis exhibited by tumor cells is gelatinase B (*MMP-9*) (11–14). Uría and López-Otín (8) have demonstrated that MMP-26 is able to cleave MMP-9, and here we examine the possibility that MMP-26 facilitates tumor cell invasion through the activation of pro-MMP-9. The highly invasive and metastatic cell line utilized for this study, an androgen-re-

* This work was supported in part by Department of Defense/United States Army Prostate Cancer Research Program Grant DAMD17-02-1-0238, National Institutes of Health Grant CA78646, American Cancer Society, Florida Division, Grant F01FSU-1, the Florida State University Research Foundation (to Q.-X. A. S.), and National Institutes of Health Grants CA82739 and CA76620 (to H. E. Z. and L. W. K. C., respectively). The costs of publication of this article were defrayed in part by the payment of page charges. This article must therefore be hereby marked "*advertisement*" in accordance with 18 U.S.C. Section 1734 solely to indicate this fact.

‖ To whom correspondence should be addressed: Dept. of Chemistry and Biochemistry, Florida State University, 203 DLC, Chemistry Research Bldg., Rm. 203, Tallahassee, FL 32306-4390. Tel.: 850-644-8683; Fax: 850-644-8281; E-mail: sang@chem.fsu.edu.

[1] The abbreviations used are: ECM, extracellular matrix; ANOVA, analysis of variance; ARCaP, androgen repressed prostate cancer cells line; BPH, benign prostate hyperplasia; FN, fibronectin; IMA, integrated morphometry analysis; MMP-7, matrix metalloproteinase-7/matrilysin; MMP-9, matrix metalloproteinase-9/gelatinase B; MMP-26, matrix metalloproteinase-26/endometase/matrilysin-2; MMPs, matrix metalloproteinases; CAPS, 3-cyclohexylamino-1-propanesulfonic acid.

pressed human prostate cancer (ARCaP), was derived from the ascites fluid of a patient with advanced prostate cancer that had metastasized to the lymph nodes, lungs, pancreas, liver, kidneys, and bones (15). This cell line produces high levels of MMP-9 and gelatinase A (MMP-2) (15, 16).

In this study, we provide evidence that MMP-26 is capable of activating pro-MMP-9, and that once activated, MMP-9 cleaves fibronectin, type IV collagen, and gelatin with great efficiency. Both the MMP-26 and MMP-9 proteins were highly expressed in the ARCaP cells, and co-localization of their expression patterns was consistently observed. The invasiveness of ARCaP cells through FN or type IV collagen was significantly decreased in the presence of antibodies specifically targeting MMP-26 or MMP-9. In addition, cells transfected with antisense *MMP-26*, showing significant reduction of MMP-26 at the protein level, exhibited a reduction of invasive potential *in vitro* in addition to a significant diminution in observed levels of active MMP-9 protein. These results support the hypothesis that activation of MMP-9 by MMP-26 may promote the *in vitro* invasiveness of ARCaP cells through FN or type IV collagen, whereas the co-expression of MMP-26 and MMP-9 in many human prostate carcinoma tissues indicates that this relationship may also occur *in vivo*.

MATERIALS AND METHODS

Cell Culture—ARCaP, DU145, PC-3, and LNCaP, which are all established human prostate carcinoma cell lines, were routinely grown in low-glucose Dulbecco's modified Eagle's medium supplemented with 10% fetal bovine serum, 100 units/ml penicillin, and 100 μg/ml streptomycin in a humidified atmosphere containing 5% CO_2 at 37 °C.

Silver Stain and Gelatin Zymography—Purified recombinant MMP-26 (6) or MMP-7 were incubated with purified pro-MMP-9 (17) or pro-MMP-2 (18) in HEPES buffer (50 mM HEPES, pH 7.5, 200 mM NaCl, 10 mM $CaCl_2$, and 0.01% Brij-35) at 37 °C. For the dosage dependence of MMP-9 activation, MMP-9 (0.2 μM, final concentration) was incubated with MMP-7 and MMP-26 at the indicated molar concentration ratio (2:1, 4:1, and 8:1) for 24 h. The MMP-9 activation was quenched by 2× SDS-PAGE sample buffer containing 50 mM EDTA. The resulting solution was further diluted five times and 5 μl of the diluted sample was loaded onto SDS-polyacrylamide gels (8%). For the time dependence of MMP-9 activation, MMP-9 (0.2 μM) was incubated with MMP-7 (0.05 μM) and MMP-26 (0.05 μM) for the indicated time periods (0, 4, 8, 24 and 48 h) before quenching with the sample buffer. For FN cleavage assays, 2 μl of FN (0.25 mg/ml) were incubated with 30 μl of MMP-26 (final concentration 0.05 μM), pro-MMP-9 (final concentration 0.2 μM), or MMP-26-activated MMP-9 solutions in 1× HEPES buffer at 37 °C for 18 h. For silver staining, the reaction was stopped by adding 4× reducing sample buffer (6% SDS, 40% glycerol, 200 mM Tris-HCl, pH 6.8, 5% β-mercaptoethanol, 200 mM EDTA, and 0.08% bromphenol blue) and boiled for 5 min. Following electrophoresis on a 9% SDS-polyacrylamide gel, the protein bands were visualized by silver staining (19). For gelatin zymogram, the gel was incubated for 3 h at 37 °C before it was stained with 0.1% Coomassie Blue solution (17, 20, 21).

Protein N-terminal Sequencing—Samples were separated by SDS-PAGE and transferred to ProBlott™ polyvinylidene difluoride membranes (Applied Biosystems) using CAPS buffer (10 mM CAPS, pH 11, 0.005% SDS). Proteins were visualized by staining with Coomassie Brilliant Blue R-250 solution (0.1% Coomassie Brilliant Blue R-250, 40% methanol, 1% acetic acid) and excised fragments were sent for sequencing. N-terminal sequencing was performed at the Bioanalytical Core Facility, Florida State University.

Reverse Transcriptase-PCR Analysis—RNA was extracted from the original cells by Trizol according to manufacturer protocols (Invitrogen, Carlsbad, CA), and 2 μg of total RNA were subjected to reverse transcriptase-PCR according to the standard protocol provided with the PCR kit (Invitrogen Corp., Carlsbad, CA). The *MMP-26* forward primer was 5′-ACCATGCAGCTCGTCATCTTAAGAG-3′; the reverse primer was 5′-AGGTATGTCAGATGAACATTTTTCTCC-3′; for glyceraldehyde-3-phosphate dehydrogenase the forward primer was 5′-ACGGATTTGGTCGTATTGGG-3′; the reverse primer was 5′-TGATTTTGGAGGGATCTCGC-3′. PCR reactions were performed using a Biometra Personal Cycler (Biometra, Germany) with 30 thermal cycles of 10 s at 94 °C denaturing, 30 s at 60 °C annealing, and 1 min at 72 °C elongation. Ten μl of the amplified PCR products were then electrophoresed on a 1.0% agarose gel containing 0.5 mg/ml ethidium bromide for analysis of size differences. To confirm the amplification of the required cDNA sequences, PCR products were digested with a restriction enzyme as directed by the manufacturer.

Generation and Characterization of Polyclonal Antibodies—Specific antigen peptides corresponding to unique sequences in the pro-domain and metalloproteinase domain of MMP-26 were synthesized by Dr. Umesh Goli at the Biochemical Analysis, Synthesis and Sequencing Services Laboratory of the Department of Chemistry and Biochemistry, Florida State University (Tallahassee, FL). The sequence selected from the pro-domain was Thr^{60}-Gln-Glu-Thr-Gln-Thr-Gln-Leu-Leu-Gln-Gln-Phe-His-Arg-Asn-Gly-Thr-Asp^{67}, and the sequence selected from the metalloproteinase domain was Asp^{188}-Lys-Asn-Glu-His-Trp-Ser-Ala-Ser-Asp-Thr-Gly-Tyr-Asn^{201} of the prepro-enzyme. Using the BLAST search method at the National Center for Biotechnology Information web site against all of the sequences in the data banks, no peptide with >45% level of identity was found (6), predicting the antibodies directed against these two peptides should be specific. The purity of these peptides was verified by reverse-phase high performance liquid chromatography and mass spectrometry. Rabbit anti-human antibodies were then generated, purified, and characterized as described previously (19, 21). Western blot analyses have demonstrated that these two antibodies are highly specific for MMP-26 because they do not cross-react with human matrilysin (MMP-7), stromelysin (MMP-3), gelatinase A (MMP-2), gelatinase B (MMP-9), and some other proteins tested (data not shown).

Western Blotting—Western blotting for MMP-26 was performed by lysing the cells with Tris-buffered saline (50 mM Tris and 150 mM NaCl, pH 7.4) containing 1.5% (v/v) Triton X-114 as described previously (21). Aliquots (20 μl) of cell lysate and media containing equal volumes (20 μl) from each treatment treated with SDS sample buffer were then loaded onto an SDS-polyacrylamide gel. Samples were electrophoresed and then electroblotted onto a nitrocellulose membrane. Immunoreactive MMP-26 bands were visualized using a horseradish peroxidase or alkaline phosphatase-conjugated secondary antibody (Jackson ImmunoResearch, West Grove, PA). Western blot analysis for MMP-9 was performed with a 1 μg/ml dilution of polyclonal anti-MMP-9 antibody (Oncogene Science, Cambridge, MA). MMP-9 bands were visualized using an alkaline phosphatase-conjugated secondary antibody (Jackson ImmunoResearch) followed by the addition of 5-bromo-4-chloro-3-indoyl phosphate and nitro blue tetrazolium. The blot membranes were then scanned, and the signal intensities were measured by integrated morphometry analysis (IMA) (Metamorph System, version 4.6r8, Universal Imaging Corporation, Inc., West Chester, PA). The signal intensities obtained were expressed as integrated optical density (the sum of the optical densities of all pixels that make up the object). All the bands used the same exclusive threshold for analysis.

Immunocytochemistry and Immunohistochemistry—Cells were fixed in 50% methanol, 50% acetone for 15 min and permeated with 1% Triton X-100 in Tris-buffered saline for 15 min. Formalin-fixed paraffin-embedded human prostate cancer tissues were sectioned to 4 μm thickness and fixed on slides. The sections were dewaxed with xylene and rehydrated in 100 and 95% ethanol. Nonspecific antibody binding in cells and sections was blocked with blocking buffer (0.2% Triton X-100, 5% normal goat serum, and 3% bovine serum albumin in Tris-buffered saline) for 1 h at room temperature prior to overnight incubation with affinity-purified specific rabbit anti-human MMP-26 antibody in the same buffer (5 μg/ml for immunocytochemistry and 10 μg/ml for inmmunohistochemistry) or goat anti-human MMP-9 antibody (25 μg/ml for immunohistochemistry, R&D Systems, Minneapolis, MN) at 4 °C. Cells and sections were incubated with alkaline phosphatase-conjugated secondary antibody (Jackson ImmunoResearch) diluted (1:5000) in the blocking buffer for 4 h at room temperature. The signals were detected by adding Fast-Red (Sigma). Purified preimmune IgGs from the same animal were used as negative controls for MMP-26. Normal goat serum was used as a negative control for MMP-9. The sections were counterstained lightly with hematoxylin for viewing negatively stained cells.

Preparation of MMP-26 Constructs—Full-length cDNA of *MMP-26* was amplified by PCR according to published sequences (6) and cloned into modified mammalian expression vector pCR™3.1-Uni with a FLAG tag at its C-terminal as described (22). Following confirmation of cDNA sequencing, plasmids containing correct inserts were used as sense vectors and plasmids with reversibly inserted cDNA were used as antisense vectors (22).

Transfections of ARCaP Cells and Isolation of MMP-26 Sense and Antisense Construct Stably Transfected Clones—ARCaP cells were

Inhibitory Effects of Anti-MMP-26 and Anti-MMP-9 Antibodies on the Invasiveness of ARCaP Cells—To determine the role of MMP-26 and MMP-9 in ARCaP cell invasiveness, antibodies targeting the metalloproteinase domain of MMP-26 and targeting MMP-9 were utilized during *in vitro* cell invasion assays.

[illegible] μg/ml (18.8%) for the MMP-26 antibody (Fig. 4*A*), and at concentrations of 10 (52.2%) and 25 μg/ml (28.0%) for the MMP-9 antibody (Fig. 4*B*), when compared with the preimmune IgG. Antibody targeting the pro-domain of MMP-26 also significantly decreased the invasive potential of ARCaP cells through

transfected with sense and antisense *MMP-26* cDNA-containing vectors using LipofectAMINE 2000 (Invitrogen) as described earlier (22, 23). Sense- and antisense-transfected cell lines were treated identically with regard to transfection conditions and maintenance in the selection

to yield the reduced signal to background ratios used for subsequent comparative analyses by ANOVA. Statistical analysis of all samples was performed with the least significant difference correction of ANOVA

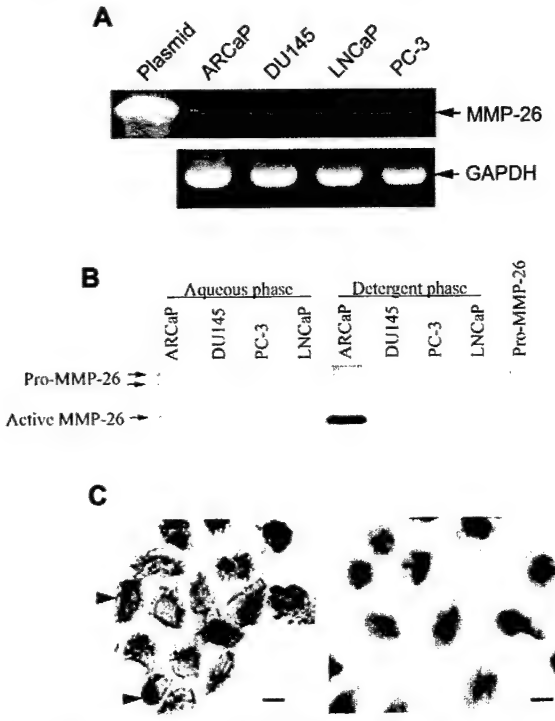

FIG. 3. ***MMP-26* mRNA and protein expression in ARCaP cells.** *A*, reverse transcriptase-PCR analysis of *MMP-26* mRNA in ARCaP, DU145, LNCaP, and PC-3 cell lines. MMP-26 plasmid is used as control (*top panel, lane 1*). The mRNA levels of a glycolysis pathway enzyme, glyceraldehyde-3-phosphate dehydrogenase (*GAPDH*), are shown in the *bottom panel* as a positive control to normalize cellular mRNA concentration. *B*, Western blot analysis of MMP-26 protein in ARCaP, DU145, LNCaP, and PC-3 cell lines. The *last lane* is recombinant pro-MMP-26 as a control. *C*, immunocytochemistry localization of MMP-26 in ARCaP cells. *Left panel*, the primary antibody is rabbit anti-MMP-26 antibody; *right panel*, the primary antibody is preimmune IgG from the same rabbit. *Red* staining indicates MMP-26 expression. *Scale bars* = 12 μm. *Arrows* show the positive staining signals. The cells were counterstained with hematoxylin for viewing of negatively stained cells (*purple*).

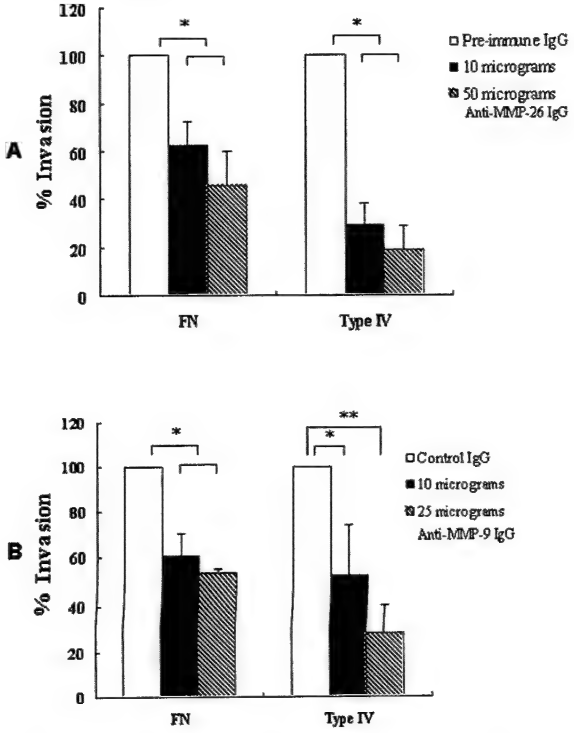

FIG. 4. **Blocking of ARCaP cell invasion through FN and type IV collagen by MMP-26 and MMP-9 antibodies.** The invasion assay was performed with modified Boyden chambers. The MMP-26 antibody is a rabbit anti-human MMP-26 metallo-domain antibody. The MMP-9 antibody is a mouse anti-human MMP-9 monoclonal antibody. The percentage of invading cells was quantified as described under "Materials and Methods." *A*, comparison of the invaded cell number in the presence of MMP-26 antibody/preimmune IgG. *Control*, preimmune rabbit IgG and the final concentration is 50 μg/ml. Ten and 50 μg of IgG means the final concentrations are 10 and 50 μg/ml, respectively. *B*, comparison of the invaded cell number in the presence of MMP-9 antibody/preimmune IgG. *Control*, preimmune mouse IgG and the concentration is 25 μg/ml. Ten and 25 μg of IgG means that the concentrations are 10 and 25 μg/ml, respectively. The invaded cell numbers of the preimmune IgG treatment were used as the 100% invasiveness. *Type IV*, type IV collagen. Data shown are the mean ± S.D. values from four separate experiments for each group. *, $p < 0.01$; **, $p < 0.001$.

FN and type IV collagen (data not shown). These results show that both anti-MMP-26 and anti-MMP-9 antibodies significantly inhibit ARCaP cell invasion through FN and type IV collagen.

MMP-26 Protein Expression in Stable Transfectants by Immunocytochemistry and Western Blotting—To further confirm the role of MMP-26 in ARCaP cell invasion, we transfected pCR 3.1 vectors containing full-length *MMP-26* cDNA in both sense and antisense orientations into ARCaP cells. Immunocytochemistry and Western blotting were performed to determine MMP-26 protein expression levels in the parental cells in addition to the sense and antisense *MMP-26* construct-transfected cells. Immunocytochemistry showed very strong MMP-26 staining in both the parental ARCaP and sense *MMP-26* construct-transfected cells, whereas the antisense *MMP-26* construct-transfected cells exhibited only minimal staining for MMP-26 (Fig. 5*A*). Western blotting revealed strong MMP-26 bands in the parental ARCaP and sense *MMP-26* construct-transfected cells, whereas only a very faint band was detected in the antisense *MMP-26* construct-transfected cells. No MMP-26 was detected in the cell culture media (Fig. 5*B*).

Reduction of Invasiveness of MMP-26 Antisense Stable Transfectants—Both the parental ARCaP and sense *MMP-26* construct-transfected cell lines invaded through either FN or type IV collagen *in vitro* during cell invasion assays (Fig. 6*A*), but without a marked difference ($p > 0.05$) in their invasive potentials (Fig. 6*B*). Antisense *MMP-26* construct-transfected cells showed a significant ($p < 0.01$) decrease in invasive potential through the same materials (44.0 and 23.5%, respectively) when compared with parental ARCaP cells (Fig. 6, *A* and *B*). A significant ($p < 0.01$) difference between the sense and antisense *MMP-26* construct-transfected cells was also noted (Fig. 6, *A* and *B*).

Reduced Levels of Active MMP-9 in MMP-26 Antisense Stably Transfected Cells—To determine the role of MMP-26-mediated MMP-9 activation in ARCaP cell invasion, the level of MMP-9 in conditioned media samples collected from the Boyden chambers during *in vitro* cell invasion assays was detected. Western blotting revealed a strong 86-kDa band of active MMP-9 in the conditioned media from parental ARCaP and sense *MMP-26* construct-transfected cells. A similar band, but of weaker intensity, was detected in the conditioned media collected from the antisense *MMP-26* construct-transfected cells (Fig. 7*A*). Semiquantitative analysis revealed that the active form of MMP-9 was significantly decreased ($p < 0.01$) in both the FN and type IV collagen invasive assay media from the antisense *MMP-26* construct-transfected cells (Fig. 7*B*).

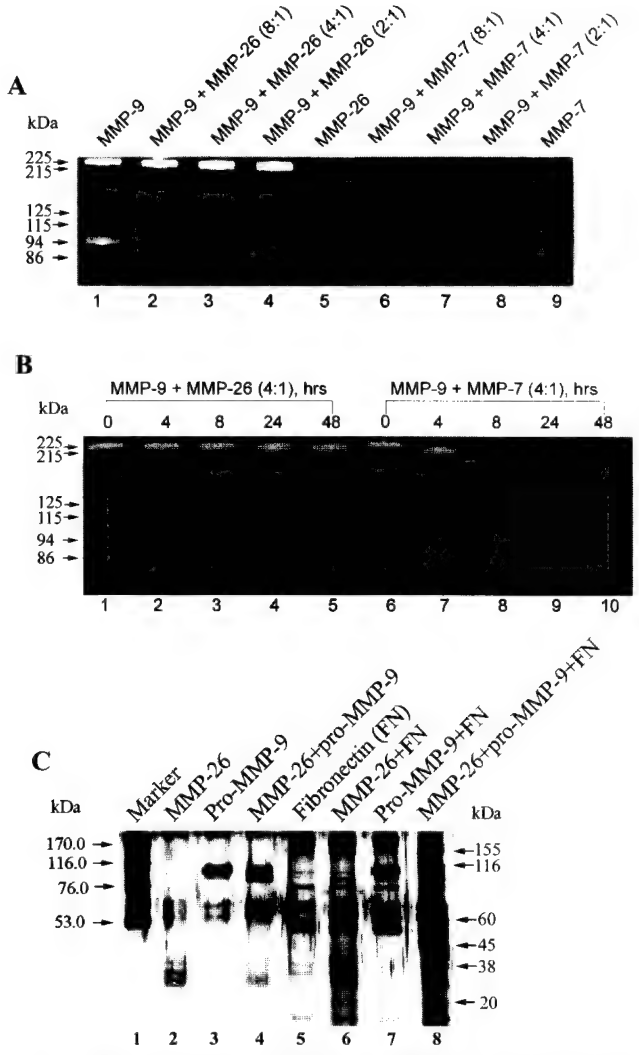

FIG. 1. **Activation of pro-MMP-9 by MMP-26.** *A* and *B*, gelatin zymogram of MMP-9 activity before and after activation of pro-MMP-9 by MMP-26 under non-reducing conditions. The 225-kDa band is a homodimer of pro-MMP-9, the 125-kDa band is a heterodimer of pro-MMP-9 and neutrophil gelatinase-associated lipocalin, and the 94-kDa band is a monomer of pro-MMP-9 (17, 26, 27). The activation reactions were incubated at 37 °C. *A*, dose-dependent analysis of pro-MMP-9 activation by MMP-26 (*lanes 1–4*) and MMP-7 (*lanes 6–8*). The activation reaction was incubated 37 °C for 24 h. The gelatin zymogram reaction was incubated at 37 °C for 3 h. The 86-kDa band was sequenced and the sequence is MRTPRXG, which is a product cleaved at the Ala^{93}–Met^{94} site. *B*, time-dependent analysis of pro-MMP-9 activation by MMP-26 (*lanes 1–5*) and MMP-7 (*lanes 6–10*). The gelatin zymogram reaction was incubated at 37 °C for 3 h. The ratio labeled in *A* and *B* is the molar concentration ratio. *C*, pro-MMP-9 activated by MMP-26 and cleavage of FN by MMP-26 and MMP-9 as detected by a silver-stained gel under reducing conditions. The molar concentration ratio for pro-MMP-9:MMP-26 is 4:1 and the reaction was incubated at 37 °C for 24 h. The molecular mass standards are labeled on the *left* and the estimated molecular masses of the FN cleavage products are labeled on the *right*.

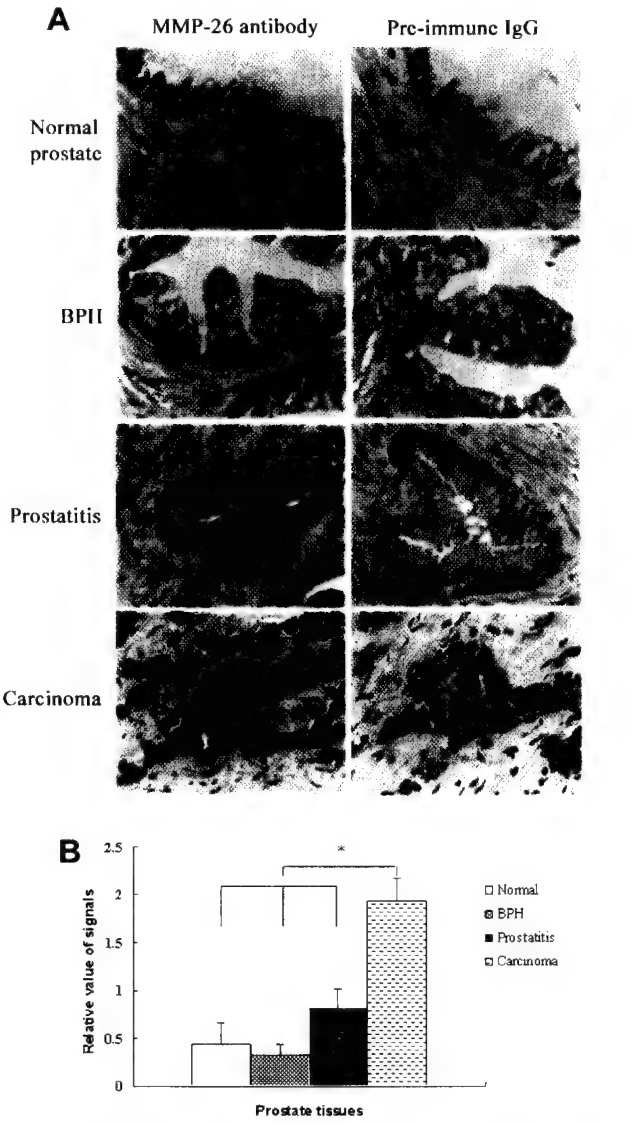

FIG. 2. **Comparison of MMP-26 expression in human normal and pathological prostate tissues.** *A*, immunohistochemistry and localization of MMP-26 in human prostate carcinoma (15 patient cases), prostatitis (9 cases), benign prostate hyperplasia (12 cases), and normal prostate gland tissues (7 cases). Cells stained *red* indicate MMP-26 expression. Photographs were taken under a microscope with ×400 magnification. *B*, densitometric analysis of MMP-26 expression in human prostate tissues. The quantification analysis was described under "Materials and Methods." Four pictures were taken from each sample with ×200 magnification. The epithelial regions were selected and the staining area and total selected area were obtained by IMA and analyzed by one-way ANOVA with LSD correction. Data shown are the mean ± S.D. values from the different prostate tissues. *, $p < 0.01$. *BPH*, benign prostate hyperplasia; *Normal*, normal prostate tissue; *Carcinoma*, prostate adenocarcinoma.

not detected in the DU145, LNCaP, or PC-3 cell lines (Fig. 3*B*), or in the ARCaP media under these experimental conditions (data not shown). Immunocytochemistry data confirmed that MMP-26 was localized inside the ARCaP cells (Fig. 3*C*) in a polarized manner.

Inhibitory Effects of Anti-MMP-26 and Anti-MMP-9 Antibodies on the Invasiveness of ARCaP Cells—To determine the role of MMP-26 and MMP-9 in ARCaP cell invasiveness, antibodies targeting the metalloproteinase domain of MMP-26 and targeting MMP-9 were utilized during *in vitro* cell invasion assays. We found significant ($p < 0.01$) reduction in the invasive potential of ARCaP cells through FN at concentrations of 10 (62.4%) and 50 μg/ml (46.0%) for the MMP-26 antibody (Fig. 4*A*), and at concentrations of 10 (55.9%) and 25 μg/ml (53.1%) for the MMP-9 antibody (Fig. 4*B*), when compared with the preimmune IgGs. We also found significantly ($p < 0.01$) reduced invasive potential in the movement of ARCaP cells through type IV collagen at concentrations of 10 (29.3%) and 50 μg/ml (18.8%) for the MMP-26 antibody (Fig. 4*A*), and at concentrations of 10 (52.2%) and 25 μg/ml (28.0%) for the MMP-9 antibody (Fig. 4*B*), when compared with the preimmune IgG. Antibody targeting the pro-domain of MMP-26 also significantly decreased the invasive potential of ARCaP cells through

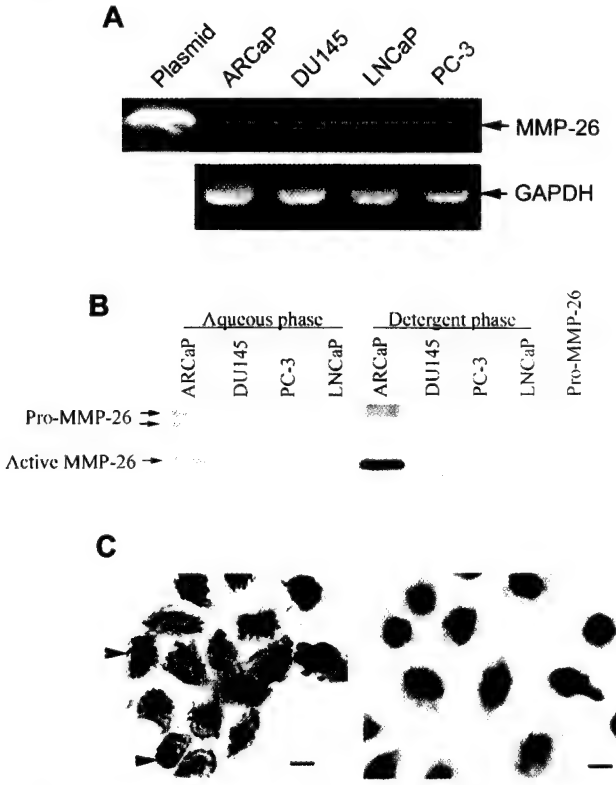

FIG. 3. ***MMP-26* mRNA and protein expression in ARCaP cells.** *A*, reverse transcriptase-PCR analysis of *MMP-26* mRNA in ARCaP, DU145, LNCaP, and PC-3 cell lines. MMP-26 plasmid is used as control (*top panel*, *lane 1*). The mRNA levels of a glycolysis pathway enzyme, glyceraldehyde-3-phosphate dehydrogenase (*GAPDH*), are shown in the *bottom panel* as a positive control to normalize cellular mRNA concentration. *B*, Western blot analysis of MMP-26 protein in ARCaP, DU145, LNCaP, and PC-3 cell lines. The *last lane* is recombinant pro-MMP-26 as a control. *C*, immunocytochemistry localization of MMP-26 in ARCaP cells. *Left panel*, the primary antibody is rabbit anti-MMP-26 antibody; *right panel*, the primary antibody is preimmune IgG from the same rabbit. *Red* staining indicates MMP-26 expression. *Scale bars* = 12 μm. *Arrows* show the positive staining signals. The cells were counterstained with hematoxylin for viewing of negatively stained cells (*purple*).

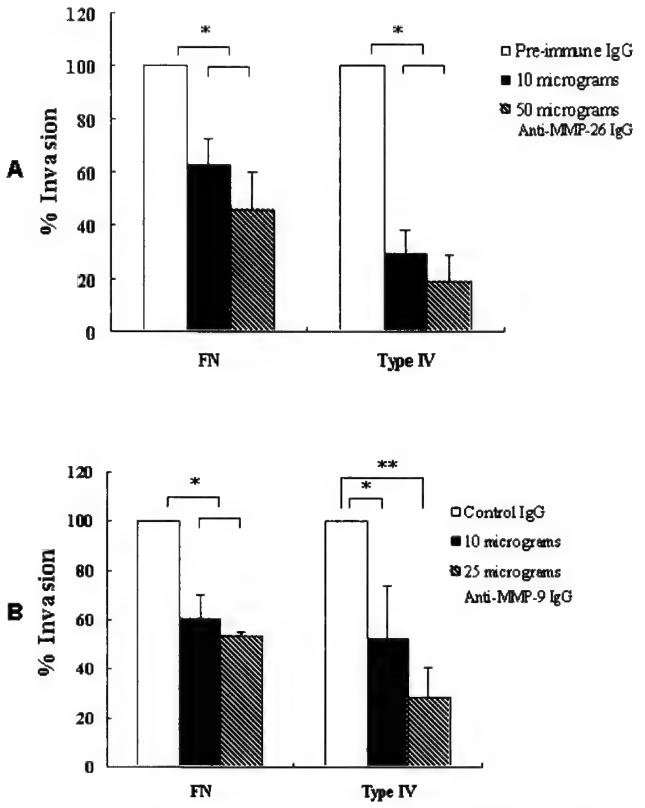

FIG. 4. **Blocking of ARCaP cell invasion through FN and type IV collagen by MMP-26 and MMP-9 antibodies.** The invasion assay was performed with modified Boyden chambers. The MMP-26 antibody is a rabbit anti-human MMP-26 metallo-domain antibody. The MMP-9 antibody is a mouse anti-human MMP-9 monoclonal antibody. The percentage of invading cells was quantified as described under "Materials and Methods." *A*, comparison of the invaded cell number in the presence of MMP-26 antibody/preimmune IgG. *Control*, preimmune rabbit IgG and the final concentration is 50 μg/ml. Ten and 50 μg of IgG means the final concentrations are 10 and 50 μg/ml, respectively. *B*, comparison of the invaded cell number in the presence of MMP-9 antibody/preimmune IgG. *Control*, preimmune mouse IgG and the concentration is 25 μg/ml. Ten and 25 μg of IgG means that the concentrations are 10 and 25 μg/ml, respectively. The invaded cell numbers of the preimmune IgG treatment were used as the 100% invasiveness. *Type IV*, type IV collagen. Data shown are the mean ± S.D. values from four separate experiments for each group. *, $p < 0.01$; **, $p < 0.001$.

FN and type IV collagen (data not shown). These results show that both anti-MMP-26 and anti-MMP-9 antibodies significantly inhibit ARCaP cell invasion through FN and type IV collagen.

MMP-26 Protein Expression in Stable Transfectants by Immunocytochemistry and Western Blotting—To further confirm the role of MMP-26 in ARCaP cell invasion, we transfected pCR 3.1 vectors containing full-length *MMP-26* cDNA in both sense and antisense orientations into ARCaP cells. Immunocytochemistry and Western blotting were performed to determine MMP-26 protein expression levels in the parental cells in addition to the sense and antisense *MMP-26* construct-transfected cells. Immunocytochemistry showed very strong MMP-26 staining in both the parental ARCaP and sense *MMP-26* construct-transfected cells, whereas the antisense *MMP-26* construct-transfected cells exhibited only minimal staining for MMP-26 (Fig. 5*A*). Western blotting revealed strong MMP-26 bands in the parental ARCaP and sense *MMP-26* construct-transfected cells, whereas only a very faint band was detected in the antisense *MMP-26* construct-transfected cells. No MMP-26 was detected in the cell culture media (Fig. 5*B*).

Reduction of Invasiveness of MMP-26 Antisense Stable Transfectants—Both the parental ARCaP and sense *MMP-26* construct-transfected cell lines invaded through either FN or type IV collagen *in vitro* during cell invasion assays (Fig. 6*A*), but without a marked difference ($p > 0.05$) in their invasive potentials (Fig. 6*B*). Antisense *MMP-26* construct-transfected cells showed a significant ($p < 0.01$) decrease in invasive potential through the same materials (44.0 and 23.5%, respectively) when compared with parental ARCaP cells (Fig. 6, *A* and *B*). A significant ($p < 0.01$) difference between the sense and antisense *MMP-26* construct-transfected cells was also noted (Fig. 6, *A* and *B*).

Reduced Levels of Active MMP-9 in MMP-26 Antisense Stably Transfected Cells—To determine the role of MMP-26-mediated MMP-9 activation in ARCaP cell invasion, the level of MMP-9 in conditioned media samples collected from the Boyden chambers during *in vitro* cell invasion assays was detected. Western blotting revealed a strong 86-kDa band of active MMP-9 in the conditioned media from parental ARCaP and sense *MMP-26* construct-transfected cells. A similar band, but of weaker intensity, was detected in the conditioned media collected from the antisense *MMP-26* construct-transfected cells (Fig. 7*A*). Semiquantitative analysis revealed that the active form of MMP-9 was significantly decreased ($p < 0.01$) in both the FN and type IV collagen invasive assay media from the antisense *MMP-26* construct-transfected cells (Fig. 7*B*).

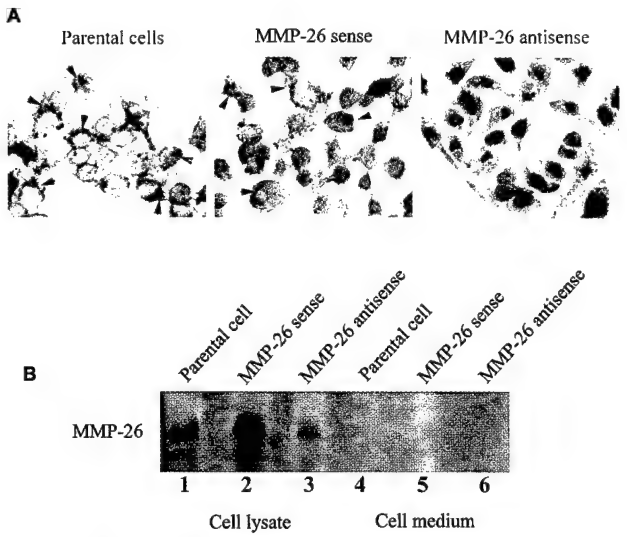

FIG. 5. **MMP-26 protein expression in parental ARCaP, sense *MMP-26* construct, and antisense *MMP-26* construct stably transfected cells.** *A*, immunocytochemistry of MMP-26 expression in parental ARCaP, sense *MMP-26* construct, and antisense *MMP-26* construct stably transfected cells. *Red* staining indicates MMP-26 expression. *Arrows* show examples of the positive staining signals. The cells were counterstained with hematoxylin for viewing of MMP-26 negative cells (*purple*). *B*, Western blot analysis of MMP-26 protein expression. Parental ARCaP, sense *MMP-26* construct, and antisense *MMP-26* construct stably transfected cells were cultured utilizing an equivalent number of cells. Conditioned medium samples were collected prior to cell lysis.

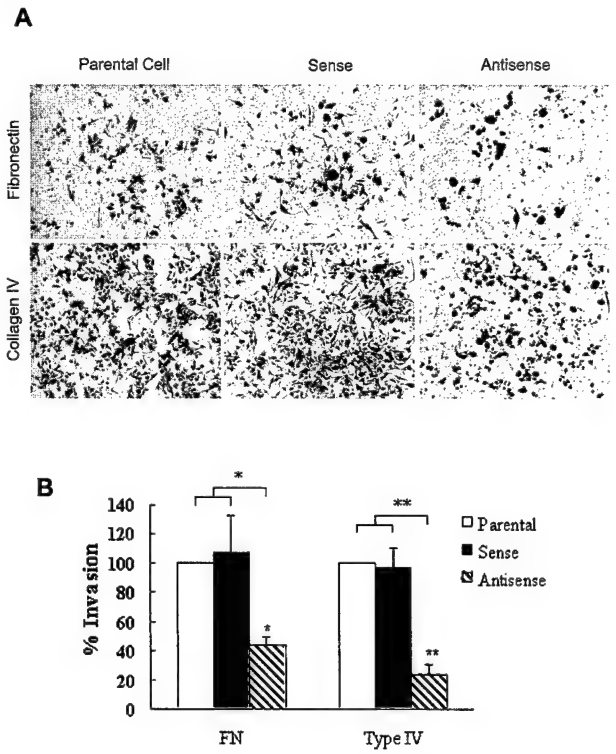

FIG. 6. **Invasion of parental ARCaP, sense, or antisense *MMP-26* construct stably transfected cells through FN and type IV collagen.** *A*, cells that invaded to the lower surface of the membrane were photographed under a microscope with ×40 magnification. *B*, the percentage of invading cells in parental and *MMP-26* sense or antisense construct stably transfected ARCaP cells. The cell numbers of the invaded parental cells were used as 100% invasiveness. The cells were counted and analyzed as described under "Materials and Methods." Data shown are the mean ± S.D. values from three separate experiments for each group. *, $p < 0.01$; **, $p < 0.001$.

Co-localization of MMP-26 with MMP-9 in Parental and MMP-26 Sense Gene Stably Transfected ARCaP Cells, and Co-expression of MMP-26 and MMP-9 in Human Prostate Carcinoma Tissue Samples—Double immunofluorescence experiments were performed in parental ARCaP and *MMP-26* stably transfected cells with human *MMP-26* sense or antisense genes. The red color indicates MMP-26 and the green color indicates MMP-9 protein staining. Merged images show a color shift to orange-yellow, indicating co-localization between MMP-26 and MMP-9. Confocal laser scanning microscopic analysis revealed co-localization of both proteins in the cytoplasm of parental ARCaP (Fig. 8*A*, *a–d*) and sense-transfected cells (Fig. 8*A*, *e–h*), but not in the antisense-transfected cells (Fig. 8*A*, *i–l*). Very weak signals were detected in parental ARCaP control cells using purified preimmune IgG for the detection of MMP-26 and nonimmune goat sera for the detection of MMP-9 (Fig. 8*A*, *m–p*). MMP-26 and MMP-9 proteins were also found to be co-expressed in human prostate carcinoma tissue samples (Fig. 8*B*).

DISCUSSION

MMP-26 is able to activate MMP-9 by cleavage at the Ala^{93}–Met^{94} site of the prepro-MMP-9, which is the same cleavage site detected previously during activation with $HgCl_2$ (28), human fibroblast-type collagenase (17), phenylmercuric acid (29), and aminophenylmercuric acid (30). This activation was confirmed by the effective cleavage of FN using MMP-9 activated by MMP-26. These results indicate that the zymogen form of MMP-9 can be transiently activated without the proteolytic loss of the cysteine (Cys^{99})-switch residue, even though these findings may appear to be in conflict with the original Cys-switch hypothesis (31). The 86-kDa form of MMP-9 may also be further activated to produce lower molecular mass active species similar to the process activated by other MMPs (17). Among all the MMPs, matrilysin (MMP-7) and MMP-26 share domain structures with pro- and metalloproteinase domains only and are both expressed in epithelial cells (6–9). Therefore, MMP-26 is also named as matrilysin-2 (8). Both MMP-26 and MMP-7 could activate MMP-9 but their cleavage sites in pro-MMP-9 are different. Matrilysin cleaved MMP-9 at two sites, Glu^{59}–Met^{60} and Arg^{106}–Phe^{107} of the prepro-MMP-9 (17). Our current results also demonstrated that the MMP-9 activation mediated by MMP-26 is much slower than that mediated by MMP-7, but the activation products are much more stable when compared with the products of activation by MMP-7. This indicates that activation of MMP-9 by MMP-26 is prolonged but persistent, which is consistent with the process of tumor cell invasion. MMP-26 did not cleave pro-MMP-2, another gelatinase, indicating that pro-MMP-9 activation by MMP-26 is highly selective. MMP-9 is a powerful enzyme, and is considered to be an important contributor to the processes of invasion, metastasis, and angiogenesis in various tumors (11–14, 32–36).

This work has tested the hypothesis that MMP-26 may enhance human prostate cancer cell invasion via the activation of pro-MMP-9 using an ARCaP cell line as a working model. The ARCaP cell line is a highly invasive and metastatic human prostate cancer cell line that expresses both MMP-9 (15) and MMP-26. We found that *MMP-26* mRNA was detected in the ARCaP cell line and two other human prostate carcinoma cell lines, DU145 and LNCaP, but the MMP-26 protein was only detected in ARCaP cells. More importantly, high levels of MMP-26 protein were also detected in human prostate carcinoma cells by immunohistochemistry, but only low expression was seen in prostatitis, benign prostate hyperplasia, and normal prostate tissues. This is in agreement with reports of

33. Li, Y., and Sarkar, F. H. (2002) *Cancer Lett.* **186,** 157–164
34. Mase, K., Iijima, T., Nakamura, N., Takeuchi, T., Onizuka, M., Mitsui, T., and Noguchi, M. (2002) *Lung Cancer* **36,** 271–276
35. Singer, C. F., Kronsteiner, N., Marton, E., Kubista, M., Cullen, K. J., Hirtenlehner, K., Seifert, M., and Kubista, E. (2002) *Breast Cancer Res. Treat.* **72,** 69–77
36. Nemeth, J. A., Yousif, R., Herzog, M., Che, M., Upadhyay, J., Shekarriz, B., Bhagat, S., Mullins, C., Fridman, R., and Cher, M. L. (2002) *J. Natl. Cancer Inst.* **94,** 17–25
37. Park, H. I., Turk, B. E., Gerkema, F. E., Cantley, L. C., and Sang, Q.-X. (2002) *J. Biol. Chem.* **277,** 35168–35175
38. Seftor, R. E., Seftor, E. A., Koshikawa, N., Meltzer, P. S., Gardner, L. M., Bilban, M., Stetler-Stevenson, W. G., Quaranta, V., and Hendrix, M. J. (2001) *Cancer Res.* **61,** 6322–6327
39. Marchenko, N. D., Marchenko, G. N., and Strongin, A. Y. (2002) *J. Biol. Chem.* **277,** 18967–18972
40. Nguyen, M., Arkell, J., and Jackson, C. J. (1998) *J. Biol. Chem.* **273,** 5400–5404

THE JOURNAL OF BIOLOGICAL CHEMISTRY

Vol. 278, No. 51, Issue of December 19, pp. 51646–51653, 2003
Printed in U.S.A.

The Intermediate S_1' Pocket of the Endometase/Matrilysin-2 Active Site Revealed by Enzyme Inhibition Kinetic Studies, Protein Sequence Analyses, and Homology Modeling*

Received for publication, September 11, 2003
Published, JBC Papers in Press, October 7, 2003, DOI 10.1074/jbc.M310109200

Hyun I. Park, Yonghao Jin, Douglas R. Hurst, Cyrus A. Monroe, Seakwoo Lee, Martin A. Schwartz, and Qing-Xiang Amy Sang‡

From the Department of Chemistry and Biochemistry and Institute of Molecular Biophysics, Florida State University, Tallahassee, Florida 32306-4390

Human matrix metalloproteinase-26 (MMP-26/endometase/matrilysin-2) is a newly identified MMP and its structure has not been reported. The enzyme active site S_1' pocket in MMPs is a well defined substrate P_1' amino acid residue-binding site with variable depth. To explore MMP-26 active site structure-activity, a series of new potent mercaptosulfide MMP inhibitors (MMPIs) with Leu or homophenylalanine (Homophe) side chains at the P_1' site were selected. The Homephe side chain is designed to probe deep S_1' pocket MMPs. These inhibitors were tested against MMP-26 and several MMPs with known x-ray crystal structures to distinguish shallow, intermediate, and deep S_1' pocket characteristics. MMP-26 has an inhibition profile most similar to those of MMPs with intermediate S_1' pockets. Investigations with hydroxamate MMPIs, including those designed for deep pocket MMPs, also indicated the presence of an intermediate pocket. Protein sequence analysis and homology modeling further verified that MMP-26 has an intermediate S_1' pocket formed by Leu-204, His-208, and Tyr-230. Moreover, residue 233 may influence the depth of an MMP S_1' pocket. The residue at the equivalent position of MMP-26 residue 233 is hydrophilic in intermediate-pocket MMPs (*e.g.* MMP-2, -8, and -9) and hydrophobic in deep-pocket MMPs (*e.g.* MMP-3, -12, and -14). MMP-26 contains a His-233 that renders the S_1' pocket to an intermediate size. This study suggests that MMPIs, protein sequence analyses, and molecular modeling are useful tools to understand structure-activity relationships and provides new insight for rational inhibitor design that may distinguish MMPs with deep *versus* intermediate S_1' pockets.

Matrix metalloproteinases (MMPs,[1] matrixins) are believed to participate in angiogenesis, embryonic development, morphogenesis, reproduction, tissue resorption and remodeling, and tumor growth, progression, invasion, and metastasis through breakdown of the extracellular matrix, cell surface proteins, and processing growth factors, cytokines, and chemokines (1–3). Recently, human MMP-26 (endometase/matrilysin 2) was identified and its mRNA expression was detected in normal tissues of the human uterus and placenta, and in many types of malignant tumors (4–7). Characterization of the MMP-26 promoter suggests that this proteinase may be expressed in cancer cells of epithelial origin (8). MMP-26 may play an important role in human prostate and breast cancer invasion (9–10).

MMP-26 cleaves type I gelatin, α_1-proteinase inhibitor, fibrinogen, fibronectin, vitronectin, type IV collagen, and insulin-like growth factor binding protein-1 (4, 7, 11). Studies of MMP-26 indicate that it has substrate specificity similar to other MMPs, with the exception of a preference for Ile at the P_2 and P_2' positions, for small residues at the P_3' and P_4' positions, and Lys at the P_4 position (11). MMP-26 also hydrolyzes several synthetic fluorogenic peptide substrates designed for stromelysin-1, gelatinases, collagenases, and tumor necrosis factor-α converting enzyme (4, 11). According to these peptide substrate studies, MMP-26 may be capable of cleaving a broad range of substrates, although it has less catalytic efficiency than other MMPs.

X-ray crystal structures of MMPs illustrate that overall topology and secondary structures are conserved (12–18). The S_1' pocket, a hydrophobic pocket of variable depth, is a well defined substrate P_1'-binding site in MMPs. Three types of S_1' pockets can be distinguished from the available structures of MMPs (19–20). One type is a shallow pocket, as found in MMP-1 (human fibroblast collagenase; 13) and MMP-7 (matrilysin; 16), where the pockets are limited by the side chains of Arg and Tyr, respectively, crossing the pockets. Many of the structurally known MMPs possess Leu at the corresponding site, and its side chain forms the top of the pocket rather than crossing the pocket. These Leu-containing MMPs may be further classified as deep and intermediate S_1' pocket MMPs. A deep, tunnel-like pocket is found in MMP-3 (stromelysin-1; 12), MMP-12 (metalloelastase; 17), and MMP-14 (MT1-MMP; 21), whereas MMP-2 (gelatinase A; 22), MMP-8 (human neutrophil collagenase; 15), and MMP-9 (gelatinase B; 23) possess an intermedi-

* This work was supported by Department of Defense/U. S. Army Prostate Cancer Research Program Grant DAMD17-02-1-0238, National Institutes of Health Grant CA78646, the American Cancer Society, Florida Division F01FSU-1, and the Florida State University Research Foundation (to Q.-X. A. S.), a grant from the Molecular Design and Synthesis (MDS) Research Foundation (to M. A. S.), National Science Foundation Postdoctoral Training Grant DBI 9602233 (to H. I. P.), Department of Defense/U. S. Army Breast Cancer Research Program Predoctoral Fellowship DAMD17-00-1-0243 (to D. R. H.), and a Pfizer Summer Undergraduate Student Research Fellowship (to C. A. M.). The costs of publication of this article were defrayed in part by the payment of page charges. This article must therefore be hereby marked "*advertisement*" in accordance with 18 U.S.C. Section 1734 solely to indicate this fact.

‡ To whom correspondence should be addressed: Dept. of Chemistry and Biochemistry, Florida State University, Chemistry Research Bldg. DLC, Rm. 203, Tallahassee, FL 32306-4390. Tel.: 850-644-8683; Fax: 850-644-8281; E-mail: sang@chem.fsu.edu.

[1] The abbreviations used are: MMP, matrix metalloproteinase; Boc, *tert*-butoxycarbonyl; Brij-35, polyoxyethylene lauryl ether; Homophe, homophenylalanine; Mca, (7-methoxycoumarin-4-yl)acetyl; Dpa, *N*-3-(2,4-dinitrophenyl)-2,3-diaminopropionyl; MMPI, matrix metalloproteinase inhibitor.

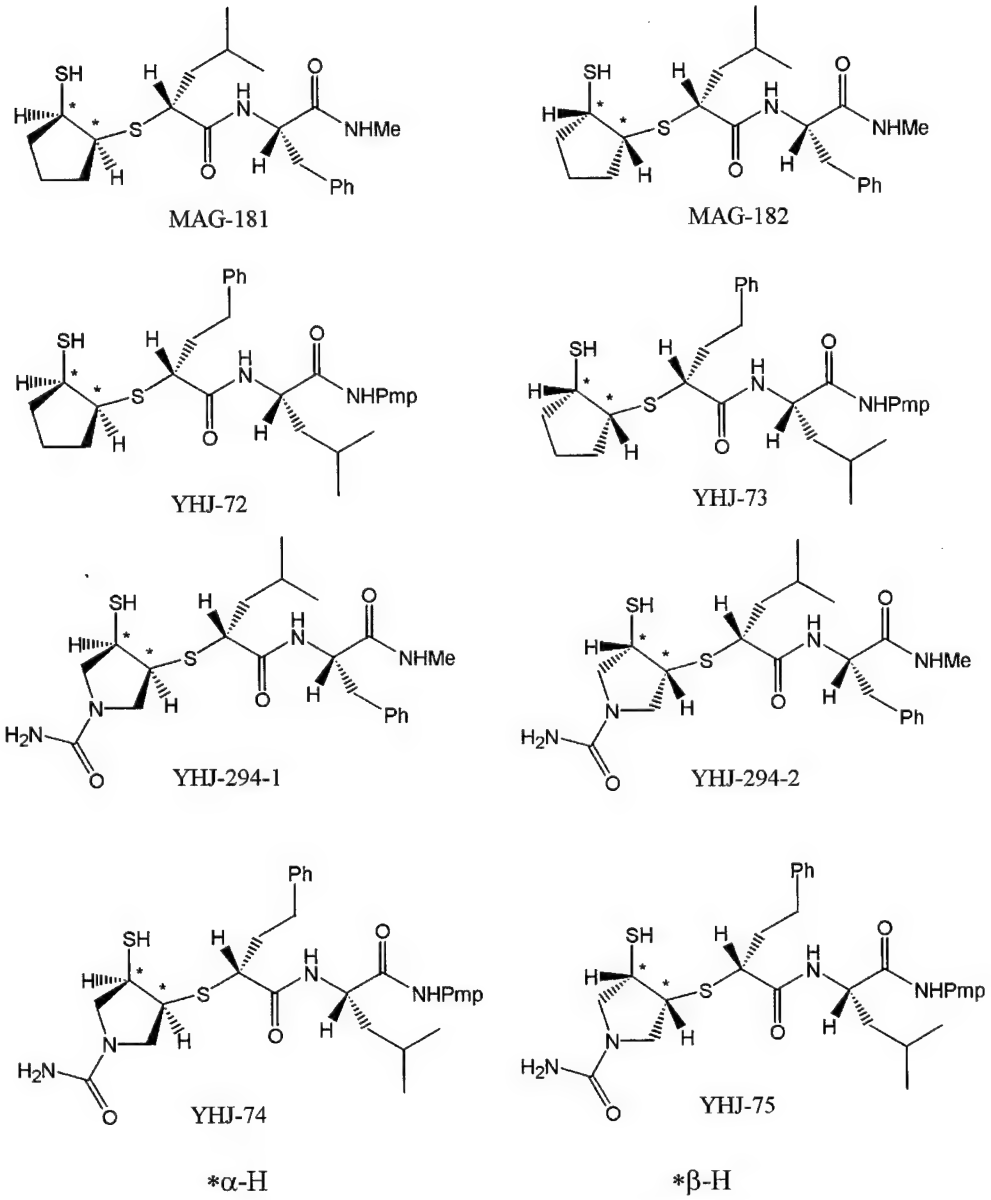

Abbreviations: Me, Methyl; Ph, Phenyl; Pmp, *p*-methoxyphenyl.

FIG. 1. **Structures of new mercaptosulfide MMP inhibitors.** The diastereomer notation in the ring system is started from the α carbon of the mercapto group.

TABLE I
Inhibition of human MMPs by mercaptosulfide MMP inhibitors

Inhibitor	K_i^{app}								
	Shallow		Deep			Intermediate			
	MMP-1	MMP-7	MMP-3	MMP-12	MMP-14	MMP-2	MMP-8	MMP-9	MMP-26
	nM			*nM*				*nM*	
MAG-181	680	710	2500	1,300	259	85	4.1	44	81
MAG-182	49	40	470	130	24	1.1	0.89	0.57	17
YHJ-72	$>12 \times 10^3$	5,500	150	130	380	930	530	180	160
YHJ-73	$>12 \times 10^3$	1,000	100	13	16	20	70	8.6	28
YHJ-294–1	5,200	3,500	$>40 \times 10^3$	16,000	3,000	430	130	550	450
YHJ-294–2	100	26	360	93	13	6.1	1.2	1.2	2.8
YHJ-74		3600	270	117	20	88	300	220	82
YHJ-75	2400	300	21	5.6	3.7	6.9	44	3.0	8.6

ate-sized pocket, which is neither deep nor shallow. An enzyme with a shallow pocket prefers large, aliphatic residues in the P_1' position, such as Leu and Met (24–25). The remainder of the MMPs can accommodate larger amino acid derivatives, such as homophenylalanine, in the P_1' position (26).

MMP-26, composed of 261 amino acid residues and lacking a hemopexin-like domain, represents the smallest member of the MMP family. The primary structure of MMP-26 can be divided into three regions that include a signal peptide, a propeptide domain, and a catalytic domain. MMP-26 identification, ex-

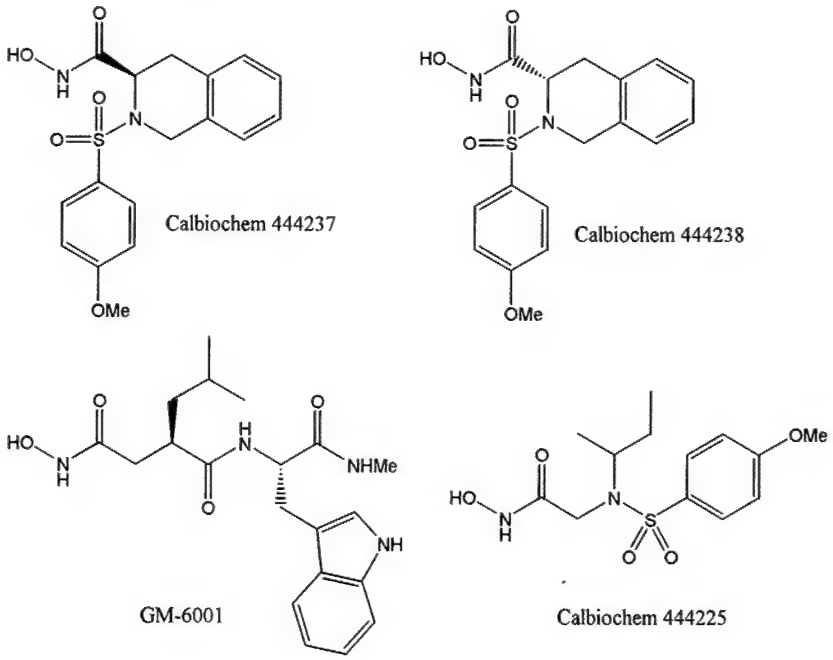

FIG. 2. **Structures of commercially available hydroxamate MMP inhibitors.** Calbiochem 444237, 444238, and 444225 are three known inhibitors of deep S_1' pocket MMPs.

TABLE II
Inhibition of MMP-26, MMP-7, and MMP-12 by hydroxamate MMP inhibitors

Inhibitor	K_i^{app}		
	MMP-26	MMP-7	MMP-12
		nM	
GM6001	0.36[a]	3.7	3.6
444237	1.5[a]	225	0.20
444238	60[a]	5.7×10^3	36
444225	43	2100	3.4

[a] Values from Ref. 11.

Shallow S_1' Pocket MMPs

```
      203                                          235
MMP-1   HRVAAHELGH SLGLSHSTDI GALMYPSYTFSGD
MMP-7   LYAATHELGH SLGMGHSSDP NAVMYPTYGNGDP
```

Deep S_1' Pocket MMPs

```
MMP-3   FLVAAHEIGH SLGLFHSANT EALMYPLYHSLTD
MMP-12  FLTAVHEIGH SLGLGHSSDP KAVMFPTYKYVDI
MMP-14  FLVAVHELGH ALGLEHSSDP SAIMAPFYQWMDT
```

Intermediate S_1' Pocket MMPs

```
MMP-2   FLVAAHEFGH AMGLEHSQDP GALMAPIYTYTKN
MMP-8   FLVAAHEFGH SLGLAHSSDP GALMYPNYAFRET
MMP-9   FLVAAHEFGH ALGLDHSSVP EALMYPMYRFTEG
MMP-26  FLVATHEIGH SLGLQHSGNQ SSIMYPTYWYHDP
```

FIG. 3. **The sequence alignment of eight MMPs.** The alignment was determined using the Genetic Computer Group (Wisconsin Package, version 10, Madison, WI, 2002) program PILEUP with a default gap weight of 8 and a gap length weight of 2 based on the full protein sequences without propeptide regions. *Boldface* amino acid residues form the S_1' pocket. *Italicized* sequences are metal binding consensus sequences. *Underlined* residues may determine S_1' pocket characteristics. To align MMP-2 and MMP-9, the 183-residue insert of fibronectin type II-like modules were deleted before the alignment. The residue numbering system is based on the sequence of MMP-26 (4).

pression, and substrate specificity have been explored by several groups (4–11). However, the S_1' pocket characteristics of MMP-26 are unknown because of the absence of an MMP-26 x-ray crystallographic structure. Therefore, in this study we have utilized previously characterized and newly developed mercaptosulfide MMPIs (27–29) together with protein sequence analyses and molecular modeling to understand the S_1' pocket characteristics of MMP-26.

EXPERIMENTAL PROCEDURES

Materials—The fluorescent peptide substrates for MMPs used in this study were purchased from Bachem Chemical Co. The metal salts and Brij-35 were purchased from Fisher Scientific Inc. The hydroxamate MMPIs 444237, 444238, 444225, and GM6001 were purchased from Calbiochem. All other chemicals were purchased from Sigma.

The mercaptosulfide inhibitors were prepared and characterized as previously described (27–29). *cis*-1-Acetylthio-2-*tert*-butoxycarbonylthiocyclopentane and *cis*-3-acetylthio-4-*tert*-butoxycarbonylthio-*N*-*tert*-butoxycarbonylpyrrolidine were synthesized (29) and *S*-alkylated with (2*S*)-2-bromo-4-methylpentanoic acid or (2*S*)-2-bromo-4-phenylbutanoic acid; the latter bromoacids were derived from L-leucine and L-homophenylalanine, respectively (27). Subsequent coupling with L-PheNHMe or L-leucine-*p*-methoxyanilide (27) afforded the *S*-Boc and *N*-Boc protected inhibitors as mixtures of two diastereomers. The *N*-Boc group was selectively removed and replaced by the other acyl groups (29). The diastereomers were separated by flash chromatography on silica gel or by reverse-phase preparative high performance liquid chromatography on a C18 column. The slower-eluting *S*-Boc protected diastereomer exhibited the more potent MMP inhibition in each case. Its stereochemistry was assigned by ^{1}H NMR NOE analysis (MAG-182), x-ray crystallography (YHJ-294-2) (29), or by analogy. Finally, the *S*-Boc protecting groups were removed by brief treatment with 2 *N* HCl in acetic acid and the mercaptosulfide inhibitors were isolated by lyophilization of the reaction mixture.

MAG-181: m.p. 174–176 °C; $[\alpha]^{25}_D$ + 11.2° (*c* = 0.4, MeOH); analysis (CHNS). *S*-Boc derivative: m.p. 118–119 °C; $[\alpha]^{25}_D$ + 33.5° (*c* = 0.49, MeOH); analysis (CHNS).

MAG-182: m.p. 173–174 °C; $[\alpha]^{25}_D$ + 98.6° (*c* = 0.45, MeOH); analysis (CHNS). *S*-Boc derivative: m.p. 159–160 °C; $[\alpha]^{25}_D$ + 63.4 (*c* = 0.52, MeOH); analysis (CHNS).

YHJ-72: m.p. 136–137 °C; $[\alpha]^{20}_D$ − 67.9° (*c* = 0.14, $CHCl_3$); analysis (CHNS). *S*-Boc derivative: m.p. 94–95 °C; $[\alpha]^{25}_D$ +0.4° (*c* = 0.24, $CHCl_3$); analysis (CHNS).

YHJ-73: m.p. 145–146 °C; $[\alpha]^{20}_D$ − 0.7° (*c* = 0.14, $CHCl_3$); analysis (CHNS). *S*-Boc derivative: m.p. 126–127 °C; $[\alpha]^{25}_D$ − 8.8° (*c* = 0.25, $CHCl_3$); HRMS.

YHJ-294-1: m.p. 98–100 °C; $[\alpha]^{20}_D$ + 54.4° (*c* = 0.50, MeOH); analysis (CHNS). *S*-Boc derivative: m.p. 123–124 °C; $[\alpha]^{20}_D$ + 11.5° (*c* = 0.55, MeOH); analysis (CHNS).

YHJ-294-2: m.p. 128–130 °C; $[\alpha]^{20}_D$ + 38.5° (*c* = 0.40, MeOH); analysis (CHNS). *S*-Boc derivative: m.p. 173–175 °C; $[\alpha]^{20}_D$ + 82.6° (*c* = 0.50, MeOH); analysis (CHNS).

YHJ-74: m.p. 174–175 °C; $[\alpha]^{20}_D$ + 2.4° (*c* = 0.50, $CDCl_3$); HRMS. *S*-Boc derivative: m.p. 112–113 °C; $[\alpha]^{20}_D$ − 42.1° (*c* = 0.24, $CHCl_3$); analysis (CHNS).

YHJ-75: m.p. 105–106 °C; $[\alpha]^{20}_D$ − 35.4° (*c* = 0.24, $CHCl_3$); analysis (CHNS). *S*-Boc derivative: m.p. 171–172 °C; $[\alpha]^{20}_D$ + 17.2° (*c* = 0.25, $CHCl_3$); HRMS.

Enzyme Preparation and Folding of the Denatured Protein—MMP-7/matrilysin, MMP-3/stromelysin-1 (30), and MMP-12/metalloelastase (4) were kindly provided by Dr. Harold E. van Wart (Roche Diagnostics),

Professor L. Jack Windsor (Indiana University), and Dr. C. Bruun Schiødt (OsteoPro A/S), respectively. MMP-1/human fibroblast collagenase, MMP-2/human fibroblast gelatinase, MMP-8/human neutrophil collagenase, and MMP-9/human neutrophil gelatinase were described previously (30, 31). The catalytic domain of MT1-MMP/MMP-14 was provided by Professor Harald Tschesche (Bielefeld University) (32). MMP-26 was prepared as described previously (4, 11). Briefly, MMP-26 was expressed as inclusion bodies from a transformed BL-21 DE3 strain. After bacterial insoluble body preparation with B-Per™ reagent, the isolated insoluble protein was folded by following the procedures previously outlined (4–11). The total MMP-26 concentration was measured by UV absorption and calculated with the molar extinction coefficient $\epsilon_{280} = 57130\ M^{-1}\ cm^{-1}$. The active concentration of MMP-26 was determined by titration with GM6001, a tight-binding inhibitor, as described previously (11).

Kinetic Assays and Inhibition of Endometase—The substrate Mca-PLGLDpaAR-NH_2 was used to measure inhibition constants (11, 33). Enzymatic assays were performed at 25 °C in 50 mM HEPES buffer at pH 7.5 in the presence of 10 mM $CaCl_2$, 0.2 M NaCl, and 0.01 or 0.05% Brij-35 with substrate concentrations of 1 μM. The release of product was monitored by measuring fluorescence (excitation and emission wavelengths of 328 and 393 nm, respectively) with a PerkinElmer luminescence spectrophotometer LS 50B connected to a temperature controlled water bath. All stock solutions of inhibitors were in methanol. For inhibition assays, 10 μl of inhibitor stock solution, 176 μl of assay buffer, and 10 μl of enzyme stock solution were mixed and incubated for 30 to 60 min prior to initiation of the assay, which was accomplished by adding and mixing 4 μl of the substrate stock solution. Enzyme concentrations ranged from 0.2 to 7 nM during the assay. Apparent inhibition constant (K_i^{app}) values were calculated by fitting the kinetic data to the Morrison equation for tight-binding inhibitors (34, 35), where v_i and v_0 are the initial rates with and without inhibitor, respectively, and $[E]_o$ and $[I]_o$ are the initial (total) enzyme and inhibitor concentrations, respectively.

$$\frac{v_i}{v_o} = \frac{[E]_o - [I]_o - K_i^{app} + \sqrt{([I]_o + K_i^{app} - [E]_o)^2 + 4[E]_o K_i^{app}}}{2[E]_o} \quad \text{(Eq. 1)}$$

Determination of Mercaptosulfide Inhibitor Concentration—The active inhibitor concentrations were estimated by titrating the mercapto group with 5,5′-dithiobis(2-nitrobenzoic acid) (Ellman's reagent) as described previously (36, 37). Briefly, the reaction of 5,5′-dithiobis(2-nitrobenzoic acid) with the mercapto group produces 2-nitro-5-thiobenzoic acid. The concentration of 2-nitro-5-thiobenzoic acid is then measured by monitoring the absorbance at 412 nm. Cysteine was used to generate the standard curve with a molar extinction coefficient of $14{,}000 \pm 500\ M^{-1}\ cm^{-1}$, which is close to the value in the literature (37).

Computational Protein Sequence Analyses and Homology Modeling Structure of MMP-26—The sequence alignment of MMP catalytic domains was performed by the PILEUP program in Genetics Computer Group (GCG) software (Wisconsin Package version 10), with a default gap weight of 8 and gap length weight of 2. To align MMP-2 and -9, the 183-residue inserts of fibronectin type II-like modules were deleted before the alignment. The homology modeling structure of the MMP-26 catalytic domain was constructed using the Swiss Model program (38–40) with the crystal structure of the MMP-12-inhibitor complex (Protein Data Bank number 1JK3) (17) as a template. The mercaptosulfide inhibitors were computationally docked into the active site of MMP-26 with MacroModel version 7.2 (41, 42). Global minimization calculations were performed by the Monte Carlo molecular mechanical minimization method (43) with the Amber force field modified to include parameters for zinc and calcium. Residues within 7 Å of the inhibitor were included in the minimizations. All modeling was performed using the continuum solvent model. The crystallographic structures of MMP-1 (Protein Data Bank number 1HFC) (44), MMP-7 (Protein Data Bank number 1MMQ) (16), MMP-8 (Protein Data Bank number 1BZS) (45), MMP-12 (Protein Data Bank number 1JK3) (17), and MMP-14 (Protein Data Bank number 1BUV) (21) were used for comparison of the S_1' pocket.

RESULTS

Inhibition of MMPs with Mercaptosulfide MMPIs—An inhibitor set consisting of eight mercaptosulfide inhibitors was chosen to evaluate the S_1' pocket of MMP-26 (Fig. 1). These inhibitors contain P_1' and P_2' residues and have a mercapto and a sulfide group as a possible bidentate metal-binding moiety. The inhibitors contain a Leu side chain (MAG-181 and -182 and YHJ-294-1 and -2) or a Homophe side chain (YHJ-72, -73, -74, and -75) at the P_1' site. These inhibitors were tested against MMPs with known pocket characteristics (MMP-1–3, -7–9, -12, and -14). The inhibition potency of this class of inhibitors for the MMPs is significantly enhanced with a *β-H* configuration at the five-membered ring containing the mercapto and sulfide groups. The inhibitors with a Leu side chain are more potent against the shallow pocket MMPs, MMP-1/human fibroblast collagenase, and MMP-7/matrilysin than those with a Homophe side chain. Inhibitors with a Homophe side chain (YHJ-72, -73, 74, and -75) were more potent against the known deep-pocket MMPs such as MMP-3, -12, and -14 than those

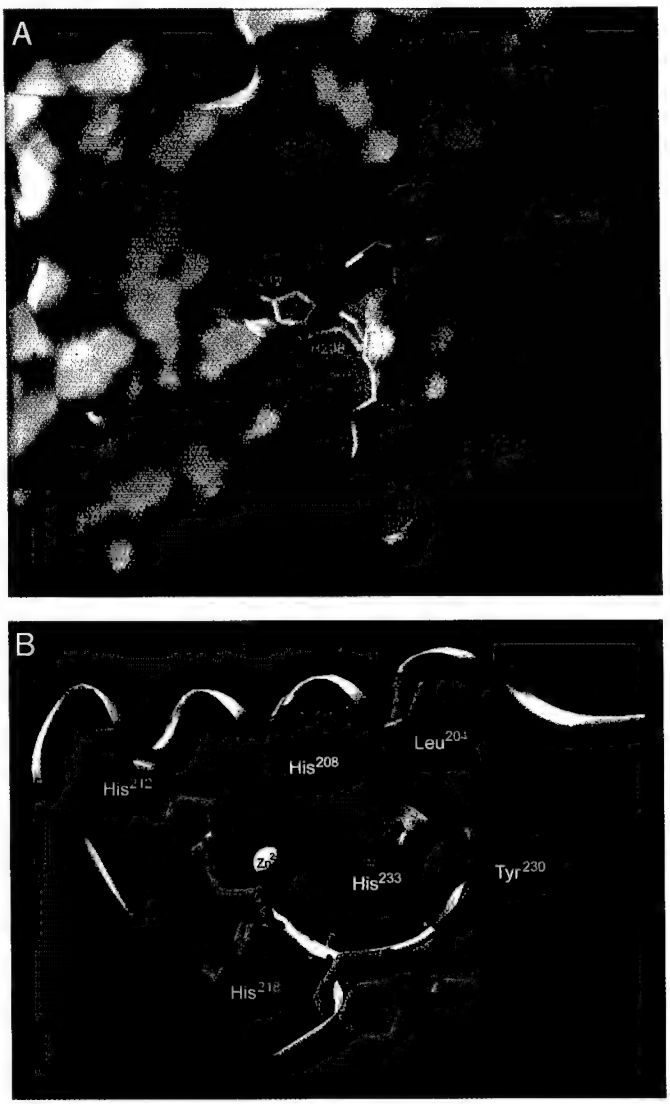

FIG. 4. **A modeled structure of MMP-26 complexed with YHJ-294-2.** *A*, the overall protein structure is shown as a molecular surface and the residues coordinating the catalytic Zn(II) (*magenta sphere*) are represented as *brown sticks* (His-208, His-212, and His-218). The inhibitor YHJ-294-2 is represented as a tube with atoms colored as follows: *green*, carbon; *red*, oxygen; *blue*, nitrogen; and *yellow*, sulfur. *B*, a close-up view of the S_1' pocket reveals that Leu-204, His-208, and Tyr-230 may be involved in formation of the pocket walls represented as *pink* molecular surfaces. The depth of the pocket may be limited by His-233 (*light blue* molecular surface). The three His residues coordinating the Zn(II) (*blue sphere*) are represented by tubes colored as described in *A*. The homology-modeled structure of MMP-26 was generated with the Swiss Model program (38–40) using the x-ray crystallographic structure of a cd-MMP-12-inhibitor complex as a template (Protein Data Bank code 1JK3) (17). The resulting MMP-26 structure was docked with YHJ-294-2 and energy-minimized as described under "Experimental Procedures."

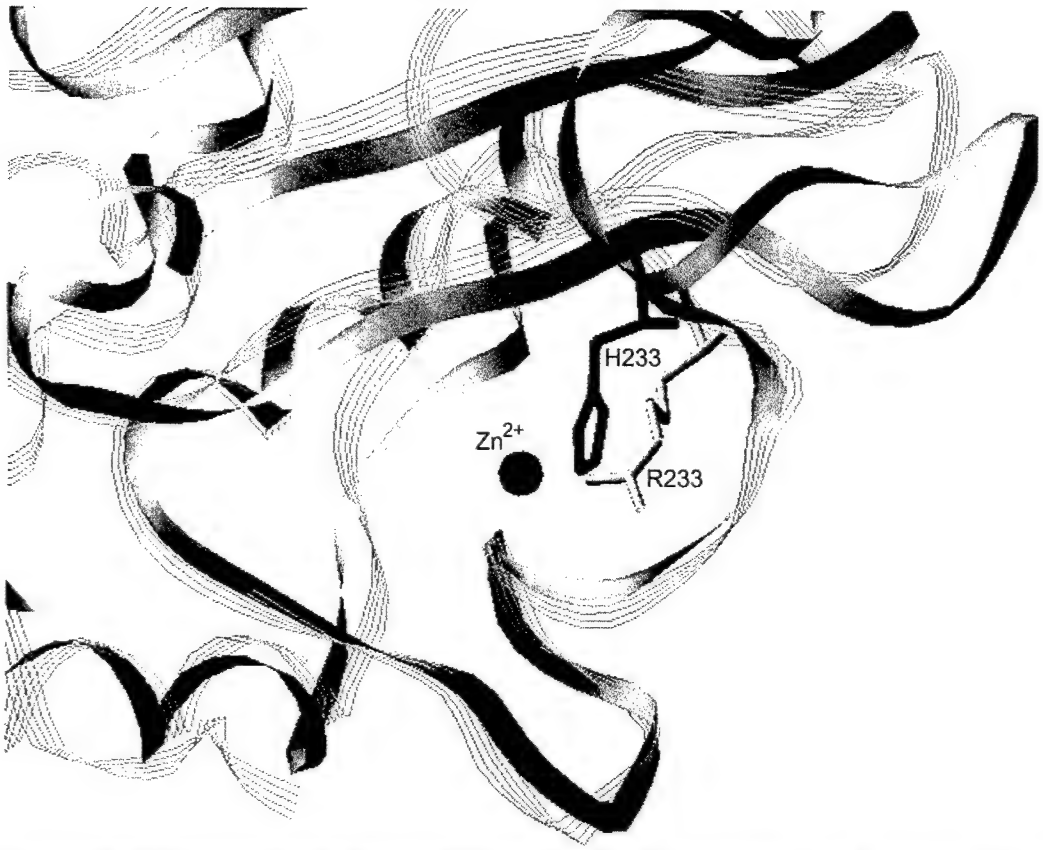

FIG. 5. **The x-ray crystallographic structure MMP-8 (Protein Data Bank number 1BZS) (45) and homology modeled MMP-26 structure are shown after superimposition of zinc (*black sphere*) and histidine N ligands with MacroModel version 7.2.** The proteins are represented by a *flat ribbon* (MMP26) or by a *line ribbon* (MMP-8). Arg-233 and His-233 from MMP-8 and -26, respectively, may limit the depth of the S_1' pocket and are represented by *gray* and *black sticks*.

with Leu side chain. The inhibitors with the Leu side chain at the P_1' site (MAG-182 and YHJ-294-2) inhibit MMP-7 (40 and 26 nM, respectively) and MMP-12 (130 and 93 nM, respectively) without significant differences in K_i^{app} values. However, the presence of Homophe at the P_1' site dramatically distinguishes MMP-12 from MMP-7. YHJ-73 efficiently inhibits MMP-12 (13 nM), however, the potency is decreased to 1 μM against MMP-7. This trend is also displayed by YHJ-75, which has a high nM K_i^{app} value against MMP-7 (300 nM) but retains potency against MMP-12 (5.6 nM). This dramatic change of potency because of changes in the P_1' site of the inhibitors is consistently observed with the remaining shallow- and deep-pocket MMPs.

MMPs with an intermediate pocket can also accommodate the Homophe at the P_1' residue. However, the difference in inhibitor potency observed with Leu or Homophe at the P_1' residue is not as remarkable as that in the shallow- and deep-pocket MMPs. Inhibitors containing Leu at the P_1' site (MAG-182 and YHJ-294-2) are only slightly more potent against MMP-2 and MMP-9 than inhibitors with Homophe (YHJ-73 and -75). These Homophe inhibitors are still potent against MMP-8 with K_i^{app} values in the low nanomolar range. In general, these results indicate that mercaptosulfide inhibitors are suitable for characterizing the S_1' pocket of MMPs.

Characteristics of the S_1' Pocket of MMP-26 as Probed by Mercaptosulfide MMPIs—Inhibition constants for the inhibitors in Fig. 1 were measured with MMP-26 (Table I). YHJ-294-2 is the most potent inhibitor of MMP-26 among the mercaptosulfide inhibitors tested, with a K_i^{app} value of 2.8 nM. MMP-26 also favors the β-*H* configuration at the cyclopentyl or pyrrolidine ring moiety in the inhibitor. Addition of the urea-substituted pyrrolidine ring in place of the cyclopentyl ring (YHJ-294-1 and -2; YHJ-74 and -75) enhances the stereoselectivity for the β-*H* configuration. Importantly, MMP-26 prefers Leu over Homophe at the S_1' site, similar to the intermediate pocket MMPs, MMP-2, -8, and -9.

Characterization of MMP-26 S_1' Pocket Using Commercial Hydroxamate MMPIs—The S_1' site of MMP-26 was further investigated with commercially available inhibitors (Fig. 2). MMP-7/matrilysin was selected as a representative member of the shallow S_1' pocket MMPs and MMP-12/metalloelastase as one of the deep S_1' pocket MMPs for comparison purposes. The K_i^{app} values of the inhibitors with MMP-7, MMP-12, and MMP-26 are summarized in Table II. GM6001 is a broad-spectrum and potent inhibitor of MMPs (K_i^{app} = 0.4 nM for MMP-1, 0.5 nM for MMP-2, 27 nM for MMP-3, 0.1 nM for MMP-8, and 0.2 nM for MMP-9) (46). It is also the most potent synthetic MMP-26 inhibitor tested, with a K_i^{app} value of 0.36 nM. It contains a Leu residue at the P_1' site, and inhibits MMP-7 (3.7 nM) and MMP-12 (3.6 nM) with similar K_i^{app} values as observed in the mercaptosulfide inhibitors with a Leu side chain at the P_1' site. The potent inhibitor 444237 of deep S_1' pocket MMPs and its less potent stereoisomer 444238 were designed for human MMP-8 (IC_{50} = 4 nM and 1 μM, respectively; 45). Inhibitor 444225 was designed to be a potent deep S_1' pocket inhibitor of MMP-3 (K_i = 130 nM; 47). The 4-methoxybenzenesulfonyl group of these inhibitors binds at the deep S_1' pocket according to the crystallographic structure (45) and the structure-activity relationship of several derivatives (47). They inhibit MMP-7 and MMP-12 with at least 150-fold lower K_i^{app} values for MMP-12 than MMP-7. These deep S_1' pocket inhibitors effectively inhibited MMP-26 with at least 90-fold lower K_i^{app} values than those of MMP-7, but were more potent against MMP-12. These results are consistent with MMP-26 having an intermediate S_1' pocket.

FIG. 6. **The x-ray crystallographic structures MMP-3 (Protein Data Bank number 1CIZ) (48) and MMP-8 (Protein Data Bank number 1BZS) (45) are shown after superimposition of zinc (*black sphere*) and histidine N ligands with MacroModel version 7.2.** The proteins are represented by a *flat ribbon* (MMP-8) or by a *line ribbon* (MMP-3). The Arg-233 in MMP-8 limits the depth of the S_1' pocket that is not restricted in MMP-3 by Leu-233.

Sequence Alignment and Homology Modeling Structure of MMP-26—The folding topology and patterns of all MMP catalytic domains are quite similar (19). Thus, homology modeling and protein sequence alignment may be useful tools to predict key residues involved in forming the S_1' pocket of MMP-26. Protein sequence alignment in Fig. 3 reveals a plausible explanation for residues participating in the formation of the S_1' pocket of MMP-26. According to the alignment, Leu-204, His-208, and Tyr-230 may be key residues in forming the S_1' pocket of MMP-26. To evaluate the prediction from the alignment, a homology modeled structure of the MMP-26 catalytic domain was constructed using the Swiss Model program (38–40) and the crystal structure of the MMP-12-inhibitor complex (Protein Data Bank number 1JK3) (17) as a template. The mercaptosulfide inhibitors were docked into the modeled MMP-26 structure using MacroModel version 7.2. The docked structures were further energy minimized as described under "Experimental Procedures." The overall MMP-26 structure complexed with YHJ-294-2 is shown in Fig. 4*A*. Consistent with other MMP family members (19), the non-primed (left) side of the MMP-26 active site is relatively flat. The primed (right) side extends deeper into the surface and the well defined S_1' pocket is clearly visible. The pocket that is formed by Leu-204, His-208, and Tyr-230 is illustrated in Fig. 4*B*. Interestingly, the depth of the pocket may be limited by His-233, consistent with the intermediate size prediction.

DISCUSSION

The inhibition characteristics of MMP-26 with mercaptosulfide inhibitors (Table I) and hydroxamate inhibitors (Table II) indicate that MMP-26 does not have a shallow S_1' pocket. According to the protein sequence alignment in Fig. 3 and the crystallographic structures of MMP-7 (16) and MMP-1 (13), Leu-204 in MMP-26 is substituted for Tyr and Arg at the equivalent position in MMP-7 and MMP-1, respectively. The side chains of Tyr and Arg terminate the S_1' pockets in these shallow-pocket MMPs. In the structure of MMP-26 (Fig. 4*B*), the side chain of Leu-204 forms the top wall of the S_1' pocket as found in most MMPs. Thus, MMP-26 appears to satisfy the requirement for a deep-pocket MMP. However, the inhibition profile of MMP-26 indicates a difference in the S_1' pocket of MMP-26 from those of other deep-pocket MMPs. The inhibitors with Homophe at the S_1' site (YHJ-73 and -75) do not show better potency than those with Leu (MAG-182 and YHJ-294-2). For the deep-pocket MMPs, the inhibition constants are consistently lower for the Homophe inhibitors than Leu inhibitors. The inhibition profile of MMP-26 with mercaptosulfide inhibitors is more similar to intermediate-pocket MMPs (MMP-2, -8, and -9) than deep-pocket MMPs (MMP-3, -12, and -14). These results suggest that MMP-26 may possess an intermediate pocket similar to those of MMP-2, MMP-8, and MMP-9.

A structural comparison of MMP-26 with MMP-8 further supports the similarity between the S_1' pockets of these two enzymes. The overlapping structures of MMP-8 (Protein Data Bank number 1BZS) (45) and MMP-26 at the S_1' pocket are displayed in Fig. 5. In MMP-8, it is known that the depth of the S_1' pocket is restricted by the Arg-233 side chain projecting toward the catalytic Zn(II) (14). In MMP-26, His-233 is present in place of Arg-233, which may restrict the depth of the pocket in a similar fashion, rendering the S_1' pocket to an intermediate size.

Based on the findings provided in this study and x-ray crystallographic structures of MMPs, the residue at the position

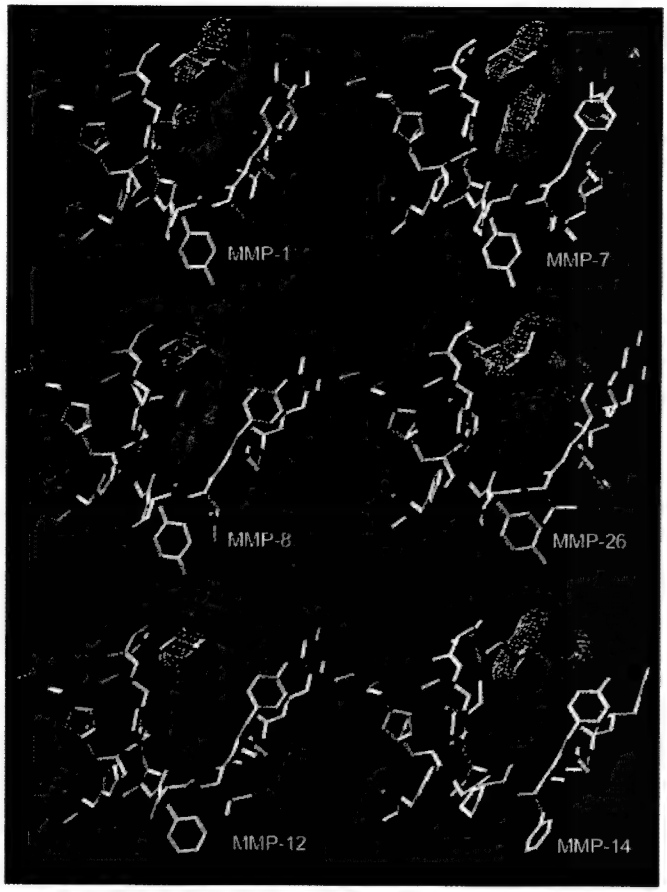

FIG. 7. **The residues forming the S_1' pocket of each enzyme are shown after superimposition of zinc (*magenta sphere*) and histidine N ligands with MacroModel version 7.2.** Inhibitors were removed from the x-ray crystallographic structures with Protein Data Bank accession numbers 1HFC (MMP-1) (44), 1MMQ (MMP-7) (16), 1BZS (MMP-8) (45), 1JK3 (MMP-12) (17), and 1BUV (MMP-14) (21). The MMP-26 structure is a homology model obtained as described under "Experimental Procedures." The key residue 204 that distinguishes a shallow pocket (MMP-1 and -7) is represented by a *yellow* molecular surface. Residue 233 may discriminate between the intermediate (MMP-8 and -26) and deep (MMP-12 and -14) pocket sizes and is represented by a *pink* molecular surface.

equivalent to His-233 of MMP-26 may play a key role in the determination of a deep or intermediate S_1' pocket. The sequence analyses (Fig. 3) showed that the residue at position 233 is hydrophobic in MMPs with deep S_1' pockets and hydrophilic in MMPs with intermediate pockets. The loop containing residue 233 may have a different orientation depending on the hydrophobicity of the side chain. The superimposed x-ray crystallographic structures of MMP-8 (Protein Data Bank number 1BZS) (45) and MMP-3 (Protein Data Bank number 1CIZ) (48) in Fig. 6 reveals this type of structural difference between an intermediate-pocket MMP (MMP-8) and a deep-pocket MMP (MMP-3). These investigations suggest that it is possible to predict the S_1' pocket properties by sequence analyses of the key residues at the Leu-204 and His-233 equivalent positions in other MMPs.

MMPs can be divided into three groups based on the characteristics of their S_1' pockets: shallow-, intermediate-, and deep-pocket MMPs (Fig. 7). Enzyme inhibition kinetic studies using MMPIs in combination with protein sequence analysis and homology modeling reveal that MMP-26 has an intermediate S_1' pocket. Our data may provide important mechanistic and structural information to design MMP-26-specific inhibitors. As the need for innovations and new strategies for MMP inhibition in cancer and inflammation is increasing (49, 50), this study may shed light on the molecular mechanisms by which highly selective and specific inhibitors targeting an individual MMP or subgroups of MMPs may be rationally designed and developed.

Acknowledgments—We thank Sara C. Monroe, Shelbourn Kent, and Katherine E. Berry for excellent assistance with the inhibitor testing, Dr. Mohammad A. Ghaffari for the synthesis of MAG-181 and MAG-182, and Robert Newcomer and Professor Jerzy R. Cioslowski for critical review of the manuscript.

REFERENCES

1. Brinckerhoff, C. E., and Matrisian, L. M. (2002) *Nat. Rev. Mol. Cell. Biol.* **3,** 207–214
2. Egeblad, M., and Werb, Z. (2002) *Nat. Rev. Cancer* **2,** 163–175
3. Overall, C. M. (2002) *Mol. Biotech.* **22,** 51–86
4. Park, H. I., Ni, J., Gerkema, F. E., Liu, D., Belozerov, V. E., and Sang, Q.-X. (2000) *J. Biol. Chem.* **275,** 20540–20544
5. Uría, J. A., and López-Otín, C. (2000) *Cancer Res.* **60,** 4745–4751
6. De Coginac, A. B., Elson, G., Delneste, Y., Magistrelli, G., Jeannin, P., Aubry, J.-P., Berthier, O., Schmitt, D., Bonnefoy, J.-Y., and Gauchat, J.-F. (2000) *Eur. J. Biochem.* **267,** 3323–3329
7. Marchenko, G. N., Ratnikov, B. I., Rozanov, D. V., Godzik, A., Deryugina, E. I., and Strongin, A. Y. (2001) *Biochem. J.* **359,** 705–718
8. Marchenko, G. N., Marchenko, N. D., Leng, J., and Strongin, A. Y. (2002) *Biochem. J.* **363,** 253–262
9. Zhao, Y.-G., Xiao, A.-Z., Newcomer, R. G., Park, H. I., Kang, T., Chung, L. W., Swanson, M. G., Zhau, H. E., Kurhanewicz, J., and Sang, Q.-X. (2003) *J. Biol. Chem.* **278,** 15056–15064
10. Zhao, Y.-G., Xiao, A.-Z., Park, H. I., Newcomer, R. G., Yan, M., Man, Y. G., Heffelfinger, S. C., and Sang, Q.-X. (2003) *Cancer Res.*, in press
11. Park, H. I., Turk, B. E., Gerkema, F. E., Cantley, L. C., and Sang, Q.-X. (2002) *J. Biol. Chem.* **277,** 35168–35175
12. Gooley, P. R., O'Connell, J. F., Marcy, A. I., Cuba, G. C., Salowe, S. P., Bush, B. L., Hermes, J. D., Esser, N. K., Hagmann, W. K., Springer, J. P., and Johnson, B. A. (1994) *Nat. Struct. Biol.* **1,** 111–118
13. Lovejoy, B., Cleasby, A., Hassell, A. M., Longley, K., Luther, M. A., Weigl, D., McGeehan, G., McElroy, A. B. Drewry, D., Lambert, M. H., and Jordon, S. R. (1994) *Science* **263,** 375–377
14. Bode, W., Reinemer, P., Huber, R., Kleine, T., Schnierer, S., and Tschesche, H. (1994) *EMBO J.* **13,** 1263–1269
15. Stams, T., Spurlino, J. C., Smith, D. L., Wahl, R. C., Ho, T. F., Qoronfleh, M. W., Banks, T. M., and Rubin, B. (1994) *Nat. Struct. Biol.* **1,** 119–123
16. Browner, M. F., Smith, W. W., and Castelhano, A. L. (1995) *Biochemistry* **34,** 6602–6610
17. Lang, R., Kocourek, A., Braun, M., Tschesche, H., Huber, R., Bode, W., and Maskos, K. (2001) *J. Mol. Biol.* **312,** 731–742
18. Nar, H., Werle, K., Bauer, M. M., Dollinger, H., and Jung, B. (2001) *J. Mol. Biol.* **312,** 743–751
19. Bode, W., Fernandez-Catalan, C., Tschesche, H., Grams, F., Nagase, H., and Maskos, K. (1999) *Cell. Mol. Life Sci.* **55,** 639–652
20. Nagase, H. (2001) in *Matrix Metalloproteinase Inhibitors in Cancer Therapy* (Clendeninn, N. J., and Appelt, K., eds) pp. 39–66, Humana Press, Totowa, NJ
21. Fernandez-Catalan, C., Bode, W., Huber, R., Turk, D., Calvete, J. J., Lichte, A., Tschesche, H., and Maskos, K. (1998) *EMBO J.* **17,** 5238–5248
22. Morgunova, E., Tuuttila, A., Bergmann, U., and Tryggvason, K. (2002) *Proc. Natl. Acad. Sci. U. S. A.* **99,** 7414–7419
23. Rowsell, S., Hawtin, P., Minshull, C. A., Jepson, H., Brockbank, S. M. V., Barratt, D. G., Slater, A. M., McPheat, W. L., Walterson, D., Henney, A. M., and Pauptit, R. A. (2002) *J. Mol. Biol.* **319,** 173–181
24. Netzel-Arnett, S., Sang, Q.-X., Moore, W. G. I., Narve, M., Birkedal-Hansen, H., and Van Wart, H. E. (1993) *Biochemistry* **32,** 6427–6432
25. Nagase, H., Fields, C. G., and Fields, G. B. (1994) *J. Biol. Chem.* **269,** 20952–20957
26. Mucha, A., Cuniasse, P., Kannan, R., Beau, F., Yiotakis, A., Basset, P., and Dive, V. (1998) *J. Biol. Chem.* **273,** 2763–2768
27. Schwartz, M. A., and Van Wart, H. E. (October 3, 1995) U. S. Patent 5455262
28. Sang, Q.-X., Jia, M. C., Schwartz, M. A., Jaye, M. C., Kleinman, H. K., Ghaffari, M. A., and Luo, Y. L. (2000) *Biochem. Biophys. Res. Commun.* **274,** 780–786
29. Jin, Y., Ghaffari, M. A., and Schwartz, M. A. (2002) *Tetrahedron Lett.* **43,** 7319–7321
30. Sang, Q.-X., Birkedal-Hansen, H., and Van Wart, H. E. (1995) *Biochim. Biophys. Acta* **1251,** 99–108
31. Sang, Q. A., Bodden, M. K., and Windsor, L. J. (1996) *J. Prot. Chem.* **15,** 243–253
32. Hurst, D. R., Schwartz, M. A., Ghaffari, M. A., Jin, Y., Tschesche, H., Fields, G. B., and Sang, Q.-X. (October 8, 2003) *Biochem. J.* 10.1042/BJ20031067
33. Knight, C. G., Willenbrock, F., and Murphy, G. (1992) *FEBS Lett.* **296,** 263–266
34. Morrison, J. F. (1969) *Biochim. Biophys. Acta* **185,** 269–286
35. Copeland, R. A. (2000) *Enzymes: A Practical Introduction to Structure, Mechanism, and Data Analysis*, 2nd Ed., Wiley-VCH, Inc., New York
36. Ellman, G. L., (1959) *Arch. Biochem. Biophys.* **82,** 70–77
37. Riddles, P. W., Blakeley, R. L., and Zerner, B., (1979) *Anal. Biochem.* **94,** 75–81
38. Peitsch, M. C. (1995) *Bio/Technology* **13,** 658–660
39. Peitsch, M. C. (1996) *Biochem. Soc. Trans.* **24,** 274–279

40. Guex, N., and Peitsch, M. C. (1997) *Electrophoresis* **18,** 2714–2723
41. Bohacek, R., de Lombaert, S., McMartin, C., Priestle, J., and Grütter, M. (1996) *J. Am. Chem. Soc.* **118,** 8231–8249
42. Arighi, C. N., Rossi, J. P., and Delfino, J. M. (1998) *Biochemistry* **37,** 16802–16814
43. Chang, G., Guida, W. C., and Still, W. C. (1989) *J. Am. Chem. Soc.* **111,** 4379–4386
44. Spurlino, J. C., Smallwood, A. M., Carlton, D. D., Banks, T. M., Vavra, K. J., Johnson, J. S., Cook, E. R., Falvo, J., Wahl, R. C., Pulvino, T. A., Wendoloski, J. J., and Smith, D. L. (1994) *Proteins* **19,** 98–109
45. Matter, H., Schwab, W., Barber, D., Billen, G., Hasse, B., Neises, B., Schudok, M., Thorwart, W., Schreuder, H., Brachvogel, V., Lönze, P., and Weithmann, K. U. (1999) *J. Med. Chem.* **42,** 1908–1920
46. Galardy, R. E., Cassabonne, M. E., Giese, C., Gilbert, J. H., Lapierre, F., Lopez, H., Schaefer, M. F., Stack, R., Sullivan, M., and Summer, B. (1994) *Ann. N. Y. Acad. Sci.* **732,** 315–323
47. MacPherson, L. J., Bayburt, E. K., Capparelli, M. P., Carroll, B. J., Goldstein, R., Justice, M. R., Zhu, L., Hu, S., Melton, R. A., Fryer, L., Goldberg, R. L., Doughty, J. R., Spirito, S., Blancuzzi, V., Wilson, D., O'Byrne, E. M., Ganu, V., and Parker, D. T. (1997) *J. Med. Chem.* **40,** 2525–2532
48. Pavlovsky, A. G., Williams, M. G., Ye, Q. Z., Ortwine, D. F., Purchase, C. F., 2nd, White, A. D., Dhanaraj, V., Roth, B. D., Johnson, L. L., Hupe, D., Humblet, C., and Blundell, T. L. (1999) *Protein Sci.* **8,** 1455–1462
49. Overall, C. M., and López-Otín, C. (2002) *Nat. Rev. Cancer* **2,** 657–672
50. Coussens, L. M., Fingleton, B., and Matrisian, L. M. (2002) *Science* **295,** 2387–2392

[CANCER RESEARCH 64, 590–598, January 15, 2004]

Endometase/Matrilysin-2 in Human Breast Ductal Carcinoma *in Situ* and Its Inhibition by Tissue Inhibitors of Metalloproteinases-2 and -4: A Putative Role in the Initiation of Breast Cancer Invasion

Yun-Ge Zhao,[1] Ai-Zhen Xiao,[1] Hyun I. Park,[1] Robert G. Newcomer,[1] Mei Yan,[2] Yan-Gao Man,[3] Sue C. Heffelfinger,[2] and Qing-Xiang Amy Sang[1]

[1]Department of Chemistry and Biochemistry and Institute of Molecular Biophysics, Florida State University, Tallahassee, Florida; [2]Department of Pathology and Laboratory of Medicine, University of Cincinnati College of Medicine, Cincinnati, Ohio; and [3]Department of Gynecology and Breast Pathology, The Armed Forces Institute of Pathology, Washington, D.C.

ABSTRACT

Local disruption of the integrity of both the myoepithelial cell layer and the basement membrane is an indispensable prerequisite for the initiation of invasion and the conversion of human breast ductal carcinoma *in situ* (DCIS) to infiltrating ductal carcinoma (IDC). We previously reported that human endometase/matrilysin-2/matrix metalloproteinase (MMP) 26-mediated pro-gelatinase B (MMP-9) activation promoted invasion of human prostate carcinoma cells by dissolving basement membrane proteins (Y. G. Zhao *et al.*, J. Biol. Chem., *278:* 15056–15064, 2003). Here we report that tissue inhibitor of metalloproteinases (TIMP)-2 and TIMP-4 are potent inhibitors of MMP-26, with apparent K_i values of 1.6 and 0.62 nM, respectively. TIMP-2 and TIMP-4 also inhibited the activation of pro-MMP-9 by MMP-26 *in vitro*. The expression levels of MMP-26, MMP-9, TIMP-2, and TIMP-4 proteins in DCIS were significantly higher than those in IDC, atypical intraductal hyperplasia, and normal breast epithelia adjacent to DCIS and IDC by immunohistochemistry and integrated morphometry analysis. Double immunofluorescence labeling and confocal laser scanning microscopy revealed that MMP-26 was colocalized with MMP-9, TIMP-2, and TIMP-4 in DCIS cells. Higher levels of MMP-26 mRNA were also detected in DCIS cells by *in situ* hybridization.

INTRODUCTION

Matrix metalloproteinases (MMPs) are known to be associated with cancer cell invasion, growth, angiogenesis, inflammation, and metastasis (1, 2). MMP-26 is a novel enzyme that was recently cloned and characterized by our group (3) and others (4–6). It has several structural features characteristic of MMPs, including a signal peptide, a propeptide domain, and a catalytic domain with a conserved zinc-binding motif, but it lacks the hemopexin-like domain (3–6). A unique "cysteine switch" sequence in the prodomain, PHCGVPD as opposed to the conserved PRCG*XX*D sequence found in many other MMPs, keeps the enzyme latent.

MMP-26 mRNA is primarily expressed in cancers of epithelial origin, such as endometrial carcinomas (3, 7), prostate carcinomas (7), lung carcinomas (7), and their corresponding cell lines (3–6), and in a small number of normal adult tissues, such as the uterus (3, 5), placenta (4, 5), and kidney (6). Some parallels exist with MMP-7, which is also expressed epithelially and also lacks the hemopexin-like domain. We have also reported that the levels of *MMP-26 gene* and protein expression are higher in a malignant choriocarcinoma cell line (JEG-3) than in normal human cytotrophoblast cells (8). Recently, we found that the levels of MMP-26 protein in human prostate carcinomas from multiple patients were significantly higher than those in prostatitis, benign prostate hyperplasia, and normal prostate tissues (9). MMP-26 is capable of activating pro-MMP-9 by cleavage at the Ala^{93}-Met^{94} site of the pro-enzyme, and this activation facilitates the efficient cleavage of fibronectin (FN), promoting the invasion of highly invasive and metastatic androgen-repressed prostate cancer cells through FN or type IV collagen (9). The activation is prolonged but persistent, which is consistent with the process of tumor cell invasion. These findings indicate that MMP-26-mediated pro-MMP-9 activation may be one biochemical mechanism contributing to human carcinoma cell invasion *in vivo*.

MMP activities are inhibited by endogenous tissue inhibitors of metalloproteinases (TIMPs). Four mammalian TIMPs have been identified: (*a*) TIMP-1 (10); (*b*) TIMP-2 (11); (*c*) TIMP-3 (12); and (*d*) TIMP-4 (13). The hydrolytic activity of MMP-26 against synthetic peptides is blocked by TIMP-1, TIMP-2, and TIMP-4 (5, 6, 8), but the inhibitory potential of TIMP-1 is lower than that of TIMP-2 and TIMP-4 (5). TIMP-1 and TIMP-2 also inhibit the cleavage of denatured type I collagen (gelatin) by MMP-26 (6). TIMPs are expressed in human breast cancer cells (14–16). Here, we continue to explore the possible roles of MMP-26 and the coordination of MMP-26 with MMP-9, TIMP-2, and TIMP-4 in human breast carcinoma invasion.

In the present study, we showed that TIMP-2 and TIMP-4 completely inhibited the activation of pro-MMP-9 by MMP-26. The expressions of MMP-26, MMP-9, TIMP-2, and TIMP-4 proteins in human breast ductal carcinomas *in situ* (DCIS) were significantly higher than those in infiltrating ductal carcinoma (IDC), atypical intraductal hyperplasia (AIDH), and normal breast epithelia around the DCIS and IDC. Furthermore, MMP-26 was colocalized with MMP-9, TIMP-2, and TIMP-4 in human breast DCIS.

MATERIALS AND METHODS

Inhibition Assays of MMP-26 by TIMP-2 and TIMP-4. The quenched fluorescence peptide substrates, *Mca-Pro-Leu-Ala-Nva-Dpa-Ala-Arg-NH_2* and *Mca-Arg-Pro-Lys-Pro-Val-Glu-Nva-Trp-Arg-Lys(Dnp)-NH_2* were purchased from Calbiochem. The MMP-26 used in this experiment is recombinant and partially active. Briefly, MMP-26 was expressed in the form of inclusion bodies from transformed *Escherichia coli* cells as described previously (3). The inclusion bodies were isolated and purified using B-PER bacterial protein extraction reagent according to the manufacturer's instructions. The insoluble protein was dissolved in 8 M urea to ~5 mg/ml. The protein solution was diluted to ~100 μg/ml in 8 M urea and 10 mM DTT for 1 h; dialyzed in 4 M urea, 1 mM DTT, and 50 mM HEPES (pH 7.5) for at least 1 h; and then folded by dialysis in 1× HEPES buffer [50 mM HEPES, 0.2 M NaCl, 10 mM $CaCl_2$, and 0.01% Brij-35 (pH 7.5)] with 20 μM $ZnSO_4$ for 16 h. To enhance the activity of MMP-26, the folded enzyme was dialyzed twice for 24 h at 4°C in the folding buffer without Zn^{2+} ions. The total enzyme concentration was measured by UV absorption using ϵ_{280} = 57,130 M^{-1} cm^{-1}, which was

Received 6/30/03; revised 10/29/03; accepted 11/7/03.

Grant support: Department of Defense Congressionally Directed Medical Research Programs Grant DAMD17-02-1-0238, NIH Grant CA78646, American Cancer Society grant, Florida Division Grant F01FSU-1 (to Q-X. A. S.), Florida State University Research Foundation grant (to Q-X. A. S. and Y-G. Z.), and Department of Defense Congressionally Directed Medical Research Programs Grants DAMD17-01-0129 and DAMD17-01-0130 (to Y-G. M.).

The costs of publication of this article were defrayed in part by the payment of page charges. This article must therefore be hereby marked *advertisement* in accordance with 18 U.S.C. Section 1734 solely to indicate this fact.

Requests for reprints: Qing-Xiang Amy Sang, Department of Chemistry and Biochemistry, Florida State University, Chemistry Research Building DLC, Room 203, Tallahassee, Florida 32306-4390. Phone: (850) 644-8683; Fax: (850) 644-8281; E-mail: sang@chem.fsu.edu.

calculated using Genetics Computer Group software. The concentration of active MMP-26 was determined by active site titration with the tight-binding inhibitor GM-6001 as described previously (17). GM-6001 was the most potent inhibitor of MMP-26 tested, with a K_i^{app} of 0.36 nM (17). Because TIMPs are tight-binding and slow-binding inhibitors of MMPs, MMP-26 was incubated for 4 h with human TIMP-2 and TIMP-4 before the measurement of substrate hydrolysis to allow the enzyme and inhibitor to reach their binding equilibrium. Human fibroblast TIMP-2 was provided by Dr. L. Jack Windsor (Indiana University, Indianapolis, IN). Recombinant human TIMP-4 was purchased from R&D Systems (Minneapolis, MN). The concentrations of TIMPs ranged from 0.2 to 60 nM. The assay was initiated by the addition of a substrate stock solution (4 μl) prepared in 1:1 water and DMSO to an enzyme-inhibitor assay buffer (196 μl) for a final concentration of 1 μM. The release of the fluorogenic cleavage product was monitored by measuring fluorescence (excitation and emission wavelengths at 328 and 393 nm, respectively) with a Perkin-Elmer Luminescence Spectrophotometer LS 50B connected to a water bath with a temperature control. All kinetic experiments were conducted in 1× HEPES buffer. Fluorogenic peptide substrate assays were performed following the procedures we reported previously (17). To assess inhibition potency, the apparent inhibition constants (apparent K_i values) were determined by fitting the two trial data sets to the Morrison equation below (18) with nonlinear regression. In this equation, v_i is the initial rate of MMP-26 catalysis in the presence of inhibitor, and v_o is the initial rate without inhibitor. [E] and [I] are the initial enzyme and inhibitor concentrations, respectively, and K_i^{app} is the apparent inhibition constant.

$$\frac{v_i}{v_o} = 1 - \frac{([E] + [I] + K_i^{app}) - \sqrt{([E] + [I] + K_i^{app})^2 - 4[E][I]}}{2[E]}$$

Pro-MMP-9 Activation by MMP-26 and Inhibition of the Activation by TIMP-2 and TIMP-4. Zymography and silver staining were performed as reported previously (3, 7, 19, 20). MMP-26, pro-MMP-9, and active MMP-9 were purified in our laboratory (3, 21). The molar concentration ratios of TIMPs, MMP-26, and pro-MMP-9 were 10:1:4. Two metal chelators/metalloproteinase inhibitors, 1, 10-phenanthroline and EDTA, were used as controls. Briefly, MMP-26 was incubated in the presence or absence of different inhibitors (TIMPs, 1,10-phenanthroline, and EDTA) in 30 μl of 1× HEPES buffer at room temperature (25°C) for 4 h. Pro-MMP-9 was then added and incubated at 37°C for 20 h. For zymography, aliquots of the reaction solution were removed and treated with a nonreducing sample buffer. MMP-9 activity was analyzed by zymography on 9% SDS-polyacrylamide gels containing 1% gelatin (22). For silver staining, aliquots were removed and treated with a reducing sample buffer and boiled for 5 min. After electrophoresis on 9% SDS-polyacrylamide gels, the protein bands were visualized by silver staining (19).

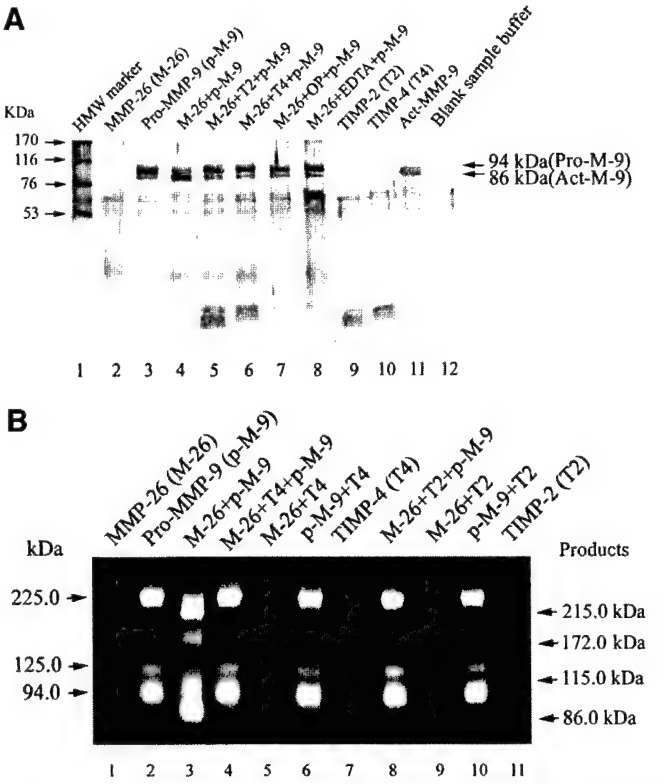

Fig. 2. Tissue inhibitor of metalloproteinases (TIMP)-2 and TIMP-4 inhibit pro-matrix metalloproteinase (MMP)-9 activation by MMP-26. *A*, pro-MMP-9 activation by MMP-26 was inhibited by both TIMP-2 and TIMP-4 (electrophoresis samples were treated under reducing conditions). MMP-26 activates pro-MMP-9, enhancing the 86-kDa band (*Lane 4*). This activation was completely blocked by adding TIMP-2 (*Lane 5*) or TIMP-4 (*Lane 6*). The inhibition by TIMP-2 and TIMP-4 is comparable with that of two broad-spectrum metal chelators/metalloproteinase inhibitors, 1,10-phenanthroline (*OP*) and EDTA (*Lanes 7* and *8*). *B*, zymogram assay of MMP-9 activation by MMP26 and inhibition by TIMP-2 and TIMP-4 (electrophoresis samples under nonreducing conditions). The 225-kDa band is a homodimer of pro-MMP-9, the 125-kDa band is a heterodimer of pro-MMP-9 and neutrophil gelatinase-associated lipocalin, and the 94-kDa band is a monomer of pro-MMP-9. MMP-26 activates pro-MMP-9 to generate new 215-, 172-, 115-, and 86-kDa active fragments (*Lane 3*). This activation was completely blocked by adding TIMP-4 (*Lane 4*) or TIMP-2 (*Lane 8*).

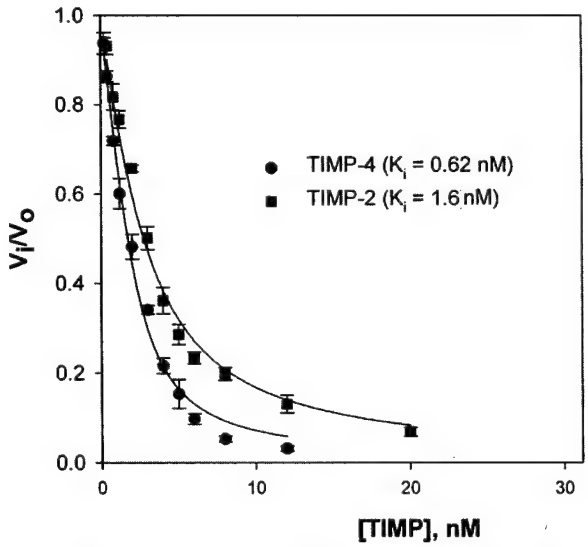

Fig. 1. Inhibition kinetics of matrix metalloproteinase 26 by tissue inhibitor of metalloproteinases (TIMP)-2 and TIMP-4. Matrix metalloproteinase 26 (2 nM) was incubated for 4 h in the presence of TIMP-2 or TIMP-4 at concentrations of 0.2–60 nM. The substrate hydrolysis assay was initiated by the addition of substrate stock solution. The data were fitted to the Morrison equation to calculate the apparent K_i values.

FN Cleavage Assay. MMP-26, pro-MMP-9, MMP-26-activated MMP-9, and TIMPs were prepared as described above. Active MMP-9, purified from human neutrophils (21), was used as a positive control. FN was incubated with MMP-26, pro-MMP-9, active MMP-9, or MMP-26 plus pro-MMP-9 in the presence or absence of TIMP-2 or TIMP-4 in 1× HEPES buffer at 37°C for 18 h. The molar concentration ratio of MMP-26:pro-MMP-9:FN:TIMP was approximately 1:4:10:10. Aliquots were removed and treated with a reducing sample buffer and boiled for 5 min. Samples were then loaded onto 9% polyacrylamide gels in the presence of SDS, electrophoresed, and subjected to silver staining (19).

***In Situ* Hybridization.** The DCIS samples were classified according to our previous reports (23, 24). Briefly, the formalin-fixed, paraffin-embedded samples were sectioned to 5-μm thickness and fixed onto slides. The full-length MMP-26 sense cDNA and antisense cDNA were amplified in pCR 3.1 and purified as described in our previous report (9). The sense and antisense plasmids were linearized with *Xho*I and *Xba*I, respectively. The sense and antisense digoxigenin-labeled RNA probes were generated by *in vitro* transcription with T7 polymerase. *In situ* hybridization was performed as per our previous report (22). Briefly, the paraffin-embedded sections (5 μm) were deparaffinized with xylene and treated with proteinase K solution [50 μg/ml in 0.2 M Tris-HCl (pH 7.5), 2 mM $MgCl_2$] for 15 min at room temperature. After prehybridization, the sections were hybridized to digoxigenin-labeled MMP-26 antisense cRNA probes for 18 h at 45°C and 100% humidity. The

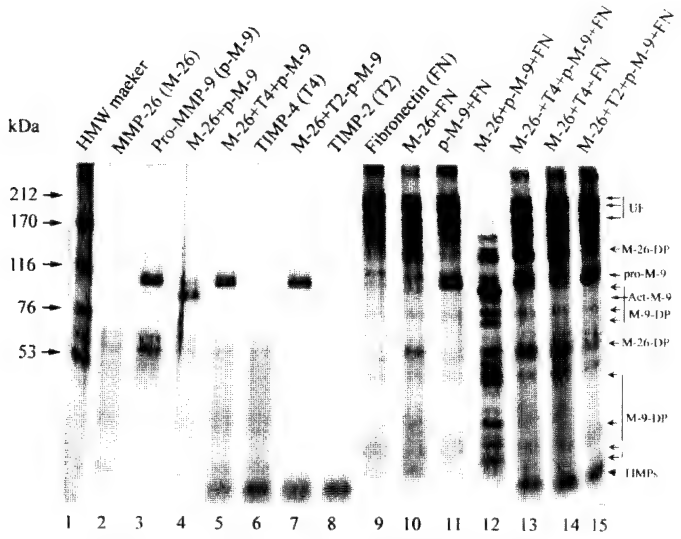

Fig. 3. Cleavage of fibronectin (FN) by matrix metalloproteinase (MMP)-9 and MMP-26. MMP-26 cleaved FN weakly, generating 125- and 58-kDa bands (*Lane 10*), pro-MMP-9 did not cleave FN (*Lane 11*), and MMP-26-activated MMP-9 (*Lane 4*) cleaved FN efficiently (*Lane 12*). Tissue inhibitor of metalloproteinases (TIMP)-4 weakly blocked FN cleavage by MMP-26 (*Lane 14*). Both TIMP-4 and TIMP-2 blocked pro-MMP-9 activation by MMP-26 (*Lanes 5* and *7*), which significantly diminished FN cleavage (*Lanes 13* and *15*). *UF*, uncleaved fibronectin; *M-26-DP*, MMP-26-degraded FN products; *M-9-DP*, MMP-9-degraded FN products; *pro-M-9*, pro-MMP-9; *Act-M-9*, activated MMP-9.

MMP-26 sense RNA probe was used under the same hybridization conditions as the control. After hybridization, the slides were washed with saline sodium citrate buffer and blocked [1% blocking reagents in Tris-buffered saline (pH 7.5)] for 30 min. The slides were then covered with anti-digoxigenin-alkaline phosphatase Fab fragments (1:400) for 2 h. Then the slides were stained with nitroblue tetrazolium/5-bromo-4-chloro-3-indolyl phosphate (Roche Applied Science, Mannheim, Germany). The expression signals were photographed under a microscope.

Immunohistochemistry. The human breast DCIS, IDC, and hyperplasia tissue samples were classified according to our reports (23–26). Immunohistochemistry was performed on consecutive sections according to our previous report (9). Briefly, the formalin-fixed, paraffin-embedded samples were sectioned to 5-μm thickness and fixed onto slides. After dewaxing and rehydrating, the slides were blocked with 3% BSA/Tris-buffered saline for 1 h at room temperature before incubation with affinity-purified, polyclonal rabbit antihuman MMP-26, MMP-9, TIMP-2, and TIMP-4 antibodies (all 25 μg/ml) at room temperature for 90 min. Sections were then incubated with alkaline phosphatase-conjugated secondary antirabbit antibody (1:500; Jackson ImmunoResearch, West Grove, PA) for 1 h at room temperature. The signals were detected with Fast-red (Sigma, St. Louis, MO). Purified preimmune IgGs from the same animal were used as negative controls.

Double Immunofluorescence and Confocal Laser Scanning Microscopy. Double immunofluorescence staining was performed as per our previous description (9). Briefly, the slides were incubated with a rabbit antihuman MMP-26 IgG (25 μg/ml) and a goat antihuman MMP-9 antibody (1:200 dilution; R&D Systems) or a mouse antihuman MMP-26 IgG (25 μg/ml; R&D Systems) and a rabbit antihuman TIMP-4 (25 μg/ml) or a rabbit antihuman TIMP-2 antibody (30 μg/ml) overnight at 4°C. The slides were then incubated with a goat antimouse-IgG IgG for 30 min at room temperature. Secondary Rhodamine Red-X-conjugated donkey antirabbit IgG and FITC-conjugated donkey antigoat IgG (Jackson ImmunoResearch) were subsequently applied at a 1:50 dilution for 30 min at room temperature. Slow Fade mounting medium was added to the slides, and fluorescence was analyzed using a Zeiss LSM510 Laser Scanning Confocal Microscope (Carl Zeiss, Heidelberg, Germany) equipped with a multi-photon laser. Images were processed for reproduction using Photoshop software version 6.0 (Adobe Systems, Mountainview, CA). Purified preimmune IgG and normal goat serum were used as negative controls.

Densitometric and Statistical Analysis. Four to 16 pictures were taken from the glandular epithelia after immunostaining by each of the four antibodies and the two preimmune IgGs in the DCIS, IDC, AIDH, and normal glands around the DCIS and IDC. Quantification of the immunostaining signals was performed using the Metamorph System (version 4.6r8; Universal Imaging Corp., Inc., West Chester, PA) according to our previous description (9). Briefly, an appropriate color threshold was determined (color model, HSI; hue, 230–255; saturation and intensity, full spectrum). The glandular epithelia

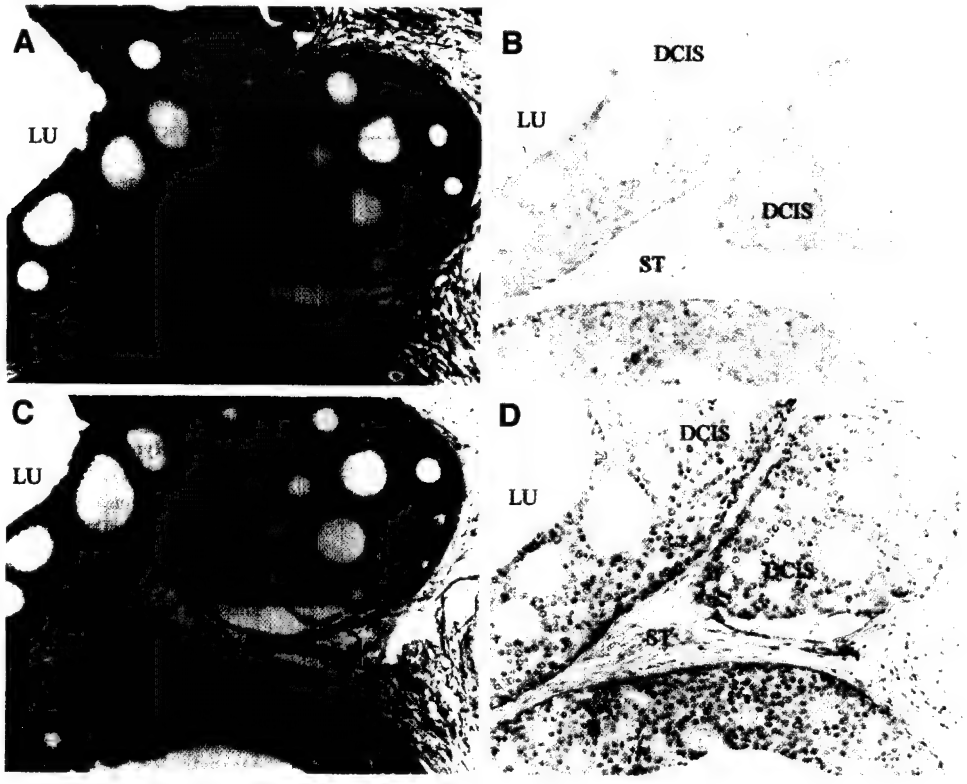

Fig. 4. Matrix metalloproteinase (MMP)-26 mRNA and protein expression in human mammary tissues. *A* and *B* are *in situ* hybridization to detect MMP-26 mRNA expression, and *C* and *D* are immunohistochemical staining to detect MMP-26 protein expression. *A*, MMP-26 antisense probe; *B*, MMP-26 sense probe; *C*, rabbit antihuman MMP-26 metallo domain IgG; *D*, pre-immune IgG. *Blue* indicates MMP-26 mRNA signals, and *red* indicates MMP-26 protein expression. Cells were counterstained lightly with hematoxylin for viewing of negatively stained epithelial and stromal cells in *C* and *D*. *DCIS*, ductal carcinoma *in situ*; *ST*, stroma; *LU*, lumen.

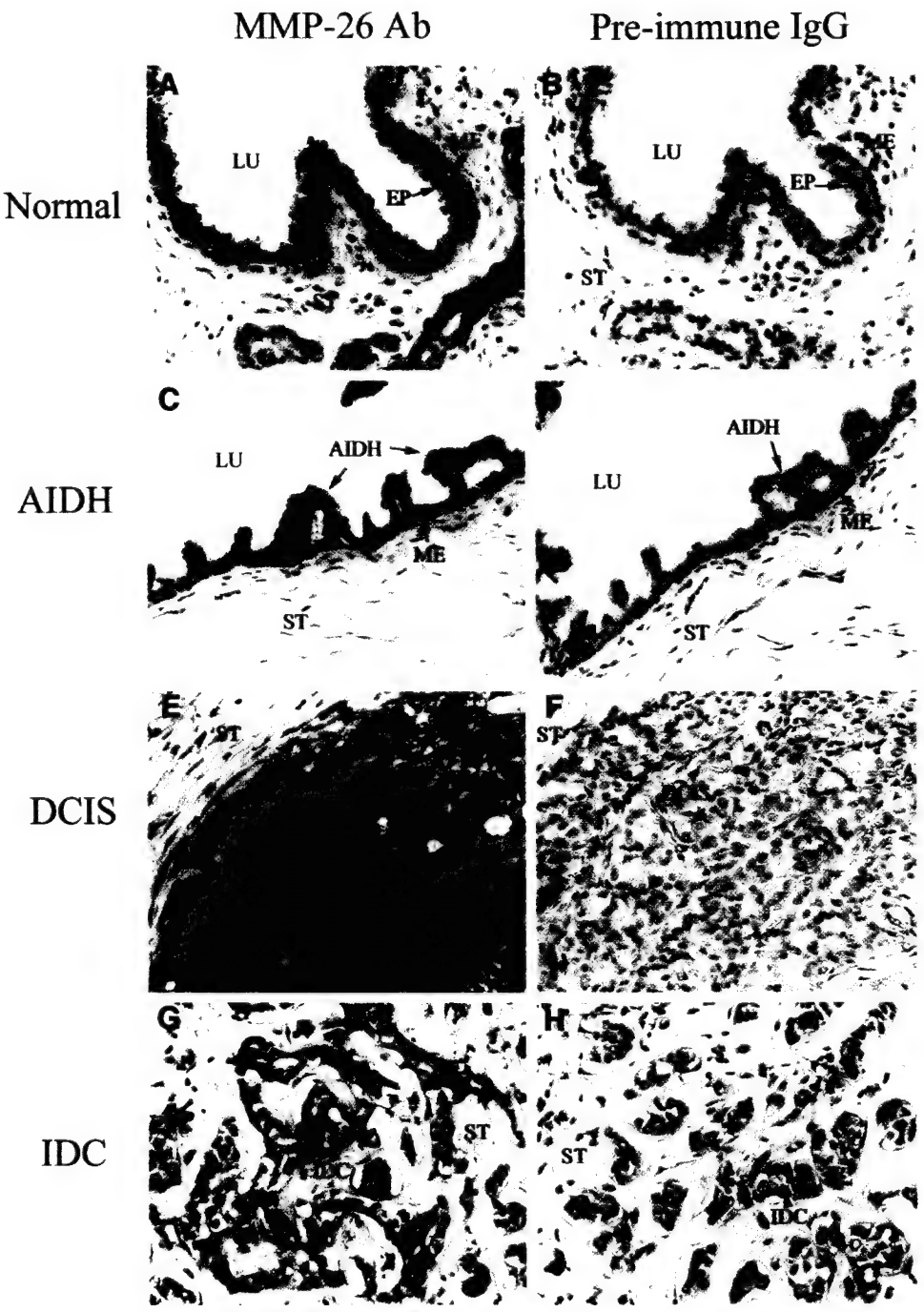

Fig. 5. Expression of matrix metalloproteinase (MMP)-26 protein in human mammary gland. Cells stained *red* indicate MMP-26 protein expression. All sections were counterstained lightly with hematoxylin for viewing negatively stained epithelial and stromal cells. *A*, *C*, *E*, and *G* are stained with anti-MMP-26 antibody, and *B*, *D*, *F*, and *H* are stained with pre-immune IgG. *A* and *B*, normal breast tissues; *C* and *D*, atypical intraductal hyperplasia (*AIDH*); *E* and *F*, breast ductal carcinoma *in situ* (*DCIS*); *G* and *H*, breast infiltrating ductal carcinoma (*IDC*). All figures are ×200 magnifications. *LU*, lumen; *EP*, epithelial cells; *ST*, stroma; *ME*, myoepithelial cells.

from each image were isolated into closed regions, and the signal areas and intensities of staining in compliance with the chosen parameters were measured by integrated morphometry analysis. The selected epithelial area was obtained by region measurement. The signal intensities were expressed as integrated absorbance (IOD, the sum of the optical densities of all pixels that make up the object). The ratio of the IOD to the selected epithelial area was determined, and the average ratios from each case were then calculated and used for statistical analysis. Statistical analysis of all samples was performed with the least significant difference correction of ANOVA for multiple comparisons. Data represent the mean ± SE, and $P < 0.05$ was considered significant.

RESULTS

Determination of the Apparent Inhibition Constants of TIMP-2 and TIMP-4 against MMP-26. The apparent K_i values of MMP-26 were measured and calculated to be 1.6 and 0.62 nM for TIMP-2 and TIMP-4, respectively (Fig. 1), using the Morrison equation (18). The apparent K_i values show that TIMP-4 is a slightly more potent inhibitor of MMP-26 than TIMP-2.

Activation of Pro-MMP-9 by MMP-26 and Inhibition of the Activation by TIMP-2 and TIMP-4. To explore the inhibition of MMP-26-mediated MMP-9 activation by TIMP-2 and TIMP-4, purified pro-MMP-9 and MMP-26 were incubated with these TIMPs, and the samples were subsequently analyzed by SDS-PAGE. MMP-26 cleaved pro-MMP-9 (94 kDa) to yield an enhanced active form 86-kDa band on a silver-stained gel under reducing conditions as per our recent report (Ref. 9; Fig. 2*A*, *Lane 4*). Zymography revealed that pro-MMP-9 presented as 225-, 125-, and 94-kDa gelatinolytic bands under nonreducing conditions. The 225-kDa band is a homodimer of pro-MMP-9, the 125-kDa band is a heterodimer of pro-MMP-9 and neutrophil gelatinase-associated lipocalin, and the 94-kDa band is a

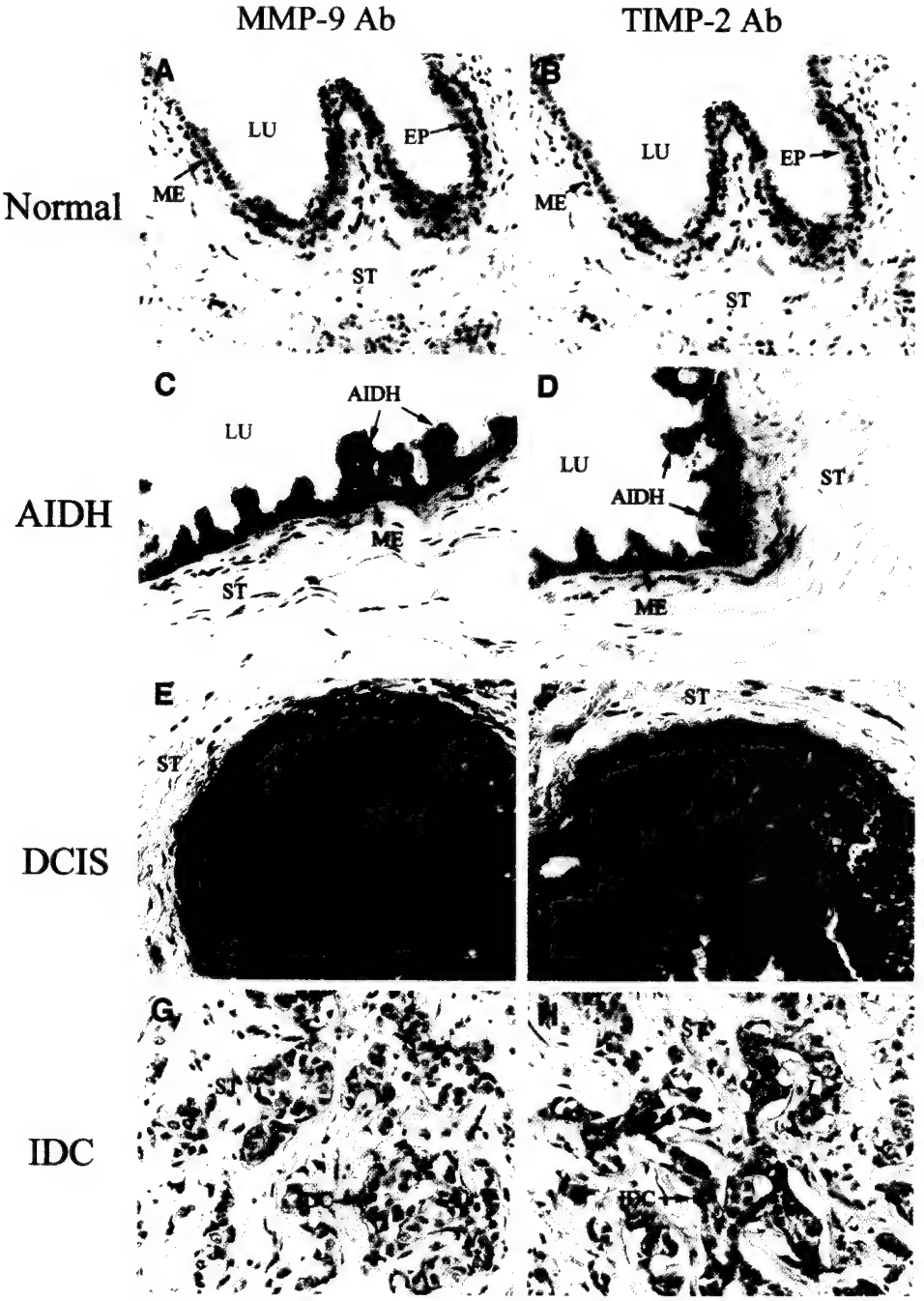

Fig. 6. Expression of matrix metalloproteinase (MMP)-9 and tissue inhibitor of metalloproteinases (TIMP)-2 proteins in human mammary gland. Cells stained *red* indicate MMP-9 or TIMP-2 protein expression. All sections were counterstained lightly with hematoxylin for viewing negatively stained epithelial and stromal cells. *A, C, E,* and *G* are stained with anti-MMP-9 antibody. *B, D, F,* and *H* are stained with TIMP-2 antibody. *A* and *B,* normal breast tissues; *C* and *D,* atypical intraductal hyperplasia (*AIDH*); *E* and *F,* ductal carcinoma *in situ* (*DCIS*); *G* and *H,* infiltrating ductal carcinoma (*IDC*). All figures are ×200 magnifications. *LU,* lumen; *EP,* epithelial cells; *ST,* stroma; *ME,* myoepithelial cells.

monomer of pro-MMP-9 (21, 27, 28). The new active 215-, 172-, 115-, and 86-kDa bands were generated after incubation with MMP-26 (Fig. 2*B, Lane 3*). The 215-, 115-, and 86-kDa bands are the active forms of the 225-, 125-, and 94-kDa forms, respectively. The 172-kDa band is a dimer of the 86-kDa forms. The activation of pro-MMP-9 by MMP-26 was completely inhibited by recombinant TIMP-2 and TIMP-4 (Fig. 2*A, Lanes 5* and *6*; Fig. 2*B, Lanes 4* and *8*). The blocking efficiencies of TIMP-2 and TIMP-4 were comparable with those of two broad-spectrum metal chelators/metalloproteinase inhibitors, 1,10-phenanthroline and EDTA (Fig. 2*A, Lanes 7* and *8*).

To further confirm the inhibition of MMP-26-mediated pro-MMP-9 activation by TIMP-2 and TIMP-4, *in vitro* FN cleavage assays were performed. MMP-26 slowly cleaved FN to generate 125- and 58-kDa bands (Fig. 3, *Lane 10*), whereas pro-MMP-9 did not cleave FN (Fig. 3, *Lane 11*). However, MMP-26-activated MMP-9 cleaved FN completely, generating at least seven new bands (Fig. 3, *Lane 12*). Both TIMP-2 and TIMP-4 completely blocked the activation of pro-MMP-9 by MMP-26, which subsequently resulted in inhibition of FN cleavage (Fig. 3, *Lanes 13* and *15*).

Expression of MMP-26 mRNA in Human Breast Tissues. *In situ* hybridization showed that MMP-26 mRNA was localized in human breast DCIS (Fig. 4*A*). On a serial section of the same tissue, MMP-26 protein was also detected in human breast DCIS (Fig. 4*C*). The MMP-26 sense probe and pre-immune IgG from the same animal as the MMP-26 antibody were used as controls (Fig. 4, *B* and *D*).

Expressions of MMP-26, MMP-9, TIMP-2, and TIMP-4 Proteins in Human Breast Tissues. MMP-26, MMP-9, TIMP-2, and TIMP-4 proteins were detected in human breast epithelia (Figs. 5–7). The expressions of the four proteins were extremely high in human breast DCIS (20 cases) cells (Fig. 5*E*; Fig. 6, *E* and *F*; Fig. 7*E*) but

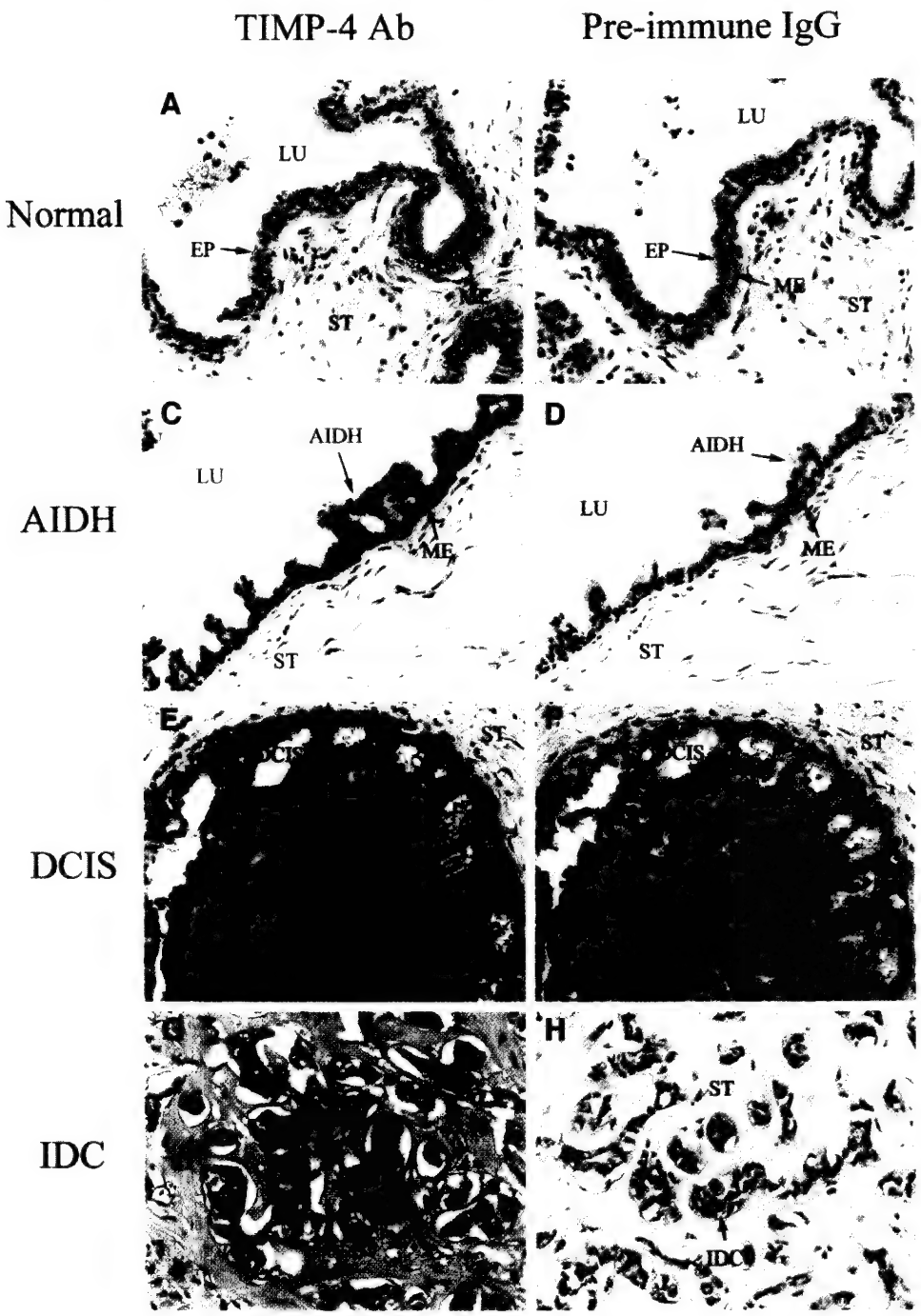

Fig. 7. Expression of tissue inhibitor of metalloproteinases (TIMP)-4 protein in human mammary gland. Cells stained *red* indicate TIMP-4 protein expression. All sections were counterstained lightly with hematoxylin for viewing negatively stained epithelial and stromal cells. *A, C, E,* and *G* are stained with antihuman TIMP-4 antibody. *B, D, F,* and *H* are stained with pre-immune IgG. *A* and *B,* normal breast tissues; *C* and *D,* atypical intraductal hyperplasia (*AIDH*); *E* and *F,* ductal carcinoma *in situ* (*DCIS*); *G* and *H,* infiltrating ductal carcinoma (*IDC*). All figures are ×200 magnifications. *LU,* lumen; *EP,* epithelial cells; *ST,* stroma; *ME,* myoepithelial cells.

very low in the normal glandular epithelial cells (25 cases) around DCIS and IDC (Fig. 5*A*; Fig. 6, *A* and *B*; Fig. 7*A*) and also in AIDH [15 cases (Fig. 5*C*; Fig. 6, *C* and *D*; Fig. 7*C*)]. Their expressions were substantially decreased in IDC [23 cases (Fig. 5*G*; Fig. 6, *G* and *H*; Fig. 7*G*)]. Statistical analysis revealed that the signal intensities of MMP-26, MMP-9, TIMP-2, and TIMP-4 proteins in DCIS were significantly higher than those in IDC, AIDH, and normal epithelia around the DCIS and IDC ($P < 0.05$ or $P < 0.01$; Fig. 8). There was no significant difference for the signals of MMP-26, MMP-9, TIMP-2, and TIMP-4 proteins among the normal epithelia around the DCIS and IDC, or in the AIDH and IDC samples ($P > 0.05$; Fig. 8). Pre-immune IgGs from the same animals as the MMP-26 or TIMP-4 antibodies were used as controls (Fig. 5, *B, D, F,* and *H*; Fig. 7, *B, D, F,* and *H*). There was no significant difference ($P > 0.05$) for the pre-immune IgG signals among the normal, AIDH, DCIS, and IDC samples.

Coexpression of MMP-26 and MMP-9 in Human Breast Carcinoma. To confirm the distributions of MMP-26, MMP-9, TIMP-2, and TIMP-4 within carcinoma cells, double immunofluorescence staining assays were performed in human breast DCIS samples. MMP-26 protein was localized mainly in the cytoplasm of the cancerous cells (Fig. 9*A*, *red*; Fig. 9*B*, *green*), which is consistent with our previous report (9). MMP-9 was localized both in the cytoplasm of the cancerous cells and at the cell surface, mainly on the cell membrane (Fig. 9*C*, *green*). The merged picture shows that MMP-26 and MMP-9 were coexpressed in the cytoplasm of the cancerous cells (Fig. 9*E*, *yellow*). The high magnification pictures in Fig. 9, *A, C,* and *E*, clearly demonstrate MMP-26 and MMP-9 colocalization (indicated by *ar-*

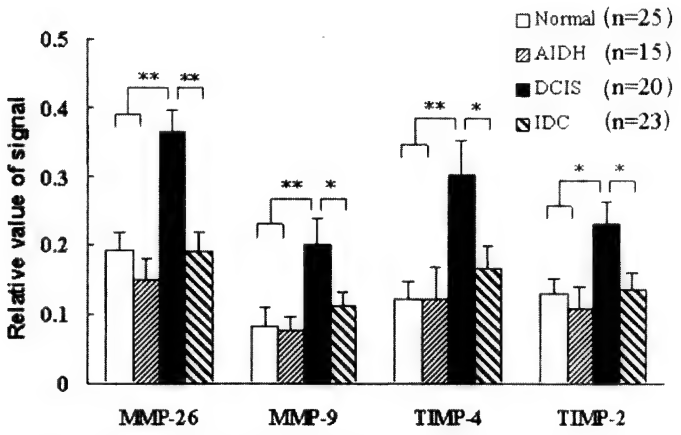

Fig. 8. Densitometric quantification analyses of matrix metalloproteinase 26, matrix metalloproteinase 9, tissue inhibitor of metalloproteinases 2, and tissue inhibitor of metalloproteinases 4 protein expression. The quantification analysis was described in "Materials and Methods." The epithelial regions were isolated, and the staining area and total selected area were obtained by Integrated Morphometry Analysis (IMA) and analyzed by one-way ANOVA with least significant difference (LSD) correction. Each value represents the mean ± SE. *, $P < 0.05$; **, $P < 0.01$. *Normal,* normal breast tissue; *AIDH,* atypical intraductal hyperplasia; *DCIS,* ductal carcinoma *in situ*; *IDC,* infiltrating ductal carcinoma; *n,* the number of cases.

rowheads). TIMP-4 is shown in Fig. 9*D* (*red*). MMP-26 and TIMP-4 were also coexpressed in the cytoplasm of the cancerous cells (Fig. 9*F, yellow*). MMP-26 and TIMP-2 were also colocalized in cancer cells, and minimal signals were detected in control tissues using purified pre-immune rabbit IgG and nonimmune goat sera (data not shown).

DISCUSSION

The epithelial component of the normal and noninvasive human breast is physically separated from the stroma by myoepithelial cells and the basement membrane, which is composed of a group of fibrous proteins, including type IV collagen, FN, laminin, and proteoglycans. The disruption of both the myoepithelial cell layer and the basement membrane is an essential prerequisite for the invasion of DCIS. In this present investigation, we found that the levels of MMP-26 and MMP-9 proteins in human breast DCIS were significantly higher than those in human breast IDC, normal mammary glands, and AIDH. MMP-26 and MMP-9 were colocalized in human breast DCIS cells. MMP-9 is a powerful enzyme associated with human breast cancer development and invasion (29, 30). Scorilas *et al.* (29) and Soini *et al.* (31) demonstrated that *MMP-9 mRNA* and protein were highly expressed in human breast carcinoma cells. MMP-9 protein is also expressed in the breast carcinoma cell lines MCF-7 (32, 33), SKBR-3 (34), MDA-MB-231 (35, 36), and MCF10A (36) and in normal breast epithelial cell lines HMT-3522 and T4-2 (32, 37). Our recent study (9) demonstrated that the level of MMP-26 protein in human prostate carcinomas is also significantly higher than those in prostatitis, benign prostate hyperplasia, and normal prostate tissues. MMP-26 and MMP-9 are not only coexpressed in human prostate carcinomas and in androgen-repressed prostate cancer cells, but they also promoted the invasion of androgen-repressed prostate cancer cells across FN or type IV collagen via MMP-26-mediated pro-MMP-9 activation.

Nguyen *et al.* (38) showed that active MMP-9 accumulates in the cytosol of human endothelial cells, where it is eventually used by invading pseudopodia, and it is possible that endogenous, self-activated MMP-26 serves as an activator for intracellular pro-MMP-9. The active form of MMP-9 may then be stored inside the cell, ready for rapid release when it is required to initiate invasion of human breast DCIS cells. Although DCIS is not invasive cancer, it may have the potential to develop into IDC, given time. The localization of *MMP-26 mRNA* and protein in carcinomas was confirmed by *in situ* hybridization and immunohistochemistry, providing evidence that MMP-26 is an epithelial cell-derived enzyme (3–6).

We demonstrated that the hydrolysis of synthetic peptides by MMP-26 is inhibited by TIMP-2 and TIMP-4, which is consistent with previous reports (5, 6, 8). TIMP-2 and TIMP-4 were also able to completely block MMP-9 activation by MMP-26, as well as the cleavage of FN by MMP-26-activated MMP-9. Therefore, one consequential function of TIMP-2 and TIMP-4 may be their inhibition of MMP-9 activation by MMP-26. TIMP-2 and TIMP-4 possess several distinct cellular functions, but their most widely appreciated biological functions are their roles in the inhibition of cell invasion *in vitro* (39–42) and their *in vivo* contributions to tumorigenesis (43, 44) and growth and metastasis (44–47). The underlying molecular mechanism for the tumor-suppressing activities of the TIMPs is thought to be dependent on their anti-MMP activities.

In our experiments, the expressions of TIMP-2 and TIMP-4 were all increased significantly in human breast DCIS but decreased in IDC, mimicking the expression of MMP-26 and MMP-9 in DCIS and IDC, which indicates that these four proteins are highly coordinated during human breast carcinoma development and progression. It may also suggest that remodeling of the extracellular matrix by MMP-26 and MMP-9 stimulates the expression of TIMP-2 and TIMP-4, implying self-regulation through a negative feedback loop. The consistently high expression of TIMP-2 and TIMP-4 proteins in human breast DCIS is in agreement with reports that the expression of TIMP-2 and TIMP-4 in human breast carcinomas is increased (14, 16,

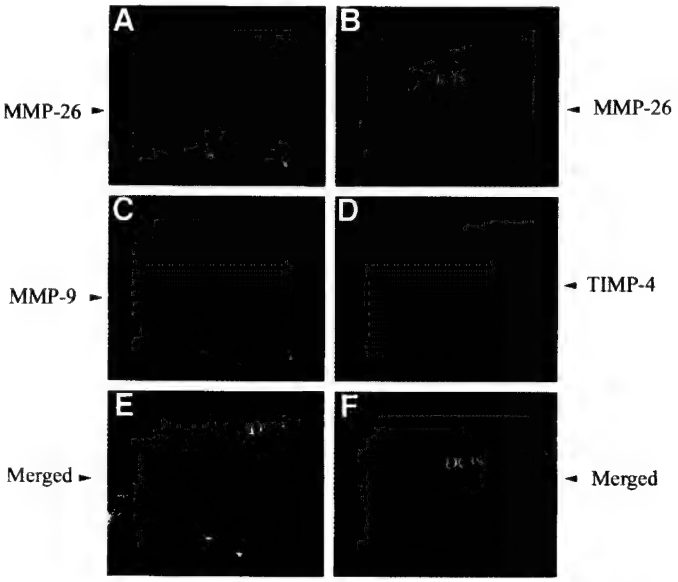

Fig. 9. Coexpression of matrix metalloproteinase (MMP)-26 with MMP-9 or tissue inhibitor of metalloproteinases (TIMP)-4 in human breast ductal carcinoma *in situ* (DCIS). In *A, C,* and *E,* the primary antibodies are rabbit antihuman MMP-26 IgG and goat antihuman MMP-9 IgG, the secondary antibodies are Rhodamine Red-X-conjugated donkey antirabbit IgG and FITC-conjugated donkey antigoat IgG. *A, red* indicates MMP-26 protein staining, which is localized mainly in the cytoplasm of DCIS cells. *C, green* indicates MMP-9 protein staining, which is localized mainly on the cell surface of the cancerous cells. *E,* merged images show a color shift to *orange-yellow,* indicating colocalization between MMP-26 and MMP-9 proteins in DCIS. In *B, D,* and *F,* the primary antibodies are mouse antihuman MMP-26 IgG and rabbit antihuman TIMP-4 IgG. After incubation with primary antibodies, the slides were incubated with goat antimouse-IgG IgG. The secondary antibodies are the same as those described in *A, C,* and *E. B, green* indicates MMP-26 protein staining, which is localized mainly in the cytoplasm of DCIS cells. *D, red* indicates TIMP-4 protein staining. *F,* merged images show a color shift to *orange-yellow,* indicating colocalization between MMP-26 and TIMP-4 proteins in DCIS. *Scale bars,* 50 μm. *ST,* stroma; *LU,* lumen.

39, 48). This may represent a compensatory response to the increased MMP-26- and MMP-9-mediated remodeling stimuli in DCIS in an attempt to reach a new balance between MMP-26/MMP-9 and TIMP-2/TIMP-4 to regulate degradation of the extracellular matrix and to suppress tumor progression by impeding MMP-26, MMP-9, and MMP-26-mediated MMP-9 activation. TIMP-2 and TIMP-4 may play multiple roles in human breast cancer in addition to inhibiting MMPs, including antiapoptotic activity and tumor-stimulating effects when administrated systemically (16). The new paradigms concerning the potential roles of TIMPs in suppressing or promoting tumor progression have been discussed previously (49).

The decreased MMP-26 and MMP-9 expression levels in IDC suggest that these two enzymes may play a role in the very early stages of DCIS invasion, but once the basement membrane has been breached, cancer cells become less dependent on the activities of MMP-26 and MMP-9. Nielsen *et al.* (50) demonstrated that MMP-9 immunostaining or *in situ* hybridization signals were not detected in human breast ductal carcinoma cells but were seen in tumor-infiltrating stromal cells including macrophages, neutrophils, and vascular pericytes. This indicates that MMP-9 may be transiently expressed in cells during the early stages of human breast carcinoma (DCIS), but not in the later stages of breast carcinoma (IDC). The controversy surrounding the expression of MMP-9 found in the literature (29, 31, 50), inclusive of our current findings, might also suggest that these different expression patterns arise from DCIS and IDC representing genetically distinct disease forms, raising the possibility that DCIS does not simply designate a transitory disease state that invariably leads to IDC.

Down-regulation of TIMPs contributed significantly to the tumorigenic and invasive potentials of cancer cells (43, 44). Decreased production of TIMP-2 resulted in increased MMP activity, leading to increased invasiveness by cancer cells (39). Therefore, maintenance of the balance between MMPs and TIMPs appears critical for the suppression of cancer cell invasion and metastasis. Once the balance between MMP-26/MMP-9 and TIMP-2/TIMP-4 in DCIS is destroyed, the inhibition by TIMP-2 and TIMP-4 may be inadequate to block the degradation of extracellular matrix components by MMP-26 and MMP-9 in DCIS, resulting in degradation of basement membrane components and initiation of the invasive processes of DCIS cells. MMP-26, MMP-9, TIMP-2, and TIMP-4 may be spatially and temporally expressed in the very early stages of DCIS invasion, whereas other enzymes/inhibitors are responsible for the late-stage invasion of IDC cells. Further investigations will provide a more complete understanding of the functions of MMP-26, MMP-9, and TIMPs in human breast cancer progression.

ACKNOWLEDGMENTS

We thank Dr. L. Jack Windsor of Indiana University for kindly providing us with TIMP-2 protein and the polyclonal anti-TIMP-2 antibody, Dr. Weiping Jiang of R&D Systems for the monoclonal anti-MMP-26 antibody, Dr. Jianzhou Wang of University of Oklahoma College of Medicine for critical review of the manuscript, and Sara C. Monroe at our laboratory at Florida State University for editorial assistance with manuscript preparation. We are also grateful to Kimberly Riddle and Jon Ekman at the Department of Biological Sciences Imaging Resources at Florida State University for their excellent assistance with confocal microscopy and integrated morphometry analysis.

REFERENCES

1. Sternlicht, M. D., and Werb, Z. How matrix metalloproteinases regulate cell behavior. Annu. Rev. Cell Dev. Biol., *17:* 463–516, 2001.
2. Egeblad, M., and Werb, Z. New functions for the matrix metalloproteinases in cancer progression. Nat. Rev. Cancer, *2:* 163–176, 2002.
3. Park, H. I., Ni, J., Gerkema, F. E., Liu, D., Belozerov, V. E., and Sang, Q. X. Identification and characterization of human endometase (matrix metalloproteinase-26) from endometrial tumor. J. Biol. Chem., *275:* 20540–20544, 2000.
4. de Coignac, A. B., Elson, G., Delneste, Y., Magistrelli, G., Jeannin, P., Aubry, J. P., Berthier, O., Schmitt, D., Bonnefoy, J. Y., and Gauchat, J. F. Cloning of MMP-26. A novel matrilysin-like proteinase. Eur. J. Biochem., *267:* 3323–3329, 2000.
5. Uría, J. A., and López-Otín, C. Matrilysin-2, a new matrix metalloproteinase expressed in human tumors and showing the minimal domain organization required for secretion, latency, and activity. Cancer Res., *60:* 4745–4751, 2000.
6. Marchenko, G. N., Ratnikov, B. I., Rozanov, D. V., Godzik, A., Deryugina, E. I., and Strongin, A. Y. Characterization of matrix metalloproteinase-26, a novel metalloproteinase widely expressed in cancer cells of epithelial origin. Biochem. J., *356:* 705–718, 2001.
7. Marchenko, G. N., Marchenko, N. D., Leng, J., and Strongin, A. Y. Promoter characterization of the novel human matrix metalloproteinase-26 gene: regulation by the T-cell factor-4 implies specific expression of the gene in cancer cells of epithelial origin. Biochem. J., *363:* 253–262, 2002.
8. Zhang, J., Cao, Y. J., Zhao, Y. G., Sang, Q. X., and Duan, E. K. Expression of matrix metalloproteinase-26 and tissue inhibitor of metalloproteinase-4 in human normal cytotrophoblast cells and a choriocarcinoma cell line, JEG-3. Mol. Hum. Reprod., *8:* 659–666, 2002.
9. Zhao, Y. G., Xiao, A. Z., Newcomer, R. G., Park, H. I., Kang, T., Chung, L. W., Swanson, M. G., Zhau, H. E., Kurhanewicz, J., and Sang, Q. X. Activation of pro-gelatinase B by endometase/matrilysin-2 promotes invasion of human prostate cancer cells. J. Biol. Chem., *278:* 15056–15064, 2003.
10. Carmichael, D. F., Sommer, A., Thompson, R. C., Anderson, D. C., Smith, C. G., Welgus, H. G., and Stricklin, G. P. Primary structure and cDNA cloning of human fibroblast collagenase inhibitor. Proc. Natl. Acad. Sci. USA, *83:* 2407–2411, 1986.
11. Stetler-Stevenson, W. G., Brown, P. D., Onisto, M., Levy, A. T., and Liotta, L. A. Tissue inhibitor of metalloproteinases-2 (TIMP-2) mRNA expression in tumor cell lines and human tumor tissues. J. Biol. Chem., *265:* 13933–13938, 1990.
12. Uria, J. A., Ferrando, A. A., Velasco, G., Freije, J. M., and Lopez-Otin, C. Structure and expression in breast tumors of human TIMP-3, a new member of the metalloproteinase inhibitor family. Cancer Res., *54:* 2091–2094, 1994.
13. Greene, J., Wang, M., Liu, Y. E., Raymond, L. A., Rosen, C., and Shi, Y. E. Molecular cloning and characterization of human tissue inhibitor of metalloproteinase 4. J. Biol. Chem., *271:* 30375–30380, 1996.
14. Remacle, A., McCarthy, K., Noel, A., Maguire, T., McDermott, E., O'Higgins, N., Foidart, J. M., and Duffy, M. J. High levels of TIMP-2 correlate with adverse prognosis in breast cancer. Int. J. Cancer, *20:* 118–121, 2000.
15. Hurst, D. R., Li, H., Xu, X., Badisa, V. L., Shi, Y. E., and Sang, Q. X. Development and characterization of a new polyclonal antibody specifically against tissue inhibitor of metalloproteinases 4 in human breast cancer. Biochem. Biophys. Res. Commun., *281:* 166–171, 2001.
16. Jiang, Y., Wang, M., Celiker, M. Y., Liu, Y. E., Sang, Q. X., Goldberg, I. D., and Shi, Y. E. Stimulation of mammary tumorigenesis by systemic tissue inhibitor of matrix metalloproteinase 4 gene delivery. Cancer Res., *61:* 2365–2370, 2001.
17. Park, H. I., Turk, B. E., Gerkema, F. E., Cantley, L. C., and Sang, Q-X. Peptide substrate specificities and protein cleavage sites of human endometase/matrilysin-2/matrix metalloproteinase-26. J. Biol. Chem., *277:* 35168–35175, 2002.
18. Morrison, J. F. Kinetics of the reversible inhibition of enzyme-catalysed reactions by tight-binding inhibitors. Biochim. Biophys. Acta, *185:* 269–286, 1969.
19. Zhao, Y. G., Wei, P., and Sang, Q. X. Inhibitory antibodies against endopeptidase activity of human adamalysin 19. Biochem. Biophys. Res. Commun , *289:* 288–294, 2001.
20. Patterson, B. C., and Sang, Q. A. Angiostatin-converting enzyme activities of human matrilysin (MMP-7) and gelatinase B/type IV collagenase (MMP-9). J. Biol. Chem., *272:* 28823–28825, 1997.
21. Sang, Q. X., Birkedal-Hansen, H., and Van Wart, H. E. Proteolytic and nonproteolytic activation of human neutrophil progelatinase B. Biochim. Biophys. Acta, *1251:* 99–108, 1995.
22. Zhao, Y. G., Xiao, A. Z., Cao, X. M., and Zhu, C. Expression of matrix metalloproteinase-2, -9 and tissue inhibitors of metalloproteinase-1, -2, -3 mRNAs in rat uterus during early pregnancy. Mol. Reprod. Dev., *62:* 149–158, 2002.
23. Heffelfinger, S. C., Yassin, R., Miller, M. A., and Lower, E. Vascularity of proliferative breast disease and carcinoma *in situ* correlates with histological features. Clin. Cancer Res., *2:* 1873–1878, 1996.
24. Heffelfinger, S. C., Yassin, R., Miller, M. A., and Lower, E. E. Cyclin D1, retinoblastoma, p53, and Her2/neu protein expression in preinvasive breast pathologies: correlation with vascularity. Pathobiology, *68:* 129–136, 2000.
25. Moinfar, F., Man, Y. G., Lininger, R. A., Bodian, C., Tavassoli, F. A. Use of keratin 35βE12 as an adjunct in the diagnosis of mammary intraepithelial neoplasia-ductal type-benign and malignant intraductal proliferations. Am. J. Surg. Pathol., *23:* 1048–1058, 1999.
26. Bratthauer, G. L., Moinfar, F., Stamatakos, M. D., Mezzetti, T. P., Shekitka, K. M., Man, Y. G., and Tavassoli, F. A. Combined E-cadherin and high molecular weight cytokeratin immunoprofile differentiates lobular, ductal, and hybrid mammary intraepithelial neoplasias. Hum. Pathol., *33:* 620–627, 2002.
27. Tschesche, H., Zolzer, V., Triebel, S., and Bartsch, S. The human neutrophil lipocalin supports the allosteric activation of matrix metalloproteinases. Eur. J. Biochem., *268:* 1918–1928, 2001.
28. Yan, L., Borregaard, N., Kjeldsen, L., and Moses, M. A. The high molecular weight urinary matrix metalloproteinase (MMP) activity is a complex of gelatinase B/MMP-9 and neutrophil gelatinase-associated lipocalin (NGAL). Modulation of MMP-9 activity by NGAL. J. Biol. Chem., *276:* 37258–37265, 2001.

29. Scorilas, A., Karameris, A., Arnogiannaki, N., Ardavanis, A., Bassilopoulos, P., Trangas, T., and Talieri, M. Overexpression of matrix-metalloproteinase-9 in human breast cancer: a potential favourable indicator in node-negative patients. Br. J. Cancer, *84:* 1488–1496, 2001.
30. Rolli, M., Fransvea, E., Pilch, J., Saven, A., Felding-Habermann, B. Activated integrin $\alpha_v\beta_3$ cooperates with metalloproteinase MMP-9 in regulating migration of metastatic breast cancer cells. Proc. Natl. Acad. Sci. USA, *100:* 9482–9487, 2003.
31. Soini, Y., Hurskainen, T., Hoyhtya, M., Oikarinen, A., Autio-Harmainen, H. 72 KD and 92 KD type IV collagenase, type IV collagen, and laminin mRNAs in breast cancer: a study by *in situ* hybridization. J. Histochem. Cytochem., *42:* 945–951, 1994.
32. Morgan, M. P., Cooke, M. M., Christopherson, P. A., Westfall, P. R., and McCarthy, G. M. Calcium hydroxyapatite promotes mitogenesis and matrix metalloproteinase expression in human breast cancer cell lines. Mol. Carcinog., *32:* 111–117, 2001.
33. Hazan, R. B., Phillips, G. R., Qiao, R. F., Norton, L., and Aaronson, S. A. Exogenous expression of N-cadherin in breast cancer cells induces cell migration, invasion, and metastasis. J. Cell Biol., *148:* 779–790, 2000.
34. Reddy, K. B., Krueger, J. S., Kondapaka, S. B., and Diglio, C. A. Mitogen-activated protein kinase (MAPK) regulates the expression of progelatinase B (MMP-9) in breast epithelial cells. Int. J. Cancer, *82:* 268–273, 1999.
35. Duivenvoorden, W. C., Hirte, H. W., and Singh, G. Transforming growth factor β1 acts as an inducer of matrix metalloproteinase expression and activity in human bone-metastasizing cancer cells. Clin. Exp. Metastasis, *17:* 27–34, 1999.
36. Toth, M., Sado, Y., Ninomiya, Y., and Fridman, R. Biosynthesis of α 2(IV) and α (IV) chains of collagen IV and interactions with matrix metalloproteinase-9. J. Cell. Physiol., *180:* 131–139, 1999.
37. Price, D. J., Avraham, S., Feuerstein, J., Fu, Y., and Avraham, H. K. The invasive phenotype in HMT-3522 cells requires increased EGF receptor signaling through both PI 3-kinase and ERK 1,2 pathways. Cell Commun. Adhes., *9:* 87–102, 2002.
38. Nguyen, M., Arkell, J., and Jackson, C. J. Active and tissue inhibitor of matrix metalloproteinase-free gelatinase B accumulates within human microvascular endothelial vesicles. J. Biol. Chem., *273:* 5400–5404, 1998.
39. Poulsom, R., Hanby, A. M., Pignatelli, M., Jeffery, R. E., Longcroft, J. M., Rogers, L., and Stamp, G. W. Expression of gelatinase A and TIMP-2 mRNAs in desmoplastic fibroblasts in both mammary carcinomas and basal cell carcinomas of the skin. J. Clin. Pathol., *46:* 429–436, 1993.
40. Albini, A., Melchiori, A., Santi, L., Liotta, L. A., Brown, P. D., and Stetler-Stevenson, W. G. Tumor cell invasion inhibited by TIMP-2. J. Natl. Cancer Inst. (Bethesda), *83:* 775–779, 1991.
41. Imren, S., Kohn, D. B., Shimada, H., Blavier, L., and DeClerck, Y. A. Overexpression of tissue inhibitor of metalloproteinases-2 retroviral-mediated gene transfer *in vivo* inhibits tumor growth and invasion. Cancer Res., *56:* 2891–2895, 1996.
42. Liu, Y. E., Wang, M., Greene, J., Su, J., Ullrich, S., Li, H., Sheng, S., Alexander, P., Sang, Q. A., and Shi, Y. E. Preparation and characterization of recombinant tissue inhibitor of metalloproteinase 4 (TIMP-4). J. Biol. Chem., *272:* 20479–20483, 1997.
43. Khokha, R., Waterhouse, P., Yagel, S., Lala, P. K., Overall, C. M., Norton, G., and Denhardt, D. T. Antisense RNA-induced reduction in murine TIMP levels confers oncogenicity on Swiss 3T3 cells. Science (Wash. DC), *243:* 947–950, 1989.
44. Mohanam, S., Wang, S. W., Rayford, A., Yamamoto, M., Sawaya, R., Nakajima, M., Liotta, L. A., Nicolson, G. L., Stetler-Stevenson, W. G., and Rao, J. S. Expression of tissue inhibitors of metalloproteinases: negative regulators of human glioblastoma invasion *in vivo*. Clin. Exp. Metastasis, *13:* 57–62, 1995.
45. DeClerck, Y. A., Perez, N., Shimada, H., Boone, T. C., Langley, K. E., and Taylor, S. M. Inhibition of invasion and metastasis in cells transfected with an inhibitor of metalloproteinases. Cancer Res., *52:* 701–708, 1992.
46. Wang, M., Liu, Y. E., Greene, J., Sheng, S., Fuchs, A., Rosen, E. M., and Shi, Y. E. Inhibition of tumor growth and metastasis of human breast cancer cells transfected with tissue inhibitor of metalloproteinase 4. Oncogene, *14:* 2767–2774, 1997.
47. Celiker, M. Y., Wang, M., Atsidaftos, E., Liu, X., Liu, Y. E., Jiang, Y., Valderrama, E., Goldberg, I. D., and Shi, Y. E. Inhibition of Wilms' tumor growth by intramuscular administration of tissue inhibitor of metalloproteinases-4 plasmid DNA. Oncogene, *20:* 4337–4343, 2001.
48. Ree, A. H., Florenes, V. A., Berg, J. P., Maelandsmo, G. M., Nesland, J. M., and Fodstad, O. High levels of messenger RNAs for tissue inhibitors of metalloproteinases (TIMP-1 and TIMP-2) in primary breast carcinomas are associated with development of distant metastases. Clin. Cancer Res., *3:* 1623–1628, 1997.
49. Jiang, Y., Goldberg, I. D., and Shi, Y. E. Complex roles of tissue inhibitors of metalloproteinases in cancer. Oncogene, *21:* 2245–2252, 2002.
50. Nielsen, B. S., Sehested, M., Kjeldsen, L., Borregaard, N., Rygaard, J., and Dano, K. Expression of matrix metalloprotease-9 in vascular pericytes in human breast cancer. Lab. Investig., *77:* 345–355, 1997.

Catalytic- and ecto-domains of membrane type 1-matrix metalloproteinase have similar inhibition profiles but distinct endopeptidase activities

Douglas R. HURST*, Martin A. SCHWARTZ*, Mohammad A. GHAFFARI*, Yonghao JIN*, Harald TSCHESCHE†, Gregg B. FIELDS‡ and Qing-Xiang Amy SANG*[1]

*Department of Chemistry and Biochemistry and Institute of Molecular Biophysics, 203 Dittmer Laboratory of Chemistry Building, Florida State University, Tallahassee, FL 32306, U.S.A., †Department of Biochemistry, University of Bielefeld, 33615 Bielefeld, Germany, and ‡Department of Chemistry and Biochemistry, Florida Atlantic University, Boca Raton, FL 33431, U.S.A.

Membrane type 1-matrix metalloproteinase (MT1-MMP/MMP-14) is a major collagenolytic enzyme that plays a vital role in development and morphogenesis. To elucidate further the structure–function relationship between the human MT1-MMP active site and the influence of the haemopexin domain on catalysis, substrate specificity and inhibition kinetics of the cdMT1-MMP (catalytic domain of MT1-MMP) and the ecto domain ΔTM-MT1-MMP (transmembrane-domain-deleted MT1-MMP) were compared. For substrate **1** [Mca-Pro-Leu-Gly-Leu-Dpa-Ala-Arg-NH_2, where Mca stands for (7-methoxycoumarin-4-yl)acetyl- and Dpa for *N*-3-(2,4-dinitrophenyl)-L-2,3-diaminopropionyl], the activation energy E_a was determined to be 11.2 and 12.2 kcal/mol (1 cal = 4.184 J) for cdMT1-MMP and ΔTM-MT1-MMP respectively, which is consistent with k_{cat}/K_M values of 7.37 and 1.46×10^4 $M^{-1} \cdot s^{-1}$. The k_{cat}/K_M values for a series of similar single-stranded peptide substrates were determined and found to correlate with a slope of 0.17 for the two enzyme forms. A triple-helical peptide substrate was predicted to have a k_{cat}/K_M of 0.87×10^4 $M^{-1} \cdot s^{-1}$ for ΔTM-MT1-MMP based on the value for cdMT1-MMP of 5.12×10^4 $M^{-1} \cdot s^{-1}$; however, the actual value was determined to be 2.5-fold higher, i.e. 2.18×10^4 $M^{-1} \cdot s^{-1}$. These results suggest that cdMT1-MMP is catalytically more efficient towards small peptide substrates than ΔTM-MT1-MMP and the haemopexin domain of MT1-MMP facilitates the hydrolysis of triple-helical substrates. Diastereomeric inhibitor pairs were utilized to probe further binding similarities at the active site. Ratios of K_i values for the inhibitor pairs were found to correlate between the enzyme forms with a slope of 1.03, suggesting that the haemopexin domain does not significantly modify the enzyme active-site structure.

Key words: activation energy, catalytic domain, diastereomeric MMP inhibitors, ecto-domain, membrane type 1-matrix metalloproteinase (MT1-MMP), substrate specificity.

INTRODUCTION

Matrix metalloproteinases (MMPs) are a family of related zinc endopeptidases known to play prominent roles during normal and pathological extracellular matrix remodelling events including cancer progression [1]. The first identified membrane type MMP, MT1-MMP, has been shown to play a key role in tumour cell invasion and metastasis by complex mechanisms, including activation of proMMP-2 and direct hydrolysis of interstitial collagens [2,3]. MT1-MMP is tethered to the cell membrane by a type 1 transmembrane region and is expressed as an active protease on the cell surface upon activation, primarily by proprotein convertases such as furin or furin-like serine proteinases [4]. In addition, consistent with other MMP family members, MT1-MMP has a propeptide, catalytic domain linker region and a haemopexin domain [5].

The haemopexin domain has been supposed to function mainly in protein-substrate recognition [6]. It is necessary for native type I collagen cleavage for reasons that are not completely understood [7,8]. Recently, new roles have been identified for the MT1-MMP haemopexin domain including enzymic regulation and subcellular localization [9,10]. Additionally, the linker region between the catalytic and haemopexin domains has been identified as having the ability to bind the collagen [11]. It is possible that this region is necessary for triple-helical substrate hydrolysis.

Although several groups have reported the cleavage of extracellular matrix constituents by MT1-MMP [12–14], a structural comparison of the active site of the catalytic domain with and without the haemopexin domain has not been accomplished. In the present study, a comparison of the substrate specificity for two truncated forms of MT1-MMP was performed using single-stranded peptide substrates. The haemopexin domain was then found to facilitate the hydrolysis of a triple-helical substrate. To demonstrate that the haemopexin domain does not influence the architecture of the active site, diastereomeric inhibitor pairs were utilized to show identical K_i ratios.

MATERIALS AND METHODS

Materials

Quenched fluorogenic peptide substrates (see Table 1) **1** and **3**–**5** [Mca-Pro-Leu-Gly-Leu-Dpa-Ala-Arg-NH_2, Mca-Pro-Lys-Pro-Leu-Ala-Leu-Dpa-Ala-Arg-NH_2, Mca-Arg-Pro-Lys-Pro-Tyr-Ala-Nva-Trp-Met-Lys-Dpa-NH_2 and Mca-Pro-Leu-Ala-Gln-Ala-Val-Dpa-Arg-Ser-Ser-Arg-NH_2, where Mca stands for (7-methyloxycoumarin-4-yl)acetyl, Dpa stands for *N*-3-(2,4-dinitrophenyl)-L-2,3-diaminopropionyl and Nva for norvaline] were purchased from Bachem and **2** (Mca-Pro-Leu-Ala-Nva-Dpa-Ala-Arg-NH_2) was from Calbiochem (San Diego, CA, U.S.A.). The triple-helical peptide substrate **6** [{(GPP*)$_5$ GPK(Mca)GPQGLRGQK(Dnp)GVR(GPP*)$_5$-NH_2}$_3$, where Dnp stands for 2,4-dinitrophenyl and P* for 4-hydroxy-L-proline] was synthesized as described previously [15]. The mercaptosulphide

Abbreviations used: MMP, matrix metalloproteinase; MT1, membrane type 1; cdMT1-MMP, catalytic domain of MT1-MMP; Dpa, *N*-3-(2,4-dinitrophenyl)-L-2,3-diaminopropionyl; Mca, (7-methoxycoumarin-4-yl)acetyl; Nva, norvaline; RTTI, rat-tail tendon type I collagen; TIMP, tissue inhibitor of metalloproteinase; ΔTM-MT1-MMP, transmembrane-domain-deleted MT1-MMP.

[1] To whom correspondence should be addressed (e-mail qxsang@chem.fsu.edu).

inhibitors were synthesized and characterized as described previously ([16,17]; Y. Jin and M. A. Schwartz, unpublished work). Hydroxamate inhibitors 444237 and 444238 were purchased from Calbiochem. The recombinant human cdMT1-MMP (catalytic domain of MT1-MMP; Ile^{114}–Ile^{318}) was expressed in *Escherichia coli* and was activated by autocatalysis [18] and ΔTM-MT1-MMP (transmembrane-domain-deleted MT1-MMP), the recombinant human ectodomain of MT1-MMP (Tyr^{112}–Glu^{523} consisting of the catalytic domain and the haemopexin domain) was expressed in *Pichia pastoris* and activated by yeast proteinases during maturation [19]. Human TIMP-2 (tissue inhibitor of metalloproteinase-2) was kindly provided by Professor Jack Windsor of Indiana University (Indianapolis, IN, U.S.A.). All standard chemicals were purchased from Fisher with the exception of 5,5′-dithio(bis-2-nitrobenzoate), which was from Sigma.

Enzyme kinetics

Kinetic assays were performed as described previously [20] in 50 mM Hepes buffer (pH 7.5), with 10 mM $CaCl_2$, 0.2 M NaCl and 0.05 % Brij-35 (polyoxyethylene lauryl ether) at 25 °C. The final substrate concentration was 1 μM (1 % DMSO), which is at least 10-fold lower than K_M. Hence k_{cat}/K_M is calculated using the equation:

$$\frac{k_{cat}}{K_M} = \frac{v}{[E][S]}$$

where v is the initial rate and [E] and [S] are the enzyme and substrate concentrations respectively. The activation energy E_a was determined by the Arrhenius equation:

$$\ln v = -\frac{E_a}{RT} + \ln A[ES]$$

where R is the universal/ideal gas constant, T the absolute temperature in Kelvin, A the collision constant/Arrhenius A factor/pre-exponential factor and [ES] the concentration of the enzyme–substrate complex. The initial rates were determined at 283 K and then at increments of 5 K up to 313 K. The fluorescence intensity was corrected for temperature using the standard Mca-Pro-Leu-OH (Bachem). For the inhibition assays, the inhibitors were incubated with enzyme for 15–30 min before adding substrate **1** to ensure equilibrium conditions. The inhibitor dissociation constant K_i was determined as described previously [21] using the Morrison equation [22]:

$$\frac{v_i}{v_o} = \frac{[E]_o + [I]_o - K_i^{app} + \sqrt{\left([I]_o + K_i^{app} - [E]_o\right)^2 + 4[E]_o K_i^{app}}}{2[E]_o}$$

where v_i and v_o are the initial rates with and without the inhibitor respectively, $[E]_o$ and $[I]_o$ are the initial enzyme and inhibitor concentrations respectively and K_i^{app} is the apparent K_i that is equal to the true K_i under the conditions of $[S] \ll K_M$ for competitive inhibition according to the equation:

$$K_i^{app} = K_i\left(1 + \frac{[S]}{K_M}\right)$$

The active mercaptosulphide inhibitor concentration was quantified with Ellman's reagent 5,5′-dithiobis-(2-nitrobenzoate) [23,24]. Active cdMT1-MMP and ΔTM-MT1-MMP concentrations were normalized by titration with standardized preparations of recombinant TIMP-2. The titration was performed as described above for determination of K_i with an $[E]/K_i$ ratio > 100 to ensure proper titrating conditions.

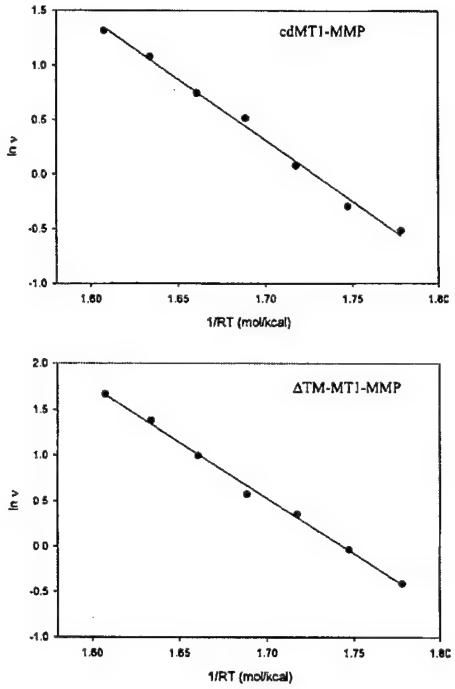

Figure 1 Arrhenius plot

E_a values were determined for the hydrolysis of substrate **1** with (**A**) cdMT1-MMP and (**B**) ΔTM-MT1-MMP as described in the Materials and methods section. Initial rates are expressed in nM/min. Fluorescence intensity was temperature-corrected. The slope of the line $-E_a$ (kcal/mol) was 11.2 and 12.2 for (**A**) and (**B**) respectively.

Collagen hydrolysis and electrophoresis

Samples containing 280 μg/ml purified RTTI (rat-tail tendon type I collagen) [20] were incubated with 80 nM enzyme at 37 °C in 50 mM Hepes (pH 7.5), 10 mM $CaCl_2$, 0.2 M NaCl and 0.05 % Brij-35. The reactions were stopped with 50 mM EDTA, 100 mM dithiothreitol and boiled for 5 min. The samples were analysed by SDS/PAGE (7 % gel) with silver staining. The cdMT1-MMP and ΔTM-MT1-MMP samples were visualized by a Western blot (12 % SDS/polyacrylamide gel) using a previously characterized antibody [3].

RESULTS

Substrate specificity

The catalytic domain alone is predicted to hydrolyse small peptide substrates more efficiently than ΔTM-MT1-MMP if the active sites are identical, possibly due to flexibility, rotational freedom or substrate exosite binding. The activation energy for enzyme hydrolysis of peptides should therefore be lower for cdMT1-MMP when compared with ΔTM-MT1-MMP. The E_a values for substrate **1** (see Table 1) with cdMT1-MMP and ΔTM-MT1-MMP were determined to be 11.2 and 12.2 kcal/mol respectively (Figure 1). Consistently, the k_{cat}/K_M values were 7.37 and $1.46 \times 10^4\ M^{-1} \cdot s^{-1}$ respectively (Table 1). If the peptide binds to a haemopexin exosite region, the effective substrate concentration would be reduced, subsequently lowering the apparent k_{cat}/K_M.

Table 1 Comparison of substrate specificity

Fluorogenic peptide substrates	k_{cat}/K_M ($\times 10^4$ $s^{-1} \cdot M^{-1}$) cdMT1	ΔTM
1 Mca-Pro-Leu-Gly ↓ Leu-Dpa-Ala-Arg-NH_2	7.37	1.46
2 Mca-Pro-Leu-Ala ↓ Nva-Dpa-Ala-Arg-NH_2	2.27	0.25
3 Mca-Pro-Lys-Pro-Leu-Ala ↓ Leu-Dpa-Ala-Arg-NH_2	7.82	1.04
4 Mca-Arg-Pro-Lys-Pro-Tyr-Ala ↓ Nva-Trp-Met-Lys-Dpa-NH_2	1.81	0.15
5 Mca-Pro-Leu-Ala ↓ Gln-Ala-Val-Dpa-Arg-Ser-Ser-Arg-NH_2	0.18	0.02
6 {(GPP*)$_5$GPK(Mca)GPQG ↓ LRGQK(Dnp)GVR(GPP*)$_5$-NH_2}$_3$*	5.12	2.18

* Single-letter amino acid abbreviations are used here. P* stands for 4-hydroxy-L-proline. The arrow indicates the putative cleavage site.

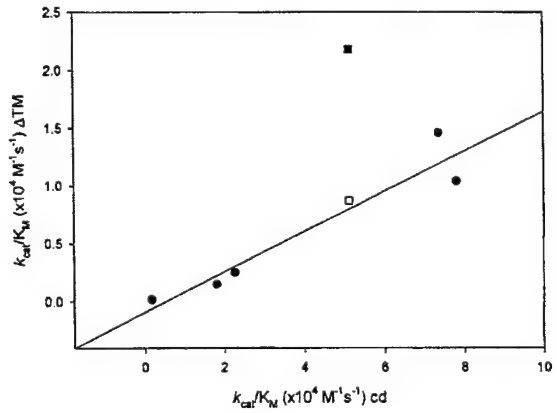

Figure 2 Correlation of specificity constants

The k_{cat}/K_M values from Table 1 for the single-stranded peptides **1–5** were plotted (●) and found to have a slope of 0.17. The triple-helical substrate **6** was predicted to have a k_{cat}/K_M value of 0.87×10^4 $M^{-1} \cdot s^{-1}$ for ΔTM-MT1-MMP (□) based on the value of 5.12×10^4 $M^{-1} \cdot s^{-1}$ for cdMT1-MMP. The actual value was determined to be 2.5-fold higher, i.e. 2.18×10^4 $M^{-1} \cdot S^{-1}$ (■).

Since the E_a and k_{cat}/K_M values correlate, exosite binding is probably not a valid reason for differences in hydrolytic efficiency. These results suggest that cdMT1-MMP is slightly more efficient than ΔTM-MT1-MMP for hydrolysing single-stranded peptides as predicted.

This trend was also noted with other similar peptides and a correlation curve was constructed with the k_{cat}/K_M values giving a slope of 0.17 (Table 1 and Figure 2). A prediction of k_{cat}/K_M values for ΔTM-MT1-MMP may then be found by multiplying the k_{cat}/K_M values for cdMT1-MMP by 0.17. The fluorescently labelled triple-helical peptide that was characterized previously [15] was tested with cdMT1-MMP and was found to have a k_{cat}/K_M value of 5.12×10^4 $M^{-1} \cdot s^{-1}$. Assuming this substrate is hydrolysed similarly to the single-stranded peptides, the predicted k_{cat}/K_M value would be 0.87×10^4 $M^{-1} \cdot s^{-1}$ for ΔTM-MT1-MMP (Figure 2, open square); however, the actual value was determined to be 2.18×10^4 $M^{-1} \cdot s^{-1}$, a value 2.5-fold higher (Figure 2, closed square).

Probing the active site

The difference in the predicted and actual values for triple-helical substrate hydrolysis by ΔTM-MT1-MMP may be due to structural differences at the active site. To probe the active-site structure, the inhibition profiles for cdMT1-MMP and ΔTM-MT1-MMP were compared with diastereomeric inhibitor pairs (Figure 3 and Table 2). The correct stereochemistry of these inhibitors is important for potency towards MT1-MMP as noted by the large differences in K_i values between inhibitor pairs. The K_i values were generally lower for cdMT1-MMP when compared with those for ΔTM-MT1-MMP, which is consistent with the peptide studies. Interestingly, the ratios of K_i values for diastereomers correlated with a slope of 1.03 between cdMT1-MMP and ΔTM-MT1-MMP (Figure 4). These results demonstrate that the haemopexin domain has no direct influence on the structure of the active site of the enzyme.

To ensure that ΔTM-MT1-MMP is a fully functional enzyme (i.e. ability to cleave collagen), RTTI was utilized as a substrate. Figure 5(B) shows the ability of this enzyme form to degrade native RTTI at 37 °C (three-quarter and one-quarter fragments not shown). The RTTI was not hydrolysed by cdMT1-MMP under the same conditions (reaction was also followed overnight with the same results; not shown). The same assay was performed with RTTI preparations that were first boiled for 5 min. Both the enzymes rapidly degraded the denatured RTTI (gelatin) samples. These results demonstrate that both enzyme forms maintain hydrolytic characteristics consistent with published reports.

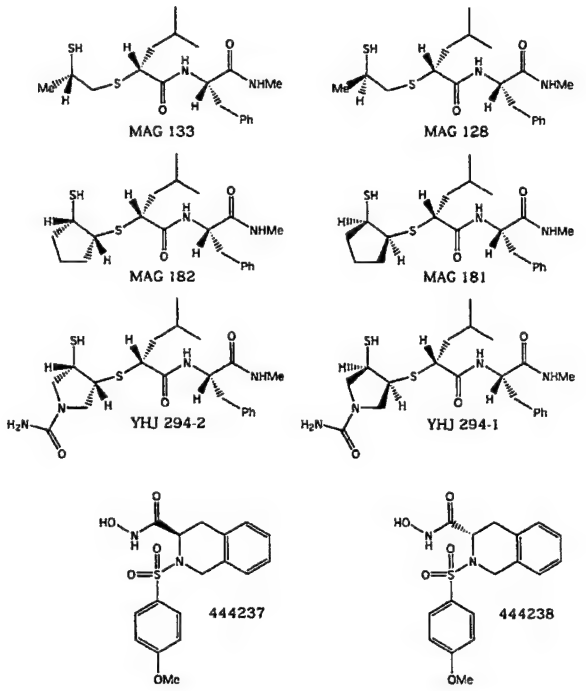

Figure 3 Inhibitor structures

The inhibitors are shown as pairs of diastereomers with the more potent inhibitor on the left. K_i values are shown in Table 2.

Table 2 K_i values of the inhibitor

Inhibitor	cdMT1 K_i (nM)	cdMT1 K_i ratio of the isomer	ΔTM-MT1 K_i (nM)	ΔTM-MT1 K_i ratio of the isomer
MAG 133	19	4	26	6
MAG 128	70		150	
MAG 182	24	11	29	19
MAG 181	259		540	
YHJ 294-2	13	231	24	242
YHJ 294-1	3000		5800	
444237	0.5	90	0.5	110
444238	45		55	

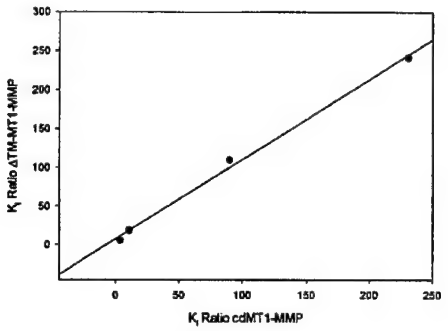

Figure 4 Correlation of diastereomer K_i ratio

The ratios from Table 2 were plotted and found to have a correlation of 1.03 ($r^2 = 0.9961$).

DISCUSSION

The haemopexin domain in MMPs is necessary for the cleavage of native interstitial type I–III collagens by mechanisms that are not completely understood [7,8]. In this study, the substrate specificity and inhibition of cdMT1-MMP was compared with ΔTM-MT1-MMP. The enzyme concentrations were normalized by titration with TIMP-2. Both forms of the enzyme were found to be fully active, as demonstrated by hydrolysis of either native or denatured RTTI, in addition to showing a single band on a Western blot. Although collagenolytic assays are typically performed at 25 °C, no cleavage was detected after incubation for up to 2 days at room temperature (23 °C). This is consistent with an earlier study that showed MT1-MMP does not hydrolyse type I collagen at 25 °C [13], although other groups have demonstrated cleavage [12,14]. The assay temperature was therefore increased to 37 °C to allow more flexibility in the collagen strands that are more readily hydrolysed. ΔTM-MT1-MMP alone is not stable after prolonged incubation at 37 °C; however, in the presence of a substrate (or an inhibitor), the stability is significantly improved (results not shown).

It may be expected that if the active sites were the same, the catalytic domain alone would be a more efficient enzyme to hydrolyse single-stranded peptides due to hindrance by the haemopexin domain. This domain may limit enzyme flexibility, diffusion of peptide into the enzyme-active site or alternatively decrease effective substrate concentration by exosite binding. The activation energies for substrate **1** are consistent with k_{cat}/K_M values which may suggest enzyme flexibility or diffusion as possible reasons for the difference. The k_{cat}/K_M values for five similar single-stranded peptides were correlated between both forms of the enzyme. The k_{cat}/K_M value for triple-helical substrates will correspond to this fit if the enzyme hydrolyses these substrates in a manner similar to the single-stranded substrates. Although the absolute k_{cat}/K_M values were slightly higher for cdMT1-MMP, the values did not correlate with the single-stranded substrates. Therefore the haemopexin domain of MT1-MMP facilitates the hydrolysis of triple-helical peptide substrates, consistent with previous studies, indicating that the haemopexin domain of

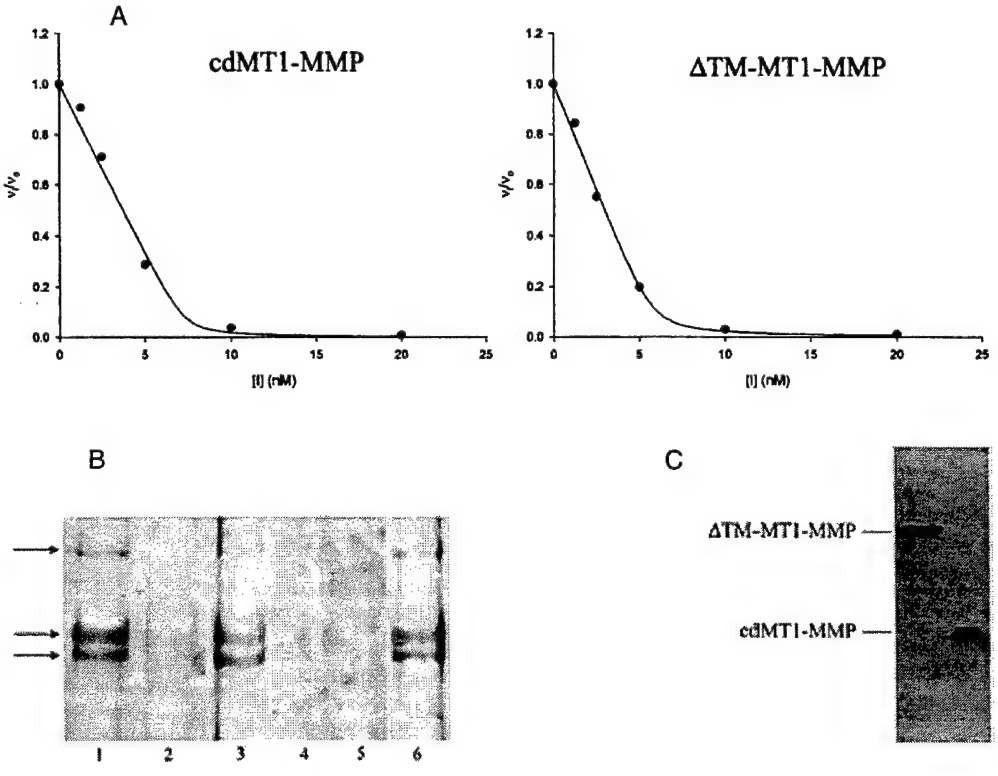

Figure 5 Enzyme titration and collagen cleavage

(**A**) The concentrations of active cdMT1-MMP and ΔTM-MT1-MMP were normalized by titration with TIMP-2 as described in the Materials and methods section: [E] = [I] at the *x*-intercept. (**B**) Collagen cleavage was verified for ΔTM-MT1-MMP with RTTI. Either ΔTM-MT1-MMP (lanes 2 and 4) or cdMT1-MMP (lanes 3 and 5) at 80 nM was incubated with 280 μg/ml RTTI (lanes 1–3 native; lanes 4–6 denatured by first boiling for 5 min) at 37 °C for 8 h. The reactions were stopped with 50 mM EDTA, 100 mM dithiothreitol and boiling for 5 min. The samples were analysed by SDS/PAGE (7 % gel) with silver staining. Lane 1 is native RTTI only and lane 6 is denatured RTTI only. (**C**) Western blot (SDS/PAGE, 12 % gel) of the purified enzymes shows one band for the ΔTM-MT1-MMP sample.

MT1-MMP modulates activity towards proteinaceous substrates [25].

Diastereomeric inhibitor pairs were utilized to probe the architecture of the enzyme-active site. Structural differences between the enzyme forms would be expected to be shown by different K_i ratios for inhibition by the pairs of stereoisomeric compounds tested. A correlation of 1 between the enzymes demonstrates that no significant differences were found at the active site. Although several groups have published the requirement of the haemopexin domain to hydrolyse native type I–III collagens, no previous report has addressed an active-site comparison for MT1-MMP with and without the haemopexin domain.

The triple-helical peptidase activities of collagenolytic enzymes (MMP-1, MMP-13 and MT1-MMP) exhibit noteworthy differences. MT1-MMP shows triple-helical peptidase activity much greater than either MMP-1 or MMP-13 [15]. The haemopexin domain of MMP-1 appears to have virtually no influence on triple-helical peptidase activity [15,26], unlike MT1-MMP. MMP-13 shows a far greater difference between single-stranded and triple-helical substrate hydrolysis compared with either MMP-1 or MT1-MMP [15,27]. Thus, although a number of MMP family members are classified as 'collagenolytic', their precise mechanisms for binding, distorting and hydrolysing triple-helical structures are almost certainly different in subtle, but as yet undefined, ways.

One important question remaining is how does the haemopexin domain influence the catalytic activity of MT1-MMP? It has been proposed that triple-helical peptidase and collagenase activity are distinguishable, as the catalytic domains of collagenases have the ability to cleave triple-helical peptides but not collagens [26]. The haemopexin domain may therefore be required for proper orientation and distortion of the collagen. Overall and co-workers [11] recently found that it is the linker region between the catalytic and haemopexin domain that is necessary for native type I collagen binding. The linker region may influence triple-helicase activity. Without knowing the three-dimensional structural organization of the linker and haemopexin domain, it is difficult to address specifically how the activities of MMPs are modulated by their structural motifs and domains.

We thank Professor L. Jack Windsor of Indiana University for providing us with purified human TIMP-2 protein and Janelle Lauer-Fields of Florida Atlantic University for synthesizing the triple-helical substrate. We are grateful to Dr Yunge Zhao for isolation of RTTI, and Robert Newcomer, Dr Hyun I. Park and Dr Tiebang Kang for a critical reading of the manuscript and valuable discussions. This work was supported by a predoctoral fellowship award from D. O. D./U.S. Army Breast Cancer Research Program DAMD17-00-1-0243 (to D. R. H.), and grants from D. O. D./U. S. Army Prostate Cancer Research Program DAMD17-02-1-238, National Institutes of Health (NIH) CA78646 (to Q.-X. A. S.), CA77402 and CA98799 (to G. B. F.), a grant from the Molecular Design and Synthesis (MDS) Research Foundation (to M. A. S.), and by the Deutsche Forschungsgemeinschaft (DFG), Bonn (SFB 549, project A05 and DFG grant Ts 8-35/3) to H. T.

REFERENCES

1 McCawley, L. J. and Matrisian, L. M. (2001) Matrix metalloproteinases: they're not just for matrix anymore! Curr. Opin. Cell Biol. **13**, 534–540
2 Sato, H., Takino, T., Okada, Y., Cao, J., Shinagawa, A., Yamamoto, E. and Seiki, M. (1994) A matrix metalloproteinase expressed on the surface of invasive tumour cells. Nature (London) **370**, 61–65
3 Li, H., Bauzon, D. E., Xu, X., Tschesche, H., Cao, J. and Sang, Q.-X. A. (1998) Immunological characterization of cell-surface and soluble forms of membrane type 1 matrix metalloproteinase in human breast cancer cells and in fibroblasts. Mol. Carcinogen. **22**, 84–94
4 Yana, I. and Weiss, S. J. (2000) Regulation of membrane type-1 matrix metalloproteinase activation by proprotein convertases. Mol. Biol. Cell. **11**, 2387–2401
5 Sternlicht, M. D. and Werb, Z. (2001) How matrix metalloproteinases regulate cell behavior. Annu. Rev. Cell Dev. Biol. **17**, 463–516
6 Murphy, G. and Knäuper, V. (1997) Relating matrix metalloproteinase structure to function: why the 'hemopexin' domain? Matrix Biol. **15**, 511–518
7 Overall, C. M. (2002) Molecular determinants of metalloproteinase substrate specificity: matrix metalloproteinase substrate binding domains, modules, and exosites. Mol. Biotech. **22**, 51–86
8 Lauer-Fields, J. L., Juska, D. and Fields, G. B. (2002) Matrix metalloproteinases and collagen catabolism. Biopolymers **66**, 19–32
9 Mori, H., Tomari, T., Koshikawa, N., Kajita, M., Itoh, Y., Sato, H., Tojo, H., Yana, I. and Seiki, M. (2002) CD44 directs membrane-type 1 matrix metalloproteinase to lamellipodia by associating with its hemopexin-like domain. EMBO J. **21**, 3949–3959
10 Lehti, K., Lohi, J., Juntunen, M. M., Pei, D. and Keski-Oja, J. (2002) Oligomerization through hemopexin and cytoplasmic domains regulates the activity and turnover of membrane-type 1 matrix metalloproteinase. J. Biol. Chem. **277**, 8440–8448
11 Tam, E., Wu, Y. I., Butler, G. S., Stack, M. S. and Overall, C. M. (2002) Collagen binding properties of the membrane type-1 matrix metalloproteinase (MT1-MMP) hemopexin C domain. The ectodomain of the 44-kDa autocatalytic product of MT1-MMP inhibits cell invasion by disrupting native type I collagen cleavage. J. Biol. Chem. **277**, 39005–39014
12 Ohuchi, E., Imai, K., Fujii, Y., Sato, H., Seiki, M. and Okada, Y. (1997) Membrane type 1 matrix metalloproteinase digests interstitial collagens and other extracellular matrix macromolecules. J. Biol. Chem. **272**, 2446–2451
13 Pei, D. and Weiss, S. J. (1996) Transmembrane-deletion mutants of the membrane-type matrix metalloproteinase-1 process progelatinase A and express intrinsic matrix-degrading activity. J. Biol. Chem. **271**, 9135–9140
14 d'Ortho, M. P., Will, H., Atkinson, S., Butler, G., Messent, A., Gavrilovic, J., Smith, B., Timpl, R., Zardi, L. and Murphy, G. (1997) Membrane-type matrix metalloproteinases 1 and 2 exhibit broad-spectrum proteolytic capacities comparable to many matrix metalloproteinases. Eur. J. Biochem. **250**, 751–757
15 Lauer-Fields, J. L., Broder, T., Sritharan, T., Chung, L., Nagase, H. and Fields, G. B. (2001) Kinetic analysis of matrix metalloproteinase activity using fluorogenic triple-helical substrates. Biochemistry **40**, 5795–5803
16 Schwartz, M. A. and van Wart, H. E. (1995) Mercaptosulfide metalloproteinase inhibitors. U.S. Patent 5455262
17 Jin, Y., Ghaffari, M. A. and Schwartz, M. A. (2002) A practical synthesis of differentially-protected *cis*-1,2-cyclopentanedithiols and *cis*-3,4-pyrrolidinedithiols. Tetrahedron Lett. **43**, 7319–7321
18 Lichte, A., Kolkenbrock, H. and Tschesche, H. (1996) The recombinant catalytic domain of membrane-type matrix metalloproteinase-1 (MT1-MMP) induces activation of progelatinase A and progelatinase A complexed with TIMP-2. FEBS Lett. **397**, 277–282
19 Roderfeld, M., Büttner, F. H., Bartnik, E. and Tschesche, H. (2000) Expression of human membrane type 1 matrix metalloproteinase in Pichia pastoris. Protein Expr. Purif. **19**, 369–374
20 Park, H. I., Ni, J., Gerkema, F. E., Liu, D., Belozerov, V. E. and Sang, Q.-X. A. (2000) Identification and characterization of human endometase (matrix metalloproteinase-26) from endometrial tumour. J. Biol. Chem. **275**, 20540–20544
21 Park, H. I., Turk, B. E., Gerkema, F. E., Cantley, L. C. and Sang, Q.-X. A. (2002) Peptide substrate specificities and protein cleavage sites of human endometase/matrilysin-2/matrix metalloproteinase-26. J. Biol. Chem. **277**, 35168–35175
22 Morrison, J. F. (1969) Kinetics of the reversible inhibition of enzyme-catalysed reactions by tight-binding inhibitors. Biochim. Biophys. Acta **185**, 269–286
23 Riddles, P. W., Blakeley, R. L. and Zerner, B. (1979) Ellman's reagent: 5,5′-dithiobis(2-nitrobenzoic acid) – a re-examination. Anal. Biochem. **94**, 75–81
24 Sang, Q.-X. A., Jia, M.-C., Schwartz, M. A., Jaye, M. C., Kleinman, H. K., Ghaffari, M. A. and Luo, Y.-L. (2000) New thiol and sulfodiimine metalloproteinase inhibitors and their effect on human microvascular endothelial cell growth. Biochem. Biophys. Res. Commun. **274**, 780–786
25 Itoh, Y., Takamura, A., Ito, N., Maru, Y., Sato, H., Suenaga, N., Aoki, T. and Seiki, M. (2001) Homophilic complex formation of MT1-MMP facilitates proMMP-2 activation on the cell surface and promotes tumour cell invasion. EMBO J. **20**, 4782–4793
26 Lauer-Fields, J. L., Tuzinski, K. A., Shimokawa, K., Nagase, H. and Fields, G. B. (2000) Hydrolysis of triple-helical collagen peptide models by matrix metalloproteinases. J. Biol. Chem. **275**, 13282–13290
27 Knäuper, V., López-Otin, C., Smith, B., Knight, G. and Murphy, G. (1996) Biochemical characterization of human collagenase-3. J. Biol. Chem. **271**, 1544–1550

Received 16 July 2003/2 September 2003; accepted 8 October 2003
Published as BJ Immediate Publication 8 October 2003, DOI 10.1042/BJ20031067

THE JOURNAL OF BIOLOGICAL CHEMISTRY
Vol. 277, No. 38, Issue of September 20, pp. 35168–35175, 2002
Printed in U.S.A.

Peptide Substrate Specificities and Protein Cleavage Sites of Human Endometase/Matrilysin-2/Matrix Metalloproteinase-26*

Received for publication, May 23, 2002, and in revised form, July 5, 2002
Published, JBC Papers in Press, July 15, 2002, DOI 10.1074/jbc.M205071200

Hyun I. Park‡, Benjamin E. Turk§, Ferry E. Gerkema‡, Lewis C. Cantley§, and Qing-Xiang Amy Sang‡¶

From the ‡Department of Chemistry and Biochemistry and Institute of Molecular Biophysics, Florida State University, Tallahassee, Florida 32306-4390 and the §Department of Medicine, Harvard Medical School, Beth Israel Deaconess Medical Center, Boston, Massachusetts 02215

Human endometase/matrilysin-2/matrix metalloproteinase-26 (MMP-26) is a novel epithelial and cancer-specific metalloproteinase. Peptide libraries were used to profile the substrate specificity of MMP-26 from the P4–P4′ sites. The optimal cleavage motifs for MMP-26 were Lys-Pro-Ile/Leu-Ser(P1)-Leu/Met(P1′)-Ile/Thr-Ser/Ala-Ser. The strongest preference was observed at the P1′ and P2 sites where hydrophobic residues were favored. Proline was preferred at P3, and Serine was preferred at P1. The overall specificity was similar to that of other MMPs with the exception that more flexibility was observed at P1, P2′, and P3′. Accordingly, synthetic inhibitors of gelatinases and collagenases inhibited MMP-26 with similar efficacy. A pair of stereoisomers had only a 40-fold difference in K_i^{app} values against MMP-26 compared with a 250-fold difference against neutrophil collagenase, indicating that MMP-26 is less stereoselective for its inhibitors. MMP-26 autodigested itself during the folding process. Two of the major autolytic sites were Leu^{49}–Thr^{50} and Ala^{75}–Leu^{76}, which still left the cysteine switch sequence (PHC^{82}GVPD) intact. This suggests that Cys^{82} may not play a role in the latency of the zymogen. Interestingly, inhibitor titration studies revealed that only ~5% of the total MMP-26 molecules was catalytically active, indicating that the thiol groups of Cys^{82} in the active molecules may be dissociated or removed from the active site zinc ions. MMP-26 cleaved Phe^{352}–Leu^{353} and Pro^{357}–Met^{358} in the reactive loop of α_1-proteinase inhibitor and His^{140}–Val^{141} in insulin-like growth factor-binding protein-1, probably rendering these substrates inactive. Among the fluorescent peptide substrates analyzed, Mca-Pro-Leu-Ala-Nva-Dpa-Ala-Arg-NH$_2$ displayed the highest specificity constant (30,000/molar second) with MMP-26. This report proposes a working model for the future studies of pro-MMP-26 activation, the design of inhibitors, and the identification of optimal physiological and pathological substrates of MMP-26 *in vivo*.

Matrix metalloproteinases (MMPs)[1] share a conservative metal binding sequence of HE*X*GH*XX*G*XX*HS and a turn containing methionine (1). Evidence suggests that MMPs may play important roles in extracellular matrix (ECM) remodeling in physiological processes (2, 3). Excessive breakdown of the ECM by MMPs is observed in pathological conditions including periodontitis, rheumatoid arthritis, and osteoarthritis. MMPs also participate in tumor cell invasion and metastasis by degrading the basement membrane and other ECM components and allowing the cancer cells to gain access to blood and lymphatic vessels (4). Analyses of a large number of peptide and protein substrates and more recent work with phage display and synthetic peptide libraries have led to the identification of consensus cleavage site motifs for a number of different MMPs (5–13). The substrate specificities of MMPs are quite similar to each other, showing strong preferences for hydrophobic residues at P1′. Although distinct MMPs often prefer the same type of amino acid residues at corresponding positions surrounding the cleavage site, differences in the orders of preference for specific residues at each position may more precisely determine MMP specificity for substrates.

Endometase (matrilysin-2/MMP-26) is the smallest member of the MMP family, with a molecular mass of 28 kDa (14–17). Sequence homology calculations identified metalloelastase (MMP-12) and stromelysin-1 (MMP-3) as the closest relatives. Nevertheless, the specificity constant profile of peptide substrates with MMP-26 was quite different from that with MMP-12 and MMP-3 (14). According to protein substrate studies *in vitro*, MMP-26 might process matrix proteins such as fibronectin, vitronectin, fibrinogen, type IV collagen, gelatinase B (MMP-9), and gelatin (14–17).

MMP-26 has been found to be highly expressed in several cancer cell lines. A significant level of expression in normal tissues was found only in the uterus and placenta. The limited occurrence of MMP-26 in normal tissues suggests that the production of this enzyme may be strictly regulated during specific events, such as implantation, and that MMP-26 could be a target enzyme for the treatment of cancer and other pathological conditions.

The biological function and substrate specificity of MMP-26 are not yet fully understood. According to the protein substrate

* This work was supported in part by a Department of Defense, U. S. Army Prostate Cancer Research Program Grant DAMD17-02-1-0238; a grant from the American Cancer Society, Florida Division F01FSU-1, the National Institutes of Health Grant CA78646; a grant from the Florida State University Research Foundation (to Q.-X. A. S.); National Science Foundation Postdoctoral Training Grant DBI 9602233 (to H. I. P.); National Institutes of Health Grant GM56203 (to L. C. C. and B. E. T.); and National Institutes of Health NRSA Fellowship GM19895 (to B. E. T.). The costs of publication of this article were defrayed in part by the payment of page charges. This article must therefore be hereby marked "*advertisement*" in accordance with 18 U.S.C. Section 1734 solely to indicate this fact.

¶ To whom correspondence should be addressed: Dept. of Chemistry and Biochemistry, Florida State University, Chemistry Research Bldg. (DLC), Rm. 203, Tallahassee, FL 32306-4390. Tel.: 850-644-8683; Fax: 850-644-8281; E-mail: qxsang@chem.fsu.edu; Website: www.chem.fsu.edu/editors/sang/sang.html.

[1] The abbreviations used are: MMP, matrix metalloproteinase; α_1-PI, α_1-protease inhibitor; Brij-35, polyoxyethylene lauryl ether; IGFBP-1, insulin-like growth factor binding protein-1; MALDI-TOF MS, matrix-assisted laser desorption ionization time-of-flight mass spectrometry; ECM, extracellular matrix; Tricine, *N*-[2-hydroxy-1,1-bis(hydroxymethyl)ethyl]glycine; Dnp, 2,4-dinitrophenyl; Dpa, *N*-3-(2,4-dinitrophenyl)-L-2,3-diaminopropionyl; Mca, (7-methoxycoumarin-4-yl)acetyl; Nva, non-valine.

studies *in vitro*, it may participate in ECM degradation. In this study, we take a step forward toward understanding the biochemical properties and functions of MMP-26 by identifying the cleavage sites of protein and peptide substrates, characterizing the substrate specificities of MMP-26 and measuring the potencies of synthetic inhibitors.

EXPERIMENTAL PROCEDURES

Materials—Dnp-Pro-Leu-Gly-Met-Trp-Ser-Arg-OH, Dnp-Pro-Leu-Ala-Tyr-Trp-Ala-Arg-OH, Mca-Pro-β-cyclohexylalanyl-Gly-Nva-His-Ala-Dpa-NH_2, Mca-Pro-Leu-Ala-Nva-Dpa-Ala-Arg-NH_2, insulin-like growth factor binding protein-1 (IGFBP-1), and MMP-specific synthetic inhibitors were purchased from Calbiochem, and Dnp-Pro-Leu-Gly-Leu-Trp-Ala-D-Arg-NH_2 and Mca-Arg-Pro-Lys-Pro-Val-Glu-Nva-Trp-Arg-Lys(Dnp)-NH_2 were purchased from Bachem. Hydroxamic acid derivatives of amino acids, buffers, cysteine, α_1-protease inhibitor (α_1-PI), and 1,10-phenanthroline were purchased from Sigma. Metal salts, Brij-35, sodium dodecyl sulfate, dithioerythreitol, and 2-mercaptoethanol were purchased from Fisher. Peptide libraries were synthesized at the Tufts University Core Facility (Boston, MA) as described previously (12).

Preparation of Partially Active MMP-26—MMP-26 was expressed in the form of inclusion bodies from transformed *E. coli* cells as described previously (14). The inclusion bodies were isolated and purified using B-PER™ bacterial protein extraction reagent according to the manufacturer's instructions. The insoluble protein was dissolved in 8 M urea to ~5 mg/ml. The protein solution was diluted to ~100 μg/ml in 8 M urea and 10 mM dithiothreitol for 1 h, dialyzed in 4 M urea, 1 mM dithiothreitol, 50 mM HEPES, or Tricine, pH 7.5, for at least 1 h and then folded by dialysis in buffer containing 50 mM HEPES or Tricine, 0.2 M NaCl, 10 mM $CaCl_2$, 20 μM $ZnSO_4$, 0.01% Brij-35, pH 7.5, for 16 h. To enhance the activity of MMP-26, the folded enzyme was dialyzed twice for 24 h at 4 °C in the folding buffer without Zn^{2+} ion. The total enzyme concentration was measured by UV absorption using $\epsilon_{280} = 57130\ M^{-1}\ cm^{-1}$, which was calculated by Genetics Computer Group software.

Peptide Library Methods—The methods were performed as described previously (12). To determine the specificity for the primed positions (18), an amino-terminally acetylated dodecamer peptide mixture (1 mM) consisting of a roughly equimolar mixture of the 19 naturally occurring L-amino acids excluding cysteine at each site was incubated with MMP-26 in 50 mM HEPES, pH 7.4, 200 mM NaCl, 5 mM $CaCl_2$ at 37 °C until 5–10% of the peptides were digested. An aliquot (10 μl) of the mixture was subjected to automated amino-terminal peptide sequencing. The data in each sequencing cycle were normalized to the total molar amount of amino acids in that cycle so that a value of 1 indicated the average value. Undigested peptides and the amino-terminal fragments of digested peptides are amino-terminally blocked and therefore do not contribute to the sequenced pool.

The specificity of the unprimed side was determined by libraries with the sequence MAXXXXXLRGAARE(K-biotin) for the P3 site and MAXXPXXLRGGGEE(K-biotin) for other sites, where X represents a degenerate position, K-biotin is ϵ-(biotinamidohexanoyl)lysine, and the amino terminus is unblocked. Libraries were partially digested with MMP-26 as described above, quenched with EDTA (10 mM), and treated in batch with 400 μl of avidin-agarose resin (Sigma). The mixture was transferred to a column, which was washed with 25 mM ammonium bicarbonate. The unbound fraction was evaporated to dryness under reduced pressure, suspended in water, and sequenced. Data were normalized as described above.

Kinetic Assays—Assays of fluorescent peptide substrates were performed by following the procedures reported in the literature (14, 29). For substrates containing the tryptophan residue, the fluorescence was observed at an excitation wavelength of 280 nm and emission wavelength of 360 nm, and for substrates containing 3-methoxycoumarin, fluorescence was measured at an excitation wavelength of 328 nm and emission wavelength of 393 nm. All of the kinetic experiments were conducted in 50 mM HEPES buffer containing 10 mM $CaCl_2$, 0.2 M NaCl, and 0.01% Brij-35. To assess inhibition potency for tight binding inhibitors, the apparent inhibitor dissociation constants (K_i^{app} values) were calculated by fitting the data to Morrison's equation (19). The inhibitor dissociation constants (K_i values) were determined by Dixon's plot (20) for less potent inhibitors. The inhibition assays were performed with a peptide substrate (1 μM), Mca-Pro-Leu-Gly-Leu-Dpa-Ala-Arg-NH_2, and 5–10 different inhibitor concentrations. The substrate stock solutions were prepared in Me_2SO and then further diluted to 50% Me_2SO in water. The final Me_2SO concentration in the assays was 1%. The inhibitors were dissolved in Me_2SO to 5 or 2 mM and diluted with methanol with the exception of inhibitor IV (Calbiochem catalogue number: 444250), which was dissolved in assay buffer. The final methanol concentration in the inhibition assays was 5% (v/v). The specificity constants (k_{cat}/K_m values) were determined by the equation $V = (k_{cat}/K_m)[E][S]$, which is modified from the Michaelis-Menten equation when $[S] \ll K_m$.

The enzyme became a mixture of several states after partial activation by dialysis. The total concentration of 400 nM MMP-26 was measured by absorption at 280 nm and calculated using a molar extinction coefficient of 57,130 $M^{-1}\ cm^{-1}$. The enzyme was titrated with MMP inhibitor I (GM-6001) to determine the concentration of catalytically active MMP-26. The titration analysis revealed the concentration of active MMP-26 to be 21 nM, which was ~5% of the total protein concentration after dialysis. For an accurate titration, the concentration of an enzyme is required to be at least 100-fold more than the inhibition constant of the titrant (21). To avoid the depletion of substrate by a high MMP-26 concentration, a less specific substrate, Mca-Arg-Pro-Lys-Pro-Val-Glu-Nva-Trp-Arg-Lys(Dnp)-NH_2, designed for MMP-3 (22), was used for detection of the initial rate. The cleavage of this substrate by MMP-26 was the slowest among peptide substrates studied in our laboratory (14).

IGFBP-1 and α_1-PI Digestion by MMP-26—IGFBP-1, α_1-PI, and MMP-26 solutions were diluted or dissolved in 50 mM HEPES buffer at pH 7.5 containing 10 mM $CaCl_2$, 0.2 M NaCl, and 0.01% Brij-35. IGFBP-1 (4 μg) and MMP-26 (0.63 μg) in a total volume of 50 μl were incubated for 2 days at room temperature. Each day, 10 μl of reaction mixture was taken, and the reaction was stopped by boiling for 5 min after 2× SDS-PAGE sample buffer containing 2% SDS, 100 mM dithiothreitol, and 50 mM EDTA was added. The cleaved products were separated by a 12% acrylamide gel and detected by silver staining. For cleavage of α_1-PI, 90 μg of α_1-PI were incubated with 1.3 μg of MMP-26 in a total volume of 100 μl. The samples were collected after 1 h, 1day, and 2 days. The cleaved products were separated by a 15% SDS-PAGE and detected by silver staining.

Determination of Cleavage Products by Matrix-assisted Laser Desorption Ionization Time-of-Flight Mass Spectrometry (MALDI-TOF MS)—The cleavage sites of fluorogenic peptide substrates and α_1-PI were determined by measuring the mass of the cleavage products with a Bruker protein time-of-flight mass spectrometer. The reaction mixture was mixed with an equivalent volume of α-cyano-4-hydroxycinamic acid (4.5 mg/ml in 50% CH_3CN, 0.05% trifluoroacetic acid) matrix solution containing synthetic peptide calibrants. Because the high salt concentration increased the noise in the mass spectra, the digestion reaction was performed with 10 mM HEPES buffer containing 5 mM $CaCl_2$ overnight at room temperature. For fluorogenic substrates, MMP-9 was used as a positive control.

RESULTS

Substrate Specificities of MMP-26—The substrate specificity of MMP-26 was investigated using a recently described peptide library method (12). Data are shown in Fig. 1. The residues preferred at each site from P4–P4′ are summarized in Table I. The strongest selectivity was seen at the P1′ site where large hydrophobic residues were preferred. Small residues, alanine and serine, were preferred at the P3′ site. Although P2′ and P4′ displayed indistinct specificity compared with the P1′ site, a lack of a preference for a basic residue (Arg or Lys) at the P2′ site was unique to MMP-26 (Table I). Among the unprimed positions, the P3 site showed the highest selectivity preferring proline and valine. The P1 site was not as selective as the P3 site, although small residues such as serine were preferred. The preference of MMP-26 for proline at P3, hydrophobic residues at P2 and P1′ sites, and serine at P1 is similar to that of other MMPs (5–13).

Inhibition of MMP-26 by Synthetic Inhibitors—Inhibition constants for several inhibitors designed for collagenases and gelatinases were measured with MMP-26, and these values are shown in Fig. 2. Among the four inhibitors tested, inhibitor I (23) was the most potent for MMP-26 with a K_i^{app} of 0.36 nM. Inhibitor II inhibited MMP-26 with a K_i^{app} of 1.5 nM, which is similar to the inhibition constant with neutrophil collagenase MMP-8 (4 nM) (24). Inhibitor III is a less potent stereoisomer of inhibitor II, and MMP-8 discriminates between the two with a 250-fold difference in their inhibition constants (1000 *versus* 4

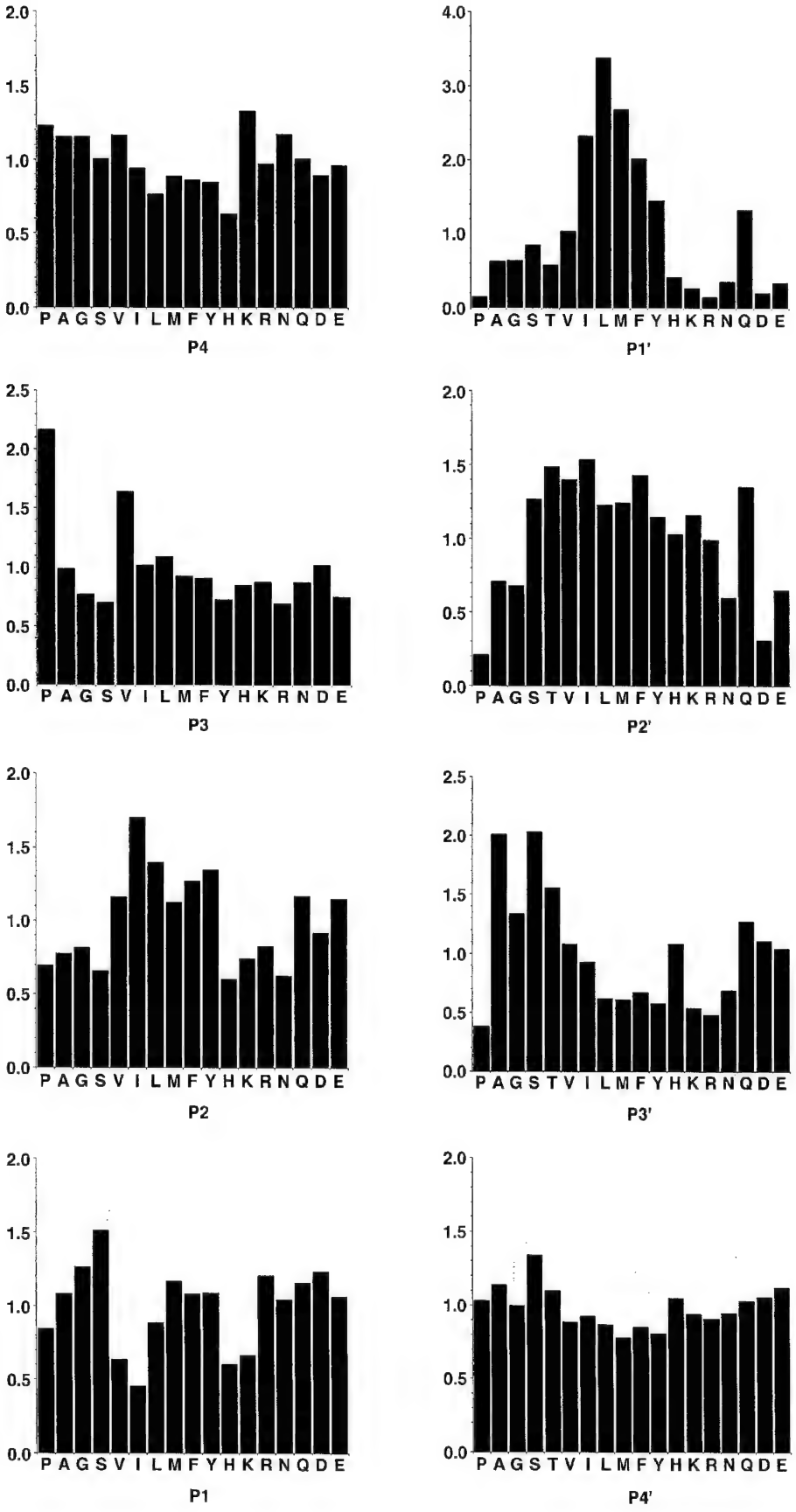

FIG. 1. **Cleavage site specificity of MMP-26 (endometase).** The *figures* on the *right* represent the relative distribution of amino acid residues at positions COOH terminus (P1'–P4') to the MMP-26 cleavage site determined by sequencing the cleavage fragments of a random dodecamer (Ac-*XXXXXXXXXXXX*). Data are normalized so that a value of 1 corresponds to the average quantity per amino acid in a given sequencing cycle and would indicate no selectivity. Tryptophan was not included in the analysis because of poor yield during sequencing. The *figures* on the *left* represent specificity of positions amino terminus to the MMP-26 cleavage site. For the P3 position, data shown were obtained using the library MA*XXXXX*LRGAARE(K-biotin). For all other positions, the P3 proline library MG*XX*P*XX*LRGGGEE(K-biotin) was used. Glutamine and threonine were omitted in some cycles because of high background on the sequencer. Data were normalized as for the primed sites.

nM). There was a 40-fold difference between the K_i^{app} values of the pair of stereoisomers with MMP-26 (60 *versus* 1.5 nM). Inhibitor IV inhibited MMP-26 with a K_i^{app} of 2.9 μM and an IC_{50} value of 3.4 μM. This IC_{50} value is similar to the IC_{50} values with interstitial collagenases MMP-1 and MMP-8 (both are 1 μM) (25).

TABLE I
Cleavage site motifs for MMP-26[a] compared with those of six other MMPs[b]

Enzyme	Cleavage position							
	P4	P3	P2	P1	P1′	P2′	P3′	P4′
MMP-26	Lup (1.3)	Pro (2.2) Val (1.6)	Ile (1.7) Leu (1.4) Tyr (1.3)	Ser (1.5)	Leu (3.4) Met (2.7) Ile (2.3) Phe (2.0) Tyr (1.5) Gln (1.3)	Ile (1.5) Iwe (1.5) Phe (1.4) Gln (1.4)	Ser (2.0) Ada (2.0) Thr (1.6) Gly (1.3)	Ser (1.3)
MMP-1	Val	Pro	Met	Ser	Met	Met	Ala	
MMP-2	Ile	Pro	Val	Ser	Leu	Arg	Ser	
MMP-3	Lys	Pro	Phe	Ser	Met	Met	Met	
MMP-7	Val	Pro	Leu	Ser	Leu	Val	Met	
MMP-9	Val	Pro	Leu	Ser	Leu	Arg	Ser	
MMP-14	Ile	Pro	Glu	Ser	Leu	Arg	Met	
MMP	Val	Pro	Leu	Ser	Leu	Arg	Ala	
Consensus[c]		Val	Tyr		Met Ile	Ile		

[a] Quantities were determined from sequencing data as described for Fig. 1, and values ≥1.3 are listed. All primed sites were obtained using the library Ac-*XXXXXXXXXXXX*. MA*XXXXX*LRGAARE(K-biotin) and MG*XXPXX*LRGGGEE(K-biotin) were used to produce the data at the unprimed sites.

[b] Data from Turk *et al.* (12). A series of consensus peptides/optimal cleavage site motifs were selected and listed for each MMP.

[c] Data summarized from Turk *et al.* (12). These listed residues were selected among amino acids that appeared at least in 5 of the 6 MMPs with values ≥1.3.

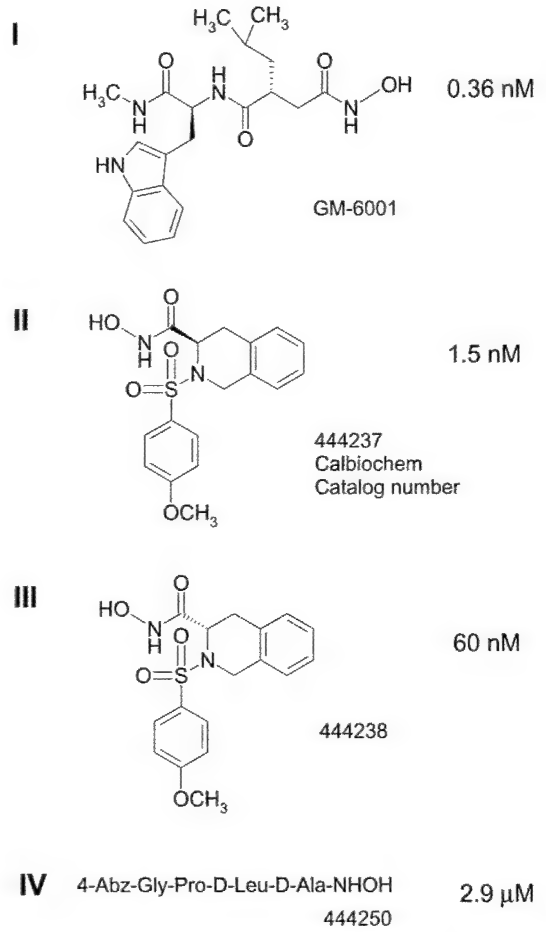

FIG. 2. **The structures of MMP inhibitors and their inhibitor dissociation constants with MMP-26.** The apparent inhibition constants (K_i^{app} values) were determined by Morrison's equation for tight binding inhibitors (compounds *I*, *II*, and *III*) (19), and the inhibition constant (K_i value) was determined by Dixon's plot for a less potent inhibitor (compound *IV*) (20). The values were 0.36, 1.5, 60, and 2900 nM for compounds I, II, III, and IV, respectively.

Autocleavage Sites of Recombinant MMP-26—Dialysis of the folded pro-form of MMP-26 results in an increase in activity because of autolysis of the prodomain. MMP-26 was collected after two 24-h dialyses with fresh buffer at 4 °C (further dialysis or incubation gradually reduced the activity). Partially activated MMP-26 was compared with the zymogen form on a silver-stained polyacrylamide gel (Fig. 3). The band near 30 kDa was confirmed to be pro-MMP-26 by amino-terminal sequencing (Fig. 3, *lane 2*) (14). Several bands below 30 kDa appeared after the dialysis, three of which were located between 20 and 25 kDa (Fig. 3, *lane 3*). One or more of the three cleavage products may be active forms of MMP-26 and was analyzed by amino-terminal sequencing. Only the top two bands were successfully sequenced. The top band resulted from cleavage of a peptide bond between Leu^{49} and Thr^{50}, and the band below it was a product of cleavage between Ala^{75} and Leu^{76} (sequence based on Ref. 14). The cleavage at either site does not remove the cysteine switch sequence PHC^{82}GVPDGSD.

Cleavage of Fluorogenic Substrates by MMP-26—Initial screening of a number of fluorogenic peptide substrates revealed that gelatinase and collagenase peptide substrates were most efficiently cleaved by MMP-26 (14, 17). Therefore, we chose peptide substrates designed for gelatinases or collagenases for further study, three of which contained Trp and two of which contained 7-methoxy coumarin as the fluorogenic group, respectively (26–30). The active MMP-26 concentration was determined by active site titration with inhibitor I (Fig. 4) using the least efficient substrate tested as described under "Experimental Procedures." The titration analysis revealed the concentration of active MMP-26 to be ~5% of the total enzyme concentration (21 of 400 nM). The cleavage sites of the six fluorogenic peptide substrates were determined by identifying the mass of the products by mass spectrometry. Mass spectra of the cleavage products revealed that the cleavage sites of the substrates by MMP-26 and MMP-9 were identical as shown in the example of peptide III (Fig. 5). The specificity constants (k_{cat}/K_m) of these six peptide substrates with MMP-26 were measured and calculated as shown in Table II. MMP-26 hydrolyzed peptide V with the highest specificity constant (3.0×10^4 M^{-1} s^{-1}), which is still 10-fold lower than the specificity constant with MMP-2 (3.97×10^5 M^{-1} s^{-1}) (26).

Cleavage Site of α_1-PI and IGFBP-1—MMP-26 cleaved α_1-PI near the COOH terminus to produce a COOH-terminal fragment of approximately 5 kDa (Fig. 6, *lanes 6* and *7*). This fragment was detected by silver staining of a 15% SDS-PAGE gel run under optimized conditions to identify proteins of molecular masses <10 kDa as described previously (31). A 24-h

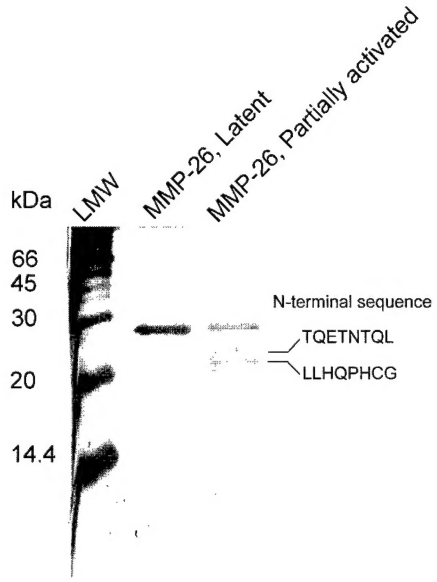

FIG. 3. **Autolysis of MMP-26 during dialysis.** *Lanes 1–3* were low molecular weight markers and the folded MMP-26 before and after dialysis at 4 °C for 24 h, respectively. The cleavage sites of MMP-26 that formed the two major bands around 20 kDa were revealed to be The^{51}–Gln^{52} and Ala^{75}–Leu^{76} by amino-terminal sequencing.

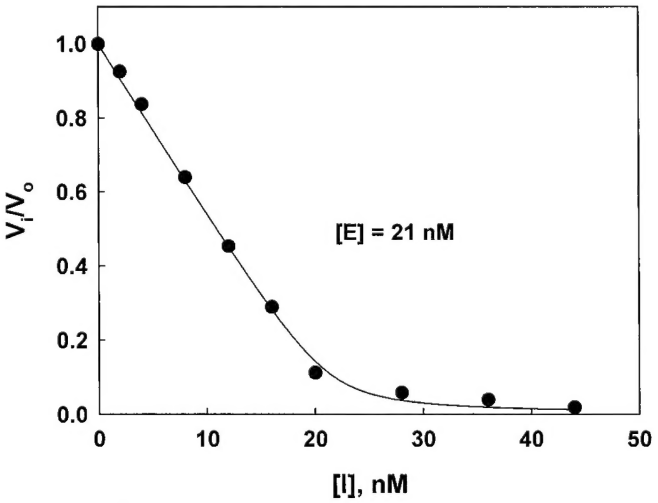

FIG. 4. **Determination of the active MMP-26 concentration by titration of MMP-26 with inhibitor I.** Total MMP-26 concentration was estimated to be 400 nM by molar absorptivity. The estimated active concentration was 21 nM by fitting the titration data into Morrison's equation (19). The assays were performed as described under "Experimental Procedures" with 1 μM of the substrate.

incubation of α_1-PI with MMP-26 at room temperature led to the formation of a fragment below 14.4 kDa (*lane 6*), which was not cleaved any further after 2 days of incubation (*lane 7*). The mass spectrum of the α_1-PI and MMP-26 mixture (Fig. 7*B*) exhibited two new peaks located at 4260 and 4774, which were not observed in the spectrum of α_1-PI alone (Fig. 7*A*). Based on molecular mass analysis, the cleavage sites resulting in these fragments should be Phe^{352}–Leu^{353} (~4774 Da) and Pro^{357}–Met^{358} (~4260 Da) near the COOH terminus of α_1-PI.

A comparison of *lanes 2* and *7* in Fig. 8 indicated that there was no detectable proteolysis of IGFBP-1 without MMP-26. The dark band around 30 kDa (IGFBP-1) disappeared, and a band below 14.4 kDa appeared when IGFBP-1 was incubated with MMP-26 for 1 or 2 days (*lanes 4* and *5*, respectively). The amino-terminal sequence of this band was determined to be Val-The-Asn-Ile-Lys-Lys-Trp-Lys, demonstrating that it arises

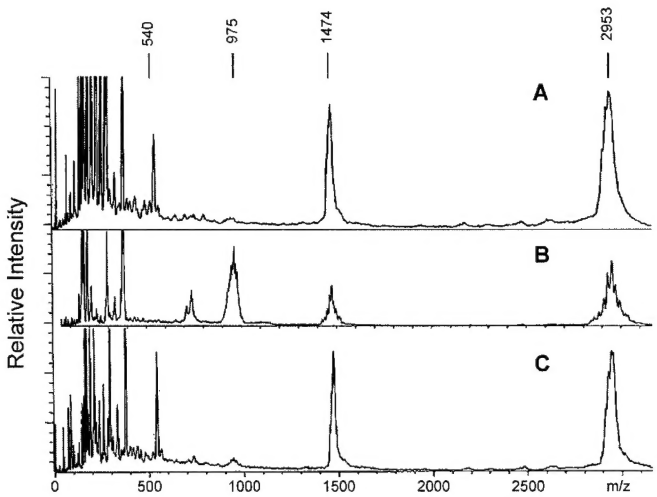

FIG. 5. **An example of the determination of fluorogenic peptide cleavage sites by MALDI TOF mass spectrometry.** 80 μM peptide substrate III (Table II), Dnp-Pro-Leu-Gly-Leu-Trp-Ala-(D)-Arg-OH) was incubated overnight with 5 nM MMP-9 (human neutrophil gelatinase) (*A*), alone (*B*), and with 20 nM endometase (*C*), pH 7.5, and 10 mM HEPES containing 5 mM $CaCl_2$ at room temperature. The two peaks observed at *m/z* 1474 and 2953 were internal synthetic peptide mass calibrants. The peaks at *m/z* 975 and 542 were the substrate and the cleaved peptide fragment, Leu-Trp-Ala-(D)-Arg-OH, produced by cleavage of the Gly–Leu peptide bond by MMP-9 and endometase, respectively.

TABLE II
Peptide substrates of MMP-26[a]

Fluorogenic substrate cleavage sites[b]	k_{cat}/K_m
	$s^{-1}\,M^{-1}$
P3 P2 P1 P1′ P2′ P3′ P4′	
Dnp-Pro-Leu-Gly-Met-Trp-Ser-Arg-OH (I)	9.4×10^3
Dnp-Pro-Leu-Ala-Tyr-Trp-Ala-Arg-OH (II)	3.5×10^3
Dnp-Pro-Leu-Gly-Leu-Trp-Ala-(D)Arg-OH (III)	4.9×10^3
Mca-Pro-Cha-Gly-Nva-His-Ala-Dpa-NH_2 (IV)	1.7×10^4
Mca-Pro-Leu-Ala-Nva-Dpa-Ala-Arg-NH_2 (V)	3.0×10^4
Mca-Pro-Leu-Gly-Leu-Dpa-Ala-Arg-NH_2 (VI)	2.2×10^4

[a] All of the assays were performed in pH 7.5 buffer containing 50 mM HEPES, 0.2 M NaCl, 0.01 M CaCl2, 0.01% Brij-35 at 25°C. The range of substrate concentrations used were 1μM, and the active MMP-26 concentration used was 2 nM for the substrates containing the Mca group and 10 nM for the substrates containing the Trp residue.

[b] The cleavage sites of the substrates were determined by mass spectrometry as described under "Experimental procedures" and Fig. 5.

from cleavage at the same site (His^{140}–Val^{141}) as stromelysin-3 (MMP-11), which produces an inactive 9-kDa fragment (32).

DISCUSSION

The results obtained from peptide library studies indicate that MMP-26 substrate specificities are similar to those of other MMPs where hydrophobic residues are preferred at P1′and P2, proline is preferred at P3, and serine is preferred at P1. The optimal cleavage motifs/consensus peptide sequences for MMP-26 were Lys-Pro-Ile/Leu-Ser(P1)-Leu/Met(P1′)-Ile/Thr-Ser/Ala-Ser (Table I), which are not identical to those of MMP-1, MMP-2, MMP-3, MMP-7, MMP-9, and MMP-14 (12). Based on this sequence specificity knowledge, new fluorescence resonance energy transfer substrates more specific for MMP-26 will be designed and developed. These data may provide critical information applicable to the design of new MMP-26-specific inhibitors and to the identification of novel physiological and pathological substrates of MMP-26 *in vivo*.

The inhibition constants of four synthetic inhibitors with MMP-26 were comparable to those with gelatinases and collagenases, the enzymes for which the inhibitors were designed. This corroborates the findings that the substrate specificity of

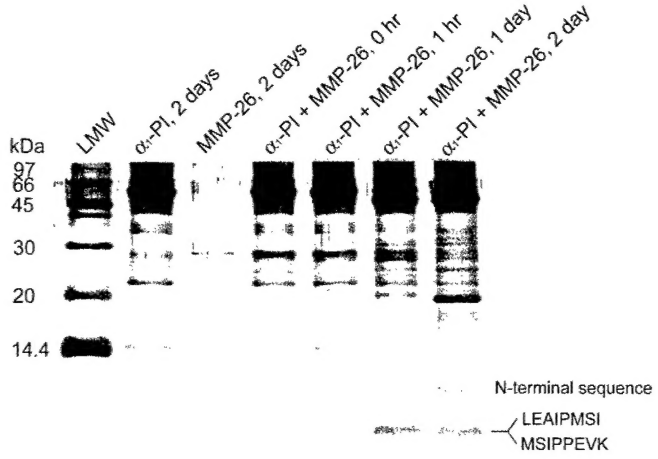

FIG. 6. **Cleavage of human α_1-PI by MMP-26.** After incubation of an α_1-PI (900 μg/ml) and MMP-26 (13 μg/ml) mixture for 1 day (*lane 6*) and 2 days (*lane 7*) at room temperature, the COOH-terminal cleavage products were detected by silver staining a 15% SDS-PAGE gel. Samples containing α_1-PI were overloaded to detect the bands of around 4.5 kDa in *lanes 6* and *7*, which might be 4.8- and 4.2-kDa fragments produced by MMP-26 proteolysis of α_1-PI. The two amino-terminal sequences were deduced from the mass spectrometry results shown in Fig. 6 compared with the primary structure of human α_1-PI.

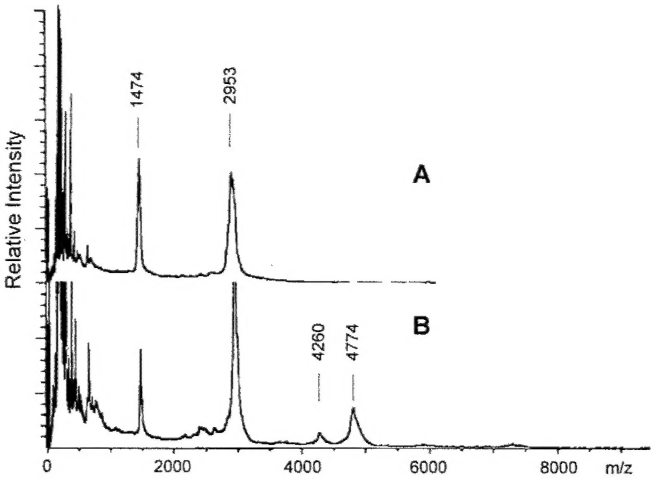

FIG. 7. **Cleavage sites of α_1-PI by MMP-26 determined by MALDI TOF mass spectrometry.** α_1-PI alone (*A*) and with MMP-26 (*B*) were incubated for 1 day in 10 mM HEPES buffer at pH 7.5 containing 5 mM $CaCl_2$. The peaks at *m/z* 1474 and 2953 were two internal calibrants. The two peaks observed at *m/z* 4260 and 4774 were produced from α_1-PI cleavage by MMP-26 at the sites Pro^{357}–Met^{358} and Phe^{352}–Leu^{353}.

MMP-26 is quite close to that of other MMPs. Inhibitor I/GM6001 was the most potent inhibitor of MMP-26 tested with a K_i^{app} of 0.36 nM. GM6001 also potently inhibits MMP-2 (K_i = 0.5 nM) and MMP-8 (K_i = 0.1 nM) but is less effective against MMP-3 (K_i = 27 nM) (23). Inhibitor III is a less potent stereoisomer of inhibitor II, and MMP-8 discriminates between the two with a 250-fold difference in their inhibition constants. There was only 40-fold difference between the K_i^{app} values of the stereoisomers with MMP-26, indicating that MMP-26 is less stereoselective for its inhibitors. Inhibitor IV was more selective for MMP-1 and MMP-8 (IC_{50} = 1 μM against both enzymes) than MMP-9 (IC_{50} = 30 μM) and MMP-3 (IC_{50} = 150 μM) (25). This inhibitor has an IC_{50} value of 3.4 μM with MMP-26, similar as that with MMP-1 and MMP-8.

A survey of known protein cleavage sites determined *in vitro* for MMP-26 is summarized in Table III. The survey indicates that hydrophobic residues are preferred at P1′ and appear in

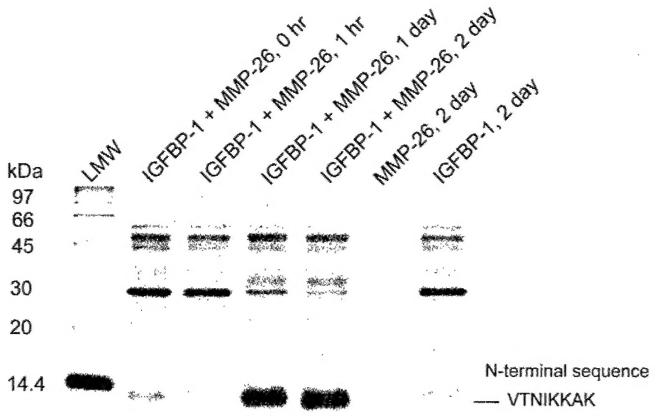

FIG. 8. **Cleavage of IGFBP-1 by MMP-26.** IGFBP-1 (80 μg/ml) was incubated with MMP-26 (13 μg/ml) for 0 h (*lane 2*), 1 h (*lane 3*), 1 day (*lane 4*), and 2 days (*lane 5*). The dense band below 14.4 kDa observed after 1 day (*lane 4*) was the product of IGFBP-1 cleavage by MMP-26 at the His^{140}–Val^{141} site.

TABLE III
Protein sequences hydrolyzed by MMP-26

Proteins	Cleavage sites[a]
α_1-PI[a]	GAMF-LEAI
	EAIP-MSIP
MMP-26 (autolysis)[b]	QMHA-LLHQ
	SPLL-TQET
MMP-26 (autolysis)[c]	QLLQ-QFHR
IGFBP-1[b]	KALH-VTNI
Fibronectin[d]	SPVA-VSQS
Vitronectin[d]	KPEG-IDSR
Fibrinogen[d]	SKPN-MIDA
	HTEK-LVTS
	GDKE-LRTG

[a] A line is inserted in the cleavage site.
[b] Data from this study.
[c] Data from Marchenko *et al.* (41).
[d] Data from Marchenko *et al.* (17).

almost all of the substrates. Residues occurring at other positions that agree with the consensus from the peptide libraries include proline (3 times) at P3, hydrophobic residues (6 times) at P2, and Ser, Ala, and Thr (4 times) at P3′. Residues at the other positions seem random and do not coincide with residue predictions by the peptide libraries, although the libraries do indicate less stringent selectivity at these positions. Accordingly, no individual protein cleavage site precisely matches the consensus motif determined by the peptide library studies, suggesting that the cleavage sites in these protein substrates are probably suboptimal for cleavage by MMP-26. The folding topology of the protein may be a contributing factor to the enzyme-substrate interactions. Although the protein cleavage site may not be the optimal sequence, the peptide chain might assume a conformation that is easily accessible to a protease active site; for example, an exposed loop is found in the bait region of α_2-macroglobulin (33), and the reactive loop is found in the bait region of α_1-PI (34). Alternatively, the cleavage of a suboptimal site may be promoted by recruitment to the enzyme via a substrate-binding exosite. In addition, the presence of unfavorable residues around the cleavage site may slow down the rate of digestion by a protease, regulating the degradation process.

MMP-26 has been shown to digest several components of the extracellular matrix, such as fibronectin, collagens, fibrinogen, and vitronectin, but not any of several plasma proteins tested with the exception of α_1-PI (14, 17). It has been reported that the cleavage of the reactive loop residues around 350–365 in α_1-PI by MMP-1 and MMP-3 inactivates the inhibitor (34–36). The digestion of α_1-PI by MMP-26 generates two major peaks

that originate from the cleavage at two sites near the COOH-terminal region, Phe^{352}–Leu^{353} (~4774 Da) and Pro^{357}–Met^{358} (~4260 Da). These are the same cleavage sites for MMP-1 (35). In addition, MMP-3 cleaves the Pro^{357}–Met^{358} bond (34). MMP-11 cleaves the Ala^{350}–Met^{351} bond (36), a site distinct from those of MMP-26 and MMP-1. Interestingly, direct evidence showed that α_1-PI was a critical substrate for MMP-9 *in vivo* in a mouse model of the autoimmune disease *bullous pemphigoid* (37). Thus, MMP-26 may inactivate α_1-PI like the other MMPs to promote serine proteinase activity, enhancing extracellular matrix degradation in cancers or other pathological processes.

The insulin-like growth factors, IGFBPs, and IGFBP proteases are involved in the regulation of somatic growth and cellular proliferation. The level of free insulin-like growth factor in a system is modulated by rates of insulin-like growth factor production and clearance and the degree of binding to IGFBPs (38). IGFBP-1 inhibits IGF-I-induced proliferation of the MCF-7 human breast adenocarcinoma (32). Through their inactivation of IGFBP-1, MMPs were able to promote cell growth and survival by the increase of the effective insulin-like growth factor concentration in the surrounding medium (32). MMP-26 cleaves the His^{140}–Val^{141} bond in IGFBP-1 as does MMP-11. Therefore, the cleavage of IGFBP-1 by MMP-26 to produce the 9-kDa inactive form may sustain the survival of cancer cells, increasing the chance of metastasis.

The cleavage sites in the fluorogenic substrates seem in good agreement with the motifs determined by the peptide library approach. Although the six commercial fluorogenic peptide substrates tested were not designed for the specificity of MMP-26, some of them resemble closely to the consensus sequences of peptide substrates for MMP-26 determined by the peptide library studies, proline at P3, a hydrophobic residue at P2, P1′, and P2′, and small residues at P3′, with the exception that serine is preferred at P1 and P4′, Lys is preferred at P4, but a basic residue is not preferred at P2′. The best substrate tested for MMP-26 was peptide V, Mca-Pro-Leu-Ala-Nva-Dpa-Ala-Arg-NH_2. This peptide appears to be very close to optimal sequences determined by the peptide library studies where there is a selected residue at essentially every position (see Fig. 1 and Table I) with the exception that the peptide libraries do not have Nva at P1′.

The cleavage sites in the protein substrates tested do not match exactly the optimal motifs identified by the peptide library approach; however, upon close examination of the protein cleavage site data presented in Table III, it seems that the amino acid residues at P1 and P4′ are less selective. This is in good agreement with the peptide library data. Furthermore, P1′ is more selective, and Leu, Met, and Ile are preferred at P1′ (Fig. 1). This finding is consistent with the protein cleavage site data shown in Table III in which 7 of the 11 residues (64%) at P1′ are these residues. Moreover, two Lys residues are found at the P4, and two Ser residues are found at P4′ of the protein cleavage sites, which is also unique to MMP-26 according to the library data.

The relative rates of cleavage in the six fluorogenic substrates also correspond to the peptide library data relatively well. The best substrate is peptide V with a specificity constant of 3.0×10^4 M^{-1} s^{-1}. In addition to peptide V, peptides IV and VI are also relatively good substrates for MMP-26 with specificity constants of 1.7×10^4 M^{-1} s^{-1} and 2.2×10^4 M^{-1} s^{-1}, respectively (Table II). The worst substrate of MMP-26 in Table II is peptide II with a specificity constant ~10 times slower than peptide V. Neither Ala at P1 nor Tyr at P1′ in the peptide II is preferred. On the other hand, the rate of cleavage of peptide V, the best peptide of MMP-26 in Table II, is 10 times slower than the rate of substrate cleavage by MMP-2 (3.97×10^5 M^{-1} s^{-1}) (26). The slower rate of peptide and protein digestion by MMP-26 suggests that this enzyme is not the most powerful MMP catalytically or the optimal substrates for MMP-26 have not been identified.

It is also possible that a manageable rate of MMP-26 catalysis may be required in biological processes such as normal implantation where tight control of substrate degradation is highly desirable. In the latter scenario, the function of MMP-26 may not be limited to the direct degradation of ECM. MMP-26 may play a more critical role in controlling the activities of growth factors or proteases that mediate such processes. Consequently, biologically significant substrates of MMP-26 may be growth factor-binding proteins, receptors, zymogens, and enzyme inhibitors.

MMP-26 is not only unique in terms of its tissue and cell-specific expression as reported by us and others (14–17) but also because of its unique cysteine switch sequence (P**H**^{81}CGVPDGSD) and thus its unique pathway of proenzyme activation. Many members of the MMP family follow the classic cysteine-switch activation model (39, 40). The inactivity of a pro-MMP is generally attributable to a complex between the sulfhydryl group of a cysteine residue in the cysteine switch sequence (P**R**CGVPDV) of the prodomain and the active site zinc atom in the catalytic domain. The activation of a pro-MMP can be achieved proteolytically by hydrolysis of the propeptide on the carboxyl-terminal side of the cysteine switch residue near the border between the propeptide and catalytic domains. This proteolytic step may be catalyzed by another proteinase or it may be an autolytic step (39, 40). However, Marchenko *et al.* (41) have challenged the cysteine-switch model. Their report showed that the activating cleavage site of pro-MMP-26 occurs at Gln^{59}–Gln^{60}, leaving the putative cysteine switch sequence intact. It was suggested that the Arg to His substitution existing in the unique P**H**^{81}CGVPDGSD cysteine-switch motif of pro-MMP-26 abolishes the ability of Cys^{82} to interact with the zinc ion of the catalytic domain (41).

We have identified two of the major autolytic sites in MMP-26 to be Leu^{49}–Thr^{50} and Ala^{75}–Leu^{76}. Although different from the Gln^{59}–Gln^{60} site, the cleavage at these two sites also does not remove the cysteine switch sequence (PH**C**^{82}GVPD) from the enzyme, suggesting that Cys^{82} may not play a role in the latency of the zymogen, which is consistent with the hypothesis proposed by Marchenko *et al.* (41). Alternatively, the thiol group of Cys^{82} could be transiently dissociated from the zinc ion at the active site, allowing a water molecule to bind to the zinc ion and the enzyme to exhibit catalytic activity. Our inhibitor titration data demonstrated that ~5% of the total enzyme molecules was active. This observation may support the concept that the thiol groups of Cys^{82} in the active enzyme molecules are dissociated or removed from the active site zinc ions and the thiol groups of the Cys^{82} in remaining 95% of the total enzyme molecules are still coordinated with the zinc ions at the active sites, forming a steady-state equilibrium between the active enzyme molecules and the zymogen molecules. However, this hypothesis and the detailed activation mechanisms of pro-MMP-26 remain to be thoroughly investigated (42). In summary, this work provides new knowledge on the MMP-26 substrate specificity to build a working model for the future design of MMP-26 inhibitors, studies of pro-MMP-26 activation, and identification of optimal physiological and pathological substrates of MMP-26 *in vivo*.

Acknowledgments—We thank Margaret Seavy at the Bioanalytical Facility for protein amino-terminal sequencing and Sara C. Monroe for editorial assistance with manuscript preparation at the Florida State University. We appreciate Dr. Jian Ni at the Human Genome Sciences Inc. for previous collaboration on the human MMP-26 project.

REFERENCES

1. Hooper, N. M. (1994) *FEBS Lett.* **354,** 1–6
2. Shapiro, S. D. (1998) *Curr. Opin. Cell Biol.* **10,** 602–608
3. Nagase, H., and Woessner, J. F. (1999) *J. Biol. Chem.* **271,** 28509–28515
4. Johansson, N., Ahonen, M., and Kähäri, V. M. (2000) *Cell. Mol. Life Sci.* **57,** 5–15
5. Netzel-Arnett, S., Sang, Q.-X., Moore, W. G., Narve, M. Birkedal-Hansen, H., and Van Wart, H. E. (1993) *Biochemistry* **32,** 6427–6432
6. McGeehan, G. M., Bickett, D. M., Green, M., Kassel, D., Wiseman, J. S., and Berman, J. (1994) *J. Biol. Chem.* **269,** 32814–32820
7. Smith, M. M., Shi, Lihong, and Narve, M. (1995) *J. Biol. Chem.* **270,** 6440–6449
8. Nagase, H., and Fields, G. B. (1996) *Biopolymers* **40,** 399–416
9. Ohkubo, S., Miyadera, K., Sugimoto, Y., Matsuo, K., Wierzba, K., and Yamada, Y. (1999) *Biochem. Biophys. Res. Commun.* **266,** 308–313
10. Deng, S., Bickett, D. M., Mitchell, J. L., Lambert, M. H., Blackburn, R. K., Carter, H. L., III, Neugebauer, J., Pahel, G., Weiner, M. P., and Moss, M. L. (2000) *J. Biol. Chem.* **275,** 31422–31427
11. Kridel, S. J., Chen, E., Kotra, L. P., Howard, E. W., Mobashery, S., and Smith, J. W. (2001) *J. Biol. Chem.* **276,** 20572–20578
12. Turk, B. E., Huang, L. L., Piro, E. T., and Cantley, L. C. (2001) *Nature Biotechnol.* **19,** 661–667
13. Chen, E. I., Kridel, S. J., Howard, E. W., Li, W., Godzik, A., and Smith, J. W. (2002) *J. Biol. Chem.* **277,** 4485–4491
14. Park, H. I., Ni, J., Gerkema, F. E., Liu, D., Belozerov, V. E., and Sang, Q.-X. A. (2000) *J. Biol. Chem.* **275,** 20540–20544
15. Uría, J. A., and López-Otín, C. (2000) *Cancer Res.* **60,** 4745–4751
16. de Coignac, A. B., Elson, G., Delneste, Y., Magistrelli, G., Jeannin, P., Aubry, J.-P. Berthier, O., Schmitt, D., Bonnefoy, J.-Y., and Gauchat, J.-F. (2000) *Eur. J. Biochem.* **267,** 3323–3329
17. Marchenko, G. N., Ratnikov, B. I., Rozanov, D. V., Godzik, A., Deryugina, E. I., and Strongin, A. Y. (2001) *Biochem. J.* **356,** 705–718
18. Schechter, I., and Berger, A. (1967) *Biochem. Biophys. Res. Comm.* **27,** 157–162
19. Morrison, J. F. (1969) *Biochim. Biophys. Acta* **185,** 269–286
20. Cornish-Bowden, A. (1974) *Biochem. J.* **137,** 143–144
21. Copeland, R. A. (2000) in *Enzymes: a Practical Introduction to Structure, Mechanism, and Data Analysis.* 2nd Ed., pp. 305–349, Wiley-VCH, Inc., New York
22. Nagase, H., Fields, C. G., and Fields, G. B. (1994) *J. Biol. Chem.* **269,** 20952–20957
23. Galardy, R. E., Cassabonne, M. E., Giese, C., Gilbert, J. H., Lapierre, F., Lopez, H., Schaefer, M. E., Stack, R., Sullivan, M., and Summers, B. (1994) *Ann. N. Y. Acad. Sci.* **732,** 315–323
24. Matter, H., Schwab, W., Barber, D., Billen, G., Haase, B., Neises, B., Schudok, M., Thorwart, W., Schreuder, H., Brachvogel, V., Lönze, P., and Weithmann, K. U. (1999) *J. Med. Chem.* **42,** 1908–1920
25. Odake, S., Morita, Y., Morikawa, T., Yoshida, N., Hori, H., and Nagai, Y. (1994) *Biochem. Biophys. Res. Comm.* **199,** 1442–1446
26. Murphy, G., Nguyen, Q., Cockett, M. I., Atkinson, S. J., Allan, J. A., Knight, C. G., Willenbrock, F., and Docherty, A. J. P. (1994) *J. Biol. Chem.* **269,** 6632–6636
27. Knäuper, V., López-Otín, C., Smith, B., Knight, G., and Murphy, G. (1996) *J. Biol. Chem.* **271,** 1544–1550
28. Knight, C. G., Willenbrock, F., and Murphy, G. (1992) *FEBS Lett.* **296,** 263–266
29. Netzel-Arnett, S., Mallya, S. K., Nagase, H., Birkedal-Hansen, H., and Van Wart, H. E. (1991) *Anal. Biochem.* **195,** 86–92
30. Stack, M. S., and Gray, R. D. (1989) *J. Biol. Chem.* **264,** 4277–4281
31. Schägger, H., and Jagow, G. (1987) *Anal. Biochem.* **166,** 368–379
32. Manes, S., Mira, E., Barbacid, M. M., Cipres, A., Fernandez-Resa, P., Buesa, J. M., Merida, I., Aracil, M., Marquez, G., and Martinez-A. C. (1997) *J. Biol. Chem.* **272,** 25706–25712
33. Sottrup-Jensen, L. (1989) *J. Biol. Chem.* **264,** 11539–11542
34. Mast, A. E., Enghild, J. J., Nagase, H., Suzuki, K., Pizzo, S. V., and Salvesen, G. (1991) *J. Biol. Chem.* **266,** 15810–15816
35. Desrochers, P. E., Jeffrey, J. J., and Weiss, S. J. (1991) *J. Clin. Invest.* **87,** 2258–2265
36. Pei, D., Majmudar, G., and Weiss, S. J. (1994) *J. Biol. Chem.* **269,** 25849–25855
37. Liu, Z., Zhou, X., Shapiro, S. D., Shipley, J. M., Twining, S. S., Diaz, L. A., Senior, R. M., and Werb, Z. (2000) *Cell* **102,** 647–655
38. Ferry, R. J., Jr., Katz, L. E. L., Grimberg, A., Cohen, P., and Weinzimer, S. A. (1999) *Horm. Metab. Res.* **31,** 192–202
39. Springman, E. B., Angleton, E. L., Birkedal-Hansen, H., and Van Wart, H. E. (1990) *Proc. Natl. Acad. Sci. U. S. A.* **87,** 364–368
40. Van Wart, H. E., and Birkedal-Hansen, H. (1990) *Proc. Natl. Acad. Sci. U. S. A.* **87,** 5578–5582
41. Marchenko, N. D., Marchenko, G. N., and Strongin, A. Y. (2002) *J. Biol. Chem.* **277,** 18967–18972
42. Sang, Q. X. (2002) in *Handbook of Proteolytic Enzymes* (Barrett, A. J., Rawlings, N. D., and Woessner, J. F., eds) 2nd Ed., Academic Press, Orlando, FL, in press